# Simulations for pearlite-to-austenite transformation in a DP590 steel for improved mechanical properties

*A Dissertation Submitted*
In Partial Fulfilment of the Requirements
for the Degree of

## Master of Engineering

in

## Production Engineering

by

**Sandeep Sharma**
Regd. No. 801382023

***Under the guidance of***

**Dr. Tarun Nanda**
Assistant Professor,
MED, TU, Patiala

**Dr. B. Ravi Kumar**
Scientist (E2),
NML, Jamshedpur


*to the*

**MECHANICAL ENGINEERING DEPARTMENT**

**THAPAR UNIVERSITY, PATIALA**

**JULY, 2015**

# CERTIFICATE

I hereby declare that the thesis entitled "**Simulations for pearlite-to-austenite transformation in a DP590 steel for improved mechanical properties**" is an authentic record of my study carried out as requirements for the award of the degree of **Master of Engineering** in **Production Engineering** at **Thapar University, Patiala** under the supervision of **Dr. Tarun Nanda,** Assistant Professor, Mechanical Engineering Department, Thapar University, Patiala and **Dr. B. Ravi Kumar**, Scientist (E2), National Metallurgical Laboratory (NML), Jamshedpur during July, 2013 to July, 2015. The matter embodied in this report has not been submitted in partial or full to any other university or institute for the award of any degree.

Sandeep Sharma

Date:

It is certified that the above statement made by the student is correct to the best of my/our knowledge and belief.

**Dr. Tarun Nanda**
Assistant Professor,
MED, TU, Patiala

**Dr. B. Ravi Kumar**
Scientist (E2),
NML, Jamshedpur

*Countersigned by*

**Dr. S.K. Mohapatra**
Sr. Professor and Head
MED, TU, Patiala

**Dr. S.S. Bhatia**
Dean of Academic Affairs
TU, Patiala

# Acknowledgement

I express my deep sense of gratitude and a very sincere thanks to my guide **Dr. Tarun Nanda** Assistant Professor, Mechanical Engineering Department, Thapar University, Patiala and **Dr. B Ravi Kumar**, Scientist (E2), National Metallurgical Laboratory (NML), Jamshedpur for their efforts and motivating me towards the goal of completion of the work.

I would also like to thank Dr. S. K. Mohapatra Head, Mechanical engineering department, Thapar University, Patiala for providing all the facilities to carry out the work. A special note of thanks to the lab technicians of NML Jamshedpur Mr Rajiv Jonko, Mr Lalan Patro and Mr Naveen Kumar for helping me polish the specimens and provide the necessary resources for the work. I would also like to thank my Parents and friends for supporting and motivating me to constantly move towards the goal of my work. At the end I would like to thank the 'ALMIGHTY' for all his blessings and kindness.

Sandeep Sharma

# Abstract

The present research work deals with the processing of third generation DP steels with lean chemistry. The main objective of the present dissertation was to understand the kinetics of formation of carbon rich austenite (i.e. austenite obtained through dissolution of pearlite only; avoiding dissolution of pro-eutectoid ferrite present in the as-received steel) to facilitate formation of carbon rich martensite (of better hardness) during processing of dual phase steels (DP steels) for enhanced mechanical performance.

DICTRA (27) was used to predict the holding time at a given annealing temperature for complete pearlite dissolution in the given hot rolled steel. The simulations were done for both equilibrium heating conditions and non-equilibrium heating conditions. The simulations for equilibrium heating rates conditions predicted that with increase in austenization temperature, the holding time required for transformation of pearlite into austenite decreases. Further, as the annealing temperature increases, the mean variation of carbon in austenite also increases i.e. heterogeneity of carbon in austenite increases. For the non-equilibrium conditions, it was predicted that as the annealing temperature increases, the mobility of carbon also increasing and also the time required for heating increases, and thus formation of stable austenite takes place. Subsequent experimentation was done to validate the results obtained through DICTRA simulations. The experimental results were found in close agreement with the simulation results and thus, establishing that the simulations done on DICTRA software were correct for the hot rolled steel.

Further, experiments were performed to investigate if the simulation results hold good for cold rolled specimens also (or not). Experiments were conducted separately for the hot rolled and cold rolled steel specimens. It was noted that the volume fractions of austenite under a given processing condition in cold rolled specimens, was higher as compared to hot rolled steel (and simulation results). The size distribution was measured using ‘analySIS FIVE’ software for both hot rolled and cold rolled steel. It was observed that ferrite and martensite phases in cold rolled annealed specimens were finer compared to the hot rolled specimens. Finally, tensile testing was performed to establish that annealing of the hot rolled steel (annealed with time periods as predicted through simulations) led to complete dissolution of pearlite (of the initial microstructure) and resulted in improved combinations of strength and ductility in the annealed steel (by formation of carbon rich austenite and hence martensite). A considerable improvement in strength-percent elongation combinations was observed for the hot rolled steels.

# Content

# List of Figures

# List of Tables

# Acronyms

| Acronym | Full Name |
|---|---|
| ACC | Accelerated Cooling |
| AHSS | Advance High Strength Steels |
| ASTM | American Society for Testing and Materials |
| ATMP | Advanced Thermo Mechanical Processing |
| BH | Bake Hardening |
| CCT | Continuous Cooling Transformation |
| CP | Complex Phase |
| CG | Coarse Grained |
| DBTT | Ductile To Brittle Transition Temperature |
| DIFT | Deformation Induced Ferrite Transformation |
| DP | Dual Phase |
| DSC | Differential Scanning Calorimetry |
| EBSD | Electron Backscatter Diffraction |
| F | Ferrite |
| FG | Fine Grained |
| GF | Gram Force |
| L-IP | Light-Weight With Induced Plasticity |
| M-A | Martensite-Austenite |
| MART | Martensite |
| MVF | Martensite Volume Fraction |
| NG-TMCP | New Generation Thermo Mechanical Controlled Processing |
| QT | Quench Temperature |
| RP | Resting Pad |
| SAED | Selected Area Electron Diffraction |
| SEM | Scanning Electron Microscopy |
| SPD | Severe Plastic Deformation |
| TEM | Transmission Electron Microscopy |
| TM | Tempered Martensite |
| TE | Total Elongation |

| | |
|---|---|
| TRIP | Transformation Induced Plasticity |
| TS | Tensile Strength |
| TWIP | Twin Induced Plasticity |
| UFC | Ultra-Fast Cooling |
| UFG | Ultrafine Grained |
| UTS | Ultimate Tensile Strength |
| XRD | X-Ray Diffraction |
| YS | Yield Strength |

# Symbols

| **Symbol** | **Full Name** |
|---|---|
| α | Ferrite |
| γ | Austenite |
| ℃ | Degree Celsius |
| $A_1$ | Lower Critical Temperature during heating |
| $A_3$ | Upper Critical Temperature during heating |
| $M_S$ | Martensite Start Temperature |
| *rm* | Plastic Strain Ratio |
| s | Second |
| t | Time |
| T | Temperature |

# Chapter 1
# Introduction

## 1.1 General

Despite the development of sophisticated composite materials in recent years, steel is still the basic construction material for industrial applications. While classical single phase steels either have good formability (ferritic steels) or strength (martensitic steels), modern multiphase steels like dual-phase (DP) or Transformation Induced Plasticity (TRIP) steels have shown high potential especially for automotive applications due to their remarkable properties combining high strength and good formability [Homberg *et al.*, 2011; Meng *et al*, 2014]. The current demands in the automobile industry for vehicle weight reduction for improved fuel economy while maintaining crash performances requires development of new and advanced high strength steels with extraordinary combination of strength and toughness. This requires new and innovative concepts of alloy design and novel processing for creation of unique microstructures in steels known as Advanced High Strength Steels (AHSS). The first generation advanced high strength steels (AHSS) were Dual Phase (DP), Complex Phase (CP) and Transformation Induced Plasticity (TRIP) steels. The advantages of first generation AHSS is that they have high strength However, these steels have several limitations such as limited deformation and fracture toughness than what is needed for significant weight reduction and energy savings in the 21st century structural components. The second generation advanced high strength steels were Twin Induced Plasticity (TWIP) and Light-weight with Induced Plasticity (L-IP) steels. These have good hardness and ductility, but these steels contain a large amount of alloying elements which makes them prohibitively expensive e.g. in Austenitic Stainless Steels, high alloying is done to get retained austenite at room temperature. Thus, there will bea need to develop third generation advanced high strength steels with combination of high strength and high toughness and that too at reasonable cost [Matlock *et al*, 2012]. The development of dual-phase (DP) steels has become an area of interest in the automobile industry because of potential weight reduction by using inexpensive alloying without sacrificing mechanical properties [Saleh and Priestner, 2001]. DP steel possesses combination of special mechanical properties such as high tensile strength, high work hardening rate at early stages of plastic deformation as well as very good ductility

[Wang and Wei, 2013]. In DP steels, combination of these properties is achieved by obtaining a ferrite/bainite or ferrite/martensite microstructure as shown in Fig. 1.1 where ferrite forms the ductile and deformable constituent and the second phase bainite/martensite strengthens the steel [Cornet and Herman, 2003].

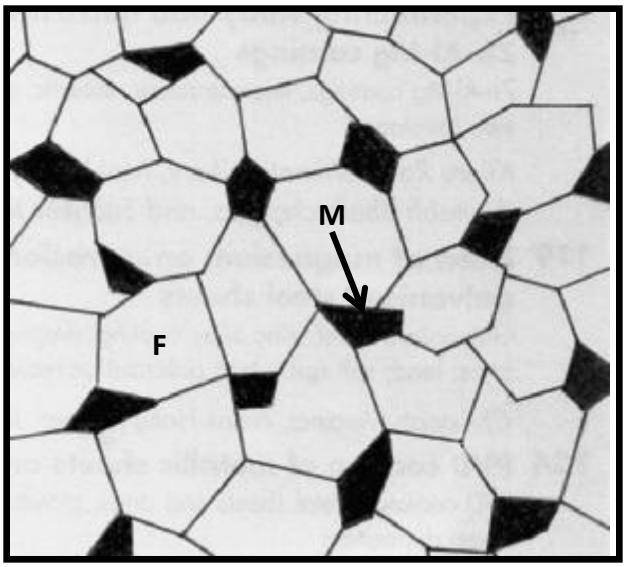


Figure 1.1: Islands of Martensite in a Matrix of Ferrite in DP Steels.
[Dziedzic and Turczyn, 2010] F= ferrite and M= martensite

## 1.2 Dual-Phase Steels

Microstructure of dual phase steels is composed of ferrite which is a ductile or deformable phase and bainite/ martensite as the second phase which provides strength [Cornet and Herman 2003]. DP steels show high strain hardening characteristics (high n value), especially at the beginning of plastic deformation. The greatest prospect of application of DP-type steels is in automotive industry. It is predicted, that their total share in a car structure can reach over 50%. These steels usually contain 0.05–0.2% C, 1.2–1.6%Mn, 0.03–0.6%Si and micro additions of V, Nb and Ti up to concentration of 0.1%. DP-type sheets can be produced by a classical heat treatment, consisting in their austenizing at a temperature slightly higher than $AC_{11}$ of the steel followed with water quenching or an energy-saving technology of the thermo mechanical treatment, integrating hot-rolling in the austenitic field or $\alpha + \gamma$ region with direct cooling [Adamczyk and Grajcar, 2006; Bhattacharya, 2006; Lorusso *et al.*, 2012; Mohrbacher, 2013].Microstructure of dual phase steels is composed of soft ferrite matrix and 10–40% of hard martensite or martensite-

austenite (M–A) particles or bainite as the third phase. This type of microstructure allows achieving an ultimate tensile strength in the range of 400–1000 MPa [Meng *et al*, 2009]. The strength of DP steel microstructure is controlled by the amount of and ductility by the size and distribution of martensite phase. This dual phase type of microstructure can exhibit the following advantageous features over the conventional high strength steels [Kuziak *et al*, 2008]:

- They do not exhibit yield point elongation
- They have low YS/UTS ratio (around 0.5) and high strain hardening characteristics (high *n* value), especially at the beginning of plastic deformation
- Grades containing low carbon content have been shown to exhibit excellent resistance to fatigue crack propagation plastic strain ratio

The microstructure of DP steels does not allow obtaining a high plastic strain ratio value of value $r_m$. This means that these steels are not good candidates for applications that require high drawability. They usually exhibit poor hole expansion ratio values. This drawback, however, can be eliminated by adding Ti with the aim of inducing precipitation strengthening in ferrite to reduce the differences in hardness between the two phases. Alternatively, M-A constituents may be replaced by bainite phase [Kuziak *et al*, 2008]. Dual phase steels can be welded with all conventional welding methods currently used in the automotive industry viz. resistance spot welding, laser welding, arc welding [Kuziak *et al*, 2008, Parkes *et al*, 2014]. The most important feature influencing mechanical properties of dual-phase microstructure includes shape, size, amount and distribution of ferrite and martensite, the carbon content of martensite, the volume fraction of retained austenite, and the grain size of martensite and ferrite phases [Patel *et al.*, 2001; Kuziak *et al.*, 2008; Lorusso *et* al., 2012].

## 1.3 Production of Dual Phase Steels

The development of DP steels has attracted great interest in the automobile industry because of a potential weight reduction by using inexpensive alloying without sacrificing mechanical properties [Saleh and Priestner, 2001]. DP steels mainly consist of two phases' viz. ferrite and martensite. But, in addition to martensite, the microstructure may also contain small amounts of other phases such as retained austenite, new ferrite, pearlite and bainite, depending on the cooling rate and thermo-mechanical processing route [Erdogan and Tekeli, 2002].Some of the authors have produced DP steels by direct quenching from temperature above $A_{C1}$temperature

(i.e. inter-critical temperature). Microstructure produced comprised of ferrite and martensite [Adamczyk and Grajcar, 2006; Demir and Erdogan, 2008]. Some authors have produced DP steels by first doing slow (air) cooling up to the desired ferrite transformation from austenite and then quenching for transforming the remaining austenite to martensite (done according to CCT diagram) [Meng *et al*., 2009].Very limited work has been reported to produce the bainite/ferrite or martensite/ ferrite microstructure of dual phase steels by first doing laminar cooling then ultra-fast cooling up to coiling temperature and then by coil cooling up to room temperature of hot rolled strip [Cornet and Herman 2003]. Mechanical properties obtained by the last method are better than all other methods due to grain refinement of microstructure and proper volume fraction of the constituent phases. The DP steels thus produced properly fit in the region of third generation AHSS. However, in this method, there is a difficulty in controlling the different rates of cooling required from the austenization temperature to the room temperature. Also, dual phase steels of ferrite/ martensite microstructure can be produced by doing ultra-fast cooling directly up to room temperature after slow laminar cooling. Mechanical properties (strength and toughness) obtained by this method are better than the properties obtained by direct water quenching [Cornet and Herman 2003].

## 1.4 Properties and Applications of Dual Phase Steels

The combination of high strength and ductility in modern AHSS can allow thinner components to be used in car construction and also to improve the safety due to their high energy-absorption capabilities. Dual-phase steels developed over the past few decades offer impressive mechanical properties, such as continuous yielding behavior and superior strength–ductility combination, high work hardening, in addition to the advantage of reduced cost, better formability, and excellent surface finish(Kumar *et al*., 2008; Dziedzic and Turczyn, 2010; Sayed and Kheirandish, 2012; Ramazani *et al*., 2014]. DP steels are strong candidates for structural applications [Han *et al*., 2013]. The usage of dual phase steels for automotive applications is increasing because they can meet the formability requirements and other properties such as high tensile strength, fatigue resistance, hole expansion, good drawing and welding properties [Cai *et al*., 2014].

## 1.5 Ultra-Fast Cooling

Ultra-fast cooling (UFC) also known as new generation thermo-mechanical controlled processing (NG-TMCP) consists in spraying the strip with jets of water under a pressure of 4–5 bar [Yong *et al*., 2012]. This cooling can be regulated in terms of cooling rate and temperature by means of the water delivery rate and the length sprayed. It allows achieving cooling rates of the order 5–10 times greater than the conventional laminar cooling rates.

The core concept in NG-TMCP includes:

1. The deformation and strain accumulation are completed at the appropriate temperature in the austenite region to obtain hardened austenite.

2. Laminar cooling is carried out after rolling to get required amount of ferrite.

3. The cooling process stops at the dynamic phase transformation point from austenite to ferrite.

4. Subsequently the cooling route is controlled based on the desired microstructure and the mechanical properties of the steel [Yong *et al*., 2012; Cai *et al*., 2014; Homberg *et al*., 2011].

The schematic of NG-TMCP is illustrated in Fig. 1.2.

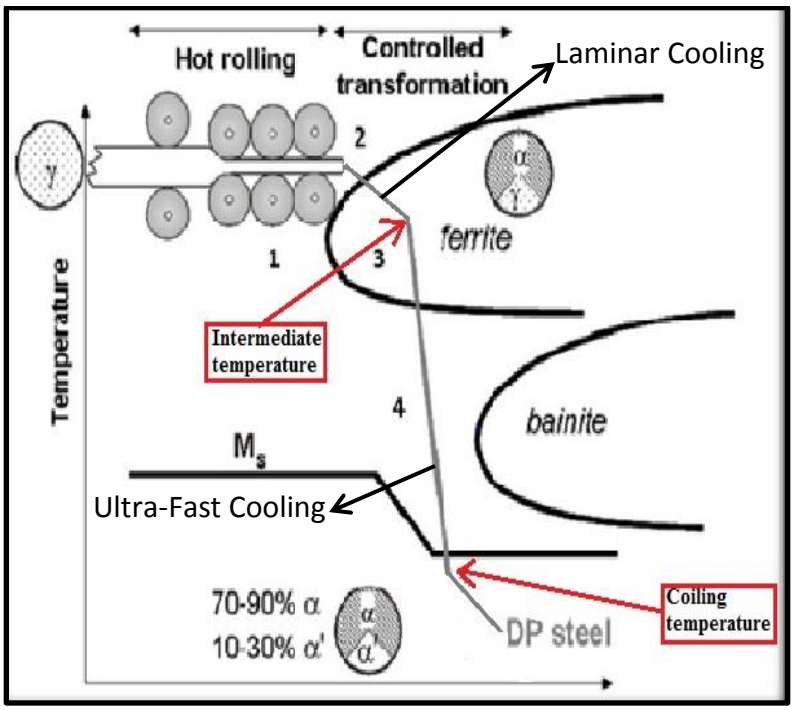


Figure 1.2: Schematic of processing scheme for hot rolled dual phase steel. [Homberg *et al*., 2011]

Depending upon the final microstructure of dual-phase steel, the UFC technique has been defined in two ways: (1) early UFC and (2) late UFC. In the early UFC technique, laminar cooling follows UFC, but the strategy is reverse in the case of late UFC. Late UFC is generally achieved by a water spray and air-assisted spray cooling process, and early ultra-fast cooling is studied by air-assisted spray only. In both types of UFC technologies, the cooling rate increases from 30 $^{o}$C/sec to 80 $^{o}$C/sec, depending on the final thickness [Cai *et al*., 2014]. The heat transfer analysis on the above cooling processes show that air-assisted spray has an excellent control on the rate of cooling [Mohapatra *et al*., 2012].

## 1.6 Etching

Identification and characterization of the type and morphology of phases in metals and alloys is very important. The type of each phase can be predicted from the chemical composition, and history of heat treatment or phase diagrams, but the appropriate qualitative and quantitative method is the experimental method. Optical microscopy, scanning and transmission electron microscopy and X-ray diffraction are usually used for microstructural investigations. Classical etchants such as nital and picral are very popular for microstructural investigation of steels. However, these etchants can only be used for simultaneous investigation of a restricted number of phases. For example, due to the similarity between bainitic and martensitic microstructures, the usual metallographic techniques are not suitable to distinguish between these phases. Electron microscopy is a very good way to distinguish martensite and bainite, but it is expensive and also may not be trustable for small regions of the specimen. Therefore, better etchants are required for multi-phase microstructures to distinguish each of microstructural components reliably and to produce a good contrast between the phases. Colour etching is widely used for visualizing different phases in metals and alloys. This method can produce different colours for different phases. Colour metallography is the best way to recognize phases such as martensite and bainite and can be used for image analyzing and determining the volume fraction of each phase. Many solutions are prepared based on thiosulfate and metablsulfite salts. These solutions produce chemical thin films on the surface of specimens that appear in different colours under polarized light [Zakerinia *et al.,* 2009]. Various type of etchants used have been discussed Table 1.1 [Hairer *et al*., 2010].

Table 1.1: Etchants used for color metallography. [Hairer *et al*., 2010]

| Etchant | Composition | Etching Principle |
|---|---|---|
| Nital | 100 ml ethanol (99%), 10 ml nitric acid (65%) | Grain boundary etching |
| LePera | 50 ml $Na_2S_2O_5$ (1% in aqueous dilution), 50 ml picric acid (4% in ethanol) | Anodic surface layer etching |
| Beraha I | 1 g potassicsulphite, 100 ml parent dilution Beraha I (1000 ml distilled water), 200 ml hydrochloric acid (32%), 24 g ammonium hydrogendifluoride | Anodic surface layer etching |
| Kalling I | 33 ml distilled water, 33 ml ethanol (99%), 33 ml hydrochloric acid (32%), 1.5 g copper(II)-chloride | Cathodic surface layer etching |
| Nital + $Na_2S_2O_5$ | Pre-etching with Nital, wet etching with $Na_2S_2O_5$ (10% in aqueous dilution) | Grain boundary and anodic surface layer etching |

## 1.7 Current Trends in the Field of Dual Phase Steels

Since the introduction of ultrafast cooling (UFC) technology, DP steels have been mostly produced using the combination of laminar cooling and ultrafast cooling and this technology also increases the controllability of the microstructure. The first laminar cooling at low cooling rate allows regulating accurately the intermediate temperature. The ultrafast cooling (UFC) regulates the coiling temperature, and consequently the nature of the second phase [Cai *et al*., 2014]. In view of the increasing demands for occupant safety and fuel efficiency, further strengthening of DP steels without a loss in ductility is also required. Grain refinement is a promising tool to achieve this aim. In recent years, a variety of new processing routes have been developed to produce ultrafine grained (UFG) low carbon steels with a ferrite grain size of 1μm and below. It is consistently found that yield strength and tensile strength are increased due to grain refinement [Calcagnotto *et al*., 2010]. Therefore ultrafine grained (UFG) steels with relatively simple chemical compositions have attracted much interest in replacing some conventional high strength alloyed steels. Methods to obtain UFG DP steels can be divided into two categories: (i) advanced thermo mechanical processing (ATMP) routes, which aim at improving conventional processing routes (ii) severe plastic deformation (SPD) techniques. In order to develop new generation steels characterized by friendly environment, low cost and light weight, hot rolled ferrite-bainite/martensite dual phase steels are produced using simple C-Mn-Si chemistry without adding expensive alloys [Tan *et al*., 2012]. Thus, it can be said that still development is going on in DP steels, using lean chemistry and different processing routes to manufacture these steels with enhanced mechanical properties.

## 1.8 Summary of the Chapter

This chapter introduces the concept of advanced high strength steels with emphasis on Dual Phase (DP) steels. The properties and applications of this steel family have been discussed. The concept of ultra-fast cooling and the role of etching have been described. A brief overview of the current developments in the area of DP steels has been discussed. The next chapter will summarize the research done by various authors in the field and will identify the gaps in the existing literature.

# Chapter 2
# Literature Review

## 2.1 General

In this chapter literature by various authors in the field of dual phase (DP) steels has been discussed. The work done by various researchers has been summarized which includes methods of producing dual phase steels, their properties and applications etc. In the last section, gaps in the present literature has been discussed which present the scope of the proposed study.

## 2.2 Literature Summary

**Patel et al. (2001) s**tudied the effects of micro-alloy additions on the properties of multi-phase hot rolled strips. Authors revealed that good toughness could be achieved through grain refinement (the Hall-Petch relationship) and a reduction in the second hard phase micro-constituent. Furthermore, a reduction in the latter also improved the cold formability. Reduction in the sulphur content significantly improved the uniform elongation, and a high uniform elongation equated directly to good cold forming properties. The presence of sulphur caused the formation of manganese-sulphide (MnS) inclusions, which would elongate during the hot rolling process. The presence of a large number of MnS inclusions (as well as alumina particles - $Al_2O_3$) would have caused cracking or splitting, during component forming due to the creation of voids at the particle-matrix interface. To retain the original globular shape of the inclusions, addition of elements such as calcium will be made, which formed sulphides of reduced plasticity at higher temperatures and allowed the globular-type inclusions, which were considerably less prone to nucleated voids, to be maintained in the final product. The relatively low carbon content permitted good ductility and weldability. Manganese acted as solid solution strengtheners whilst also lowered the austenite-ferrite transformation temperature ($Ac_3$). However, the manganese content will be usually restricted as a solid solution element to levels <1.80 wt%. For conventional hot strip rolling, niobium mainly acted as a grain refiner, vanadium mainly as a precipitation hardener and titanium's effect could be considered to lie between the two. Also, niobium had the ability to provide a dual effect in developing high strengths and also improving toughness by forming precipitates. It will be also revealed that incomplete dissolution of the

micro-alloying elements meant that their exclusion to participate in any grain refinement and/or secondary precipitation hardening. Although a reheating temperature of 1200 °C would have suffice for the vast bulk of micro-alloyed grades, a reheating temperature of 1250 °C was commonly applied in modern strip mills, thus guaranteeing an appropriate finish rolling temperature. Temperatures required for complete dissolution of the carbides and carbonitrides of niobium that were formed during the cooling of the cast slab. Minimum temperatures required for complete dissolution were determined by the niobium, carbon and nitrogen content and a higher alloy addition thus required a higher reheating temperature.

**Erdogan and Tekeli (2002)** investigated the effect of martensite particle size on tensile fracture of surface-carburized steel with dual phase core microstructure. Three specimens were made from surface carburized steel coded as A, B and C. Specimen A corresponded to normalizing and then oil quenching from the inter-critical annealing temperature of 731 $^{o}$C (dual phase with coarse martensite particles in the core). Specimen B was oil quenched from 900 $^{o}$C and then oil quenched from the inter-critical annealing temperature of 731 $^{o}$C (dual phase with fine martensite particles in the core). Specimen C was conventionally heat-treated involving directly oil quenching from 900 $^{o}$C (fully martensitic microstructure in the core). Authors observed that Specimen B exhibited higher tensile and yield strength than specimen A because microstructure of specimen B was finer than specimen A. The martensite particles were almost isolated in the ferrite matrix at 25% MVF in specimen B. The greater tensile and yield strength of specimen B was attributed to different particle size and spacing. Also, finely dispersed, hard second phase in a soft matrix offered more effective barriers to motion of dislocations and provides more effective composite strengthening for a fixed MVF. Total elongation of specimen B was superior to that of specimen A. Also, tensile strength and initial work hardening rate of specimen B were higher than in specimen A. The ratio of uniform to total elongation was lower for specimen B. Higher ductility of specimen B comparing to specimen A was explained by higher potential of specimen B for the micro-void nucleation sites. There were a greater number of martensite particles per unit volume and therefore more micro void nucleation sites in specimen B. Specimen C with wholly a martensitic structure at the core and surface region exhibited higher yield strength than both specimens A and B but almost the same tensile strength as specimen B. However, specimen C showed no difference between uniform and total elongation. In the coarse microstructure (Specimen A), a martensite particle aligned along a ferrite grain boundary could

crack easily. Martensite cracking in the fine microstructure (Specimen B) was less frequent and voids were always smaller, relative to specimen A. The fracture surface of specimen B, which had the finer martensite particle size showed ductile dimples. In specimen B cleavage facets were not observed. In specimen A, predominantly cleavage facets were observed. The specimen C with almost fully martensitic structure in the core showed completely cleavage type fracture.

**Cornet and Herman (2003)** invented a method for fabricating a multi-phase hot rolled steel strip comprising of an ultrafast cooling operation after the controlled slow cooling of the strip. In this method an ultrafast cooling operation was carried out (after slow laminar cooling) followed by final slow cooling operation. In the process, at end of the hot strip mills, temperature of the strip was kept equal to or greater than the $Ac_3$ temperature (dependent the composition of the steel). After hot rolling, the strip was subjected to a first slow cooling operation from end of roll temperature to an intermediate temperature (usually lying between 750 $^oC$ to 600 $^oC$). After the first slow cooling operation, ultrafast cooling operation was performed from intermediate temperature to a temperature referred as coiling temperature (lying between 600 $^oC$ to room temperature). Finally, a second slow cooling operation was performed from the coiling temperature to the room temperature. The first step cooling operation was performed at a high temperature under the conditions close to equilibrium conditions so that ferrite could form. The duration of the first step was dependent on the speed of the strip (during the process of hot rolling) and cooling rate was a function of degree of transformation required. The ultrafast cooling operation was performed at such a cooling rate that the product of thickness of the strip (in mm) and the cooling rate was greater than 600 $^oC/s.mm$ e.g. for a 4mm thick strip, the cooling rate must be greater than 150 $^oC/s$. In the course of final (second) slow cooling operation, residual austenite transformed to form the second phase (i.e. bainite or martensite) which was a function of the coiling temperature. For the experimentation work, authors applied the above discussed method for three different steels to obtain different microstructures. The different microstructures were obtained by careful choice and adequate control of intermediate temperature and coiling temperature. Ferrite/Bainite and Ferrite/Martensite microstructures were obtained for different samples of all the three types of steels. However, using conventional methods, multiphase microstructure could not be obtained. Finally, from the results, it was concluded that the method presented by the authors could be used to obtain multiphase microstructure in different steels. Also, it was clear from the results obtained that the

microstructure in steels not only depend upon the chemical composition but also on the application of combination of laminar and ultrafast cooling operations.

**Mohrbacher (2005)** discussed the microstructural optimization for multiphase steels with improved formability and damage resistance. The author revealed that multiphase steels typically available in the tensile strength range of 450 to 980 MPa were widely used in today's car body manufacturing. Their characteristics of high n-value and good elongation were connected with good press formability. However, practical experience has shown unexpected failure in forming operations where tight bending, stretch flanging or hole expansion were predominant due to the hardness difference between phases. The inhomogeneous microstructure of soft ferrite and hard phase constituents in combination with local straining was inherent to these problems. However this forming behaviour could be much improved by microstructural refinement and homogenization of the phases as well as modification of hardness contrasts. Although this effect was principally unavoidable, measures were taken to reduce the criticality of this phenomenon. Microstructural refinement in combination with homogenization of the individual phases was the key approach in this respect. A small addition of Nb and optimized hot–rolling were most effective in achieving such optimized microstructure. This was reflected in a clearly improved hole expansion ratio and bending angle. Grain refinement also led to better elongation and n-value. The author also explained low-carbon DP steel offer improved weldability and improved hole expansion ratio. The author concluded that the combination of microstructural refinement and reduced carbon content provided the best spectrum of application properties for dual phase steel.

**Adamczyk and Grajcar (2006)** investigated the effect of heat treatment conditions on the structure and mechanical properties of Dual Phase (DP) type steel. For the experimentation, steel of composition (C:0.09; Mn:1.5; Si:0.26; Ni:0.07; P:0.014; S:0.009; B:0.003; Al:0.029; N:0.012: Fe: balance; all in wt % ) was melted and continuous casting of 100x100mm slabs was done. After solidification the slabs were hot-rolled and forged in order to obtain the rods with a section of 24x24 mm. The heat treatment of the specimens was realized according to three routes. In the routes I and II, the steel was heated to a temperature of 910 °C ($\alpha + \gamma$ region), held at that temperature for 30min. In route I, specimen was air cooled to room temp then again heated to 750 $^{o}$C and water quenched. In route II specimen was water quenched from both temperatures viz: 910 $^{o}$C and 750 $^{o}$C. The route III consisted austenizing of steel at a temperature of 910 °C

and air cooling for 45 s to a temperature of 750 °C in order to realize the partial γ to α transformation, followed by water quenching. Route I led to formation of the ferrite structure with an irregular envelope of martensite on grain boundaries. In route II, heating the steel to an under hardening temperature, the nucleation of austenite mainly occurred on the boundaries and martensite laths were formed after primary quenching from a temperature of 910°C. The predominated martensite fraction occurred mainly as thin fibres located in surroundings of grain boundaries. Moreover, in surroundings of martensite, especially at boundary zone large grains of the alpha phase, small grains of the recrystallized ferrite could be identified. In route III, martensite was located on grain boundaries of the alpha phase. The optimum fraction of martensite averaging 20% occurred after air cooling of the specimens for 45 s. The used conditions of heat treatment led in obtaining the DP-type steels of comparable fractions of ferrite and martensite. The optimum fraction of martensite was from 21% to 24%, and the grain size of α phase was in the range 7–10 μm. The diversified morphology of martensite had influence on various mechanical properties of the steel and its deformability. The optimum strength and ductile properties were achieved by route II. The yield point of this steel was about 520 MPa, tensile strength about 800 MPa, total elongation 20%, and uniform elongation about 16%.

**Bhattacharya (2006)** reviewed various developments in the area of Advanced High Strength Steels (AHSS) which included Dual Phase steels, Multi Phase steels, Transformation Induced Plasticity (TRIP) steels and Martensitic (MART) steels. The author discussed that AHSS are replacing the conventional steels (used to manufacture structural parts) to increase fuel efficiency and safety performance. Among AHSS, the authors reported that dual phase steels provide an excellent combination of strength and ductility. All the dual phase steels developed have been based on annealing in the two-phase (inter-critical) temperature region and the consequent increase in carbon content in austenite. Higher the carbon content in austenite after inter-critical annealing results in a significant shift of $M_s$ to a lower temperature. Direct quenching from inter-critical temperature range allowed achieving very high strength of steels without expensive alloying. Multiphase steels, also referred to as complex phase steels are steels with a higher level of yield strength at the same comparable tensile strength levels of dual phase steels. The only way to gain yield strength in multiphase structure was to obtain appropriate mixture of pearlite, bainite as well as ferrite straightened by grain refinement and precipitation strengthening. TRIP steels, based on the Transformation Induced Plasticity effect, offer the highest combination of

strength and elongation, which is a measure of high level of energy absorption. In addition, they also show high bake hardening compared to dual phase steels. The relatively slow initial cooling and rapid cooling down to the temperature of isothermal holding results in further enrichment of the remaining austenite by carbon and enhancing its stability. Further growth in its stability occurred during the austenite to bainite transformation in the presence of strong ferrite forming elements. This significantly retards the carbide formation part of the bainite reaction and helps to keep all carbon in the remaining austenite. Using water quenching in a continuous annealing line, steels with 100% martensite were produced. These steels offered very high strength although ductility was lower than other AHSS steels. The strength of the steel was controlled by the carbon content and a complete austenizing temperature was used to obtain a fully martensitic structure.

**Ahmad et al. (2007)** studied the effect of thermo-mechanical processing on the hardenability and tensile fracture behaviour of dual-phase (DP) steels. Thermo-mechanical processing with various rolling reductions (0-50%) was applied in the intercritical temperature range of 725–830℃ on a low alloy hot rolled steel (0.09 C, 1.2 Mn, 0.78 Cr, 0.26 Si, 0.15 Ni, 0.2 Cu, 0.04 Mo and balance Fe, % wt) followed by quenching in the iced brine solution Metallographic examination of the as-received steel showed a microstructure comprising of ferrite and pearlite phases. Samples were inter-critically heat treated in an argon atmosphere in the range 725–830 ℃ for 20 min and then quenched in brine solution. Due to very fast cooling rate, the austenite phase almost fully transformed to martensite. Point counting method was used to determine the volume fraction of austenite. It was observed that at a temperature of 790 ℃, about 50% of austenite got formed; at this temperature, samples were rolled and cross section reductions in the range 0–50% (0, 20, 30 and 50 % reduction respectively) in lateral and longitudinal direction were achieved. All the specimens were quenched in iced brine solution, offering a cooling rate of about 500 ℃/s After grinding and polishing, specimens were etched with 5% picral followed by 2% nital solution and then immersed in a boiling alkaline chromate solution (8g $CrO_3$ + 40 g NaOH + 72 ml $H_2O$). It was observed that with rolling at a temperature of 790 ℃, for 0 to 50% thickness reduction, about 6% of ferrite increased in rolled specimens even after quenching but not in the un-rolled condition which reflected that rolling in the intercritical region decreased the hardenability. The increase in the rolling reduction resulted in more strain and martensite particles became more fibrous. In longitudinal direction, the

martensite fibres were lengthened and got reduced in thickness by rolling. In the transverse direction, they did not lengthen but thinned in the direction normal to the rolling plane. Thus, the aspect ratio of the martensite fibres was more in the longitudinal than in the transverse direction, and this affected the tensile properties to a great extent. For 30% reduction, maximum true stress in longitudinal and transverse direction were 1023 MPa and 902 MPa respectively; similarly for 50%, values were 1021 MPa and 939 MPa respectively. The UTS almost remained equal in both directions. Total elongation was also significantly affected for 50% rolling in transverse and longitudinal directions with total elongation of 12% and 18% respectively. Hot rolling in the intercritical region increased the strength of the steel without an appreciable loss in ductility. Rolling also increased the aspect ratio of the martensite more in the longitudinal direction than in the transverse directions, which developed the tensile properties.

**Kuziak et al. (2008)** presented some basic concepts of Advanced High Strength Steels (AHSS) for use in the automobile industry, which included their chemical composition design, microstructure analysis, and mechanical properties development during thermo-mechanical processing, production technology characterization, potential applications and performance in service. The authors reported that AHSS was characterized by improved formability and crash worthiness compared to the conventional steel grades. The category of AHSS covert the following generic types: dual phase (DP), transformation induced plasticity (TRIP), complex phase (CP) and martensitic steels (MART). As opposed to the conventional high strength steels in which ductility decreased with strength, modern AHSS steels combined high strength and formability/ductility. Microstructure of dual phase steels was composed of soft ferrite matrix and 10–40% of hard martensite or martensite-austenite (M–A) particles which allowed achieving the ultimate tensile strength in the range of 500–1200 MPa. The strength of the DP steel was controlled by the amount of martensite and ductility by the size and distribution of this phase. DP steels possess low YS/UTS ratio (around 0.5) and high strain hardening characteristics (high n value). Transformation-induced plasticity (TRIP) steels were based on the principle that the strain or stress induced transformation of retained austenite present in the microstructure in a sufficient amount could substantially harden the steel during deformation. The mechanical properties of TRIP steels were derived from their dispersed multi-phase microstructure which composed of ferrite (0.50–0.55), bainite (0.30–0.35), retained austenite (0.07–0.15), and possibly martensite (0.01–0.05). To obtain the best mechanical properties in a product, carbon should be

distributed to austenite and should enrich this phase as much as possible to preserve the $M_s$ below the room temperature (generally 15−25$^{o}$C below room temperature). Complex phase (CP) steels belong to a group of steels with very high ultimate tensile strength of 800 MPa or even greater. The chemical composition of CP steels contained some quantities of Nb, Ti and or V to cause the precipitation strengthening effect. CP steels have no retained austenite in the microstructure, but contained more hard phases like martensite and bainite. Their mechanical properties were characterized by continuous yielding and high uniform elongation. Martensitic (MART) steels provide the highest ultimate strength in final products, up to 1500 MPa. Microstructure of martensitic steels is mainly composed of lath martensite, which was developed by the transformation of austenite during quenching after hot rolling or annealing. AHSS were produced in complex processes involving thermo-mechanical processing followed controlled cooling. For producing DP steels, the cooling process after rolling started with slow cooling stage (on the run out table) after rolling in which the desirable amount of ferrite was obtained as a result of the austenite transformation. The ferrite transformation allowed the carbon content enrichment in the remaining austenite, which increased its hardenability and reduced $M_s$ temperature. The optimal combination of strength and ductility of TRIP steels was achieved by grain refinement and obtaining a uniform distribution of fine second phase particles. The cooling stage in the strip rolling process of TRIP steels was more complicated than that for DP strips. After producing 50–60% of ferrite in the microstructure, accelerated cooling with cooling rate greater than 20 °C/s to the coiling temperature which lied in the bainitic transformation temperature range, was realized. During coil cooling, bainitic transformation preceded further increase the carbon content in remaining austenite to around 1.2%. A part of this austenite, in the amount of 10–15%, remained untransformed accounting for the TRIP effect. The concept of CP steels was essentially similar to those of TRIP steels, however less stringent cooling practice was imposed on the hot band during the last stage of processing as no presence of retained austenite is required in their microstructure. Martensitic steels were produced by applying rapid quenching from the austenitic phase to produce the laths martensite microstructure. Finally from the discussion it was concluded that a substantial progress has been achieved during the last same years in the development of AHSS.

**Meng et al. (2009)** studied the effect of water quenching process during continuous annealing on the microstructure and tensile properties of low alloy cold rolled dual-phase (DP) steel. The chemical composition of the DP steel (taken in form of 260×100×1.0 $mm^3$ samples) was 0.06 C, 0.20 Si, 1.3 Mn, 0.017 P, 0.006 S, % weight); UTS in the as-received state was 450 MPa; and microstructure contained deformed ferrite matrix (elongated grains of ferrite) with a small quantity of non-laminar pearlite colonies. Annealing of samples was carried out in a continuous annealing simulation furnace with heating and slow cooling rates of $5^oC/s$ and $17^oC/s$, respectively. $Ac_1$ and $Ac_3$ temperatures were determined by differential scanning calorimetry (DSC) as $720^oC$ and $860^oC$ respectively. The cold rolled samples were annealed at different temperatures in the range 500-$700^oC$ with different soaking periods 0 s, 120 s and 180 s followed by direct quenching into water. Samples were prepared through standard metallographic procedure and were characterized by optical and transmission electron microscopy (etched with 4% nital solution; volume fraction estimated using standard point-counting technique). Hardness values were determined using Vicker's hardness tester (300 gf). It was observed that at $500^oC$, the recrystallization volume fraction of ferrite was approximately zero, thus only recovery process took place at $500^oC$ (for all soaking periods of 0–180 s) and this stage generally involves both annihilation of dislocations and their reorganization into lower energy configuration. The deformed ferrite grains began to re-crystallize at $550^oC$. At $600^oC$, the volume fraction of recrystallized ferrite increased sharply upto 74% at 180 s and the UTS sharply decreased with holding time. The annealing of samples at $800^oC$ showed good combination of strength and ductility. Moreover, ultimate tensile strength of some samples reached up to 600 MPa and their ductility was still good to meet the requirements of industrially used DP steels. At $820^oC$, the UTS increased upto 742 MPa and the total elongation got reduced to 13% and the volume fraction of martensite surpassed 40%. The authors reported that for good combination of strength and ductility, DP steel must have specific volume fraction of martensite (10–30%). The UTS and YS increased with increase in quenching temperature while total elongation decreased. The samples just before $Ac_1$ mainly composed of recrystallized ferrite and pearlite, while the samples just after $Ac_1$ composed of soft ferrite and hard martensite. The TEM micrographs and selected area electron diffraction (SAED) of samples subjected to intercritical annealing, after the water quenching processes showed microstructure of all samples to be comprising of ferrite and martensite (with a small amount of retained austenite and bainite). The low alloy composition

also improved the galvanizing and soldering ability. Water quenching could increase the UTS of DP steel upto 1000 MPa. The authors reported some other advantages of this method also which included reduced production cost and improved galvanizing/ soldering ability of DP steels.

**Calcagnotto et al. (2010)** studied the effect of grain refinement on the strength and toughness of dual phase steels. Large strain warm deformation at different temperatures and subsequent inter-critical annealing had been applied to obtain fine grained (2.4 μm) and ultrafine grained (1.2 μm) ferrite/martensite dual-phase (DP) steels. The mechanical properties of the produced steels were tested under tensile and impact conditions and were compared to a hot deformed coarse grained (12.4 μm) reference material. The chemical composition of the steel used was (in wt. %) 0.17 C, 1.49 Mn, 0.22 Si, 0.033 Al, 0.0033 N, 0.0017 P and 0.0031 S. To obtain the final ferrite/martensite dual-phase microstructure, the specimens were subjected to inter-critical annealing in a salt bath furnace. The temperature was held constant at 730$^{o}$C. The samples were annealed for 3 min in the salt bath; before they were quenched in water to obtain a ferrite/martensite DP structure. The martensite volume fraction and grain size were determined using the scanning electron microscope (SEM). The coarse grained (CG) steel had a grain size of 12.4 μm and contained 31.3% martensite in ferrite matrix. Fine grained (FG) steel had grain size of 2.4 μm and comprised of 30.1% martensite while the ultrafine grained (UFG) steel had grain size of 1.2 μm with 29.8% martensite. Cylindrical tensile test specimens with a diameter of 4 mm and a gauge length of 20mm were machined and tensile tests were conducted at room temperature. Relation between engineering stress and engineering can be seen in Fig. 2.1. Impact tests were also carried out in the temperature range of -40 $^{o}$C to 200 $^{o}$C. Results showed that with decrease in the grain size, ultimate tensile strength and yield strength increased remarkably while uniform elongation and total elongation were affected marginally. The ductile to brittle transition temperature (DBTT) was decreased from 127 $^{o}$C to 100 $^{o}$C for fine grained steels and for ultrafine grained steels it was decreased to 94$^{o}$C which showed the improvement in the impact toughness. The formation of the cracks and cleavage fracture was also suppressed in the fine grained and ultrafine grained steels. Therefore, it was concluded that the grain refinement affected the properties of dual phase steels and ultrafine grained dual phase steels provided better properties as compared to fine grained and coarse grained dual phase steels.

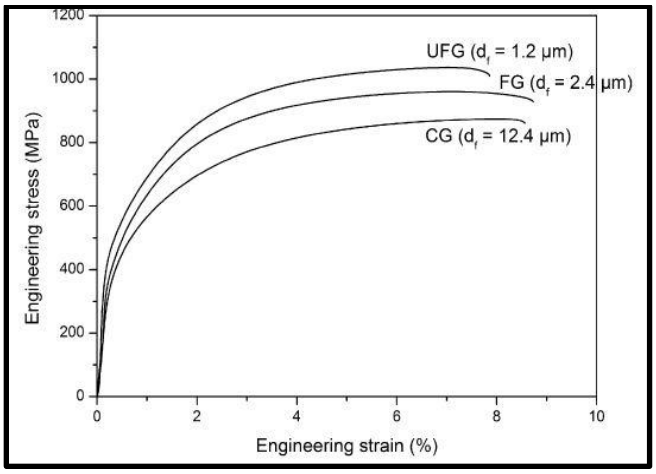


Figure 2.1: Relation of Engineering stress and Engineering Strain for Coarse Grain (CG) Fine Grain (FG) and Ultra-Fine Grain (UFG). [Calcagnotto *et al*., 2010]

**Hairer et al. (2010)** studied the various etching techniques for microstructural characterization of complex phase steels by light microscopy. The authors used different etching techniques to characterize the microstructure of complex-phase steel grade CP600 by light microscopy. Industrial complex phase (CP600) steel (0.10 C, 0.14 Si, 1.51 Mn, 0.80 Cr, 0.009 P, 0.004 Mo, % weight) with yield strength of 476 MPa, and ultimate tensile stress of 635 MPa was taken. The specimens were cut and embedded in epoxy resin, ground and polished. Specific area was marked with a diamond pyramid mount in a microscope and then the specimens were etched and the marked area was analyzed. After each analysis, the specimen was gently polished and etched with a different etchant again. By using this technique, it was possible to compare the same microstructure using different etchants. Light (optical) microscopy (LOM) was used to analyze the microstructure, images were taken at a magnification of 1500X and linear intercept method was applied for quantitative description of the microstructure of the investigated steel grade. The volume fraction of retained austenite was determined via magnetic-volumetric measurements. Micro-hardness (indentation load of 19.6133 mN, penetration speed of 1.96 mN/sec and dwell time of 15 s) were also conducted on the grains of ferrite and bainite/tempered martensite (TM). It was found that when specimens were etched with LePera (50 ml $Na_2S_2O_5$ 1% in aqueous dilution, 50 ml picric acid 4% in ethanol), ferrite formed a light brown, martensite formed a white, tempered martensite formed a brown structure, bainite formed a dark structured surface layer and pearlite formed a dark surface layer. This etchant enabled to distinguish ferrite from martensite but it did not allow the distinct identification of tempered martensite, bainite and

retained austenite. Consecutive etchings were applied with Beraha I (1 g potassic sulphite, 100 ml parent dilution Beraha I (1000 ml distilled water, 200 ml hydrochloric acid 32%, 24 g ammonium hydrogendifluoride), Kalling I (33 ml distilled water, 33 ml ethanol 99%, 33 ml hydrochloric acid 32%, 1,5 g copper(II)-chloride) and Nital + $Na_2S_2O_5$. All three etchings colored the ferrite phase as white and martensite as black or dark brown. Beraha I in addition colored the bainite and tempered martensite as light brown. By a combination of Nital and $Na_2S_2O_5$, tempered martensite and bainite both appeared brown structured and pearlite became black. Nital + $Na_2S_2O_5$ etching provided a high contrast of grain boundaries because of the combination of grain boundary etching with anodic surface layer etching. The content of retained austenite was determined magnetically. The micro-hardness measurements showed that the bainite/TM was approximately three times harder than ferrite; the hardness difference between bainite/TM and the ferrite grains is caused by grain boundary effects. Because of the small grain size, the indentation was very close to the grain boundaries and the measurement detected the hardening effect of the grain boundaries. A measurement with even a lower load (ultra-micro-hardness) could remedy the grain boundary effects. The results also showed that the hardness of ferrite grains and the mean hardness longitudinal and transverse to the rolling direction were nearly the same.

**Sodjit and Uthaisangsuk (2011)** studied the high strength dual phase steels and flow curve modelling approach and compared the mechanical properties of the DP steels experimentally as well as by modelling approach. Low carbon steels grade JIS G3101 SS400 (0.112 C, 0.018 Si, 0.013 S, 0.015 P, 0.519 Mn, 0.065 Ni, 0.044 Cu and balance Fe %wt.) and JIS G3106 SM 490 (0.173 C, 0.0235 Si, 0.010 S, 0.016 P, 0.809 Mn, 0.009 Ni, 0.025 Cu and balance Fe %wt.) called as S1 and S2 respectively. Steel strips with a thickness of 100 × 300 × 2.6 $mm^3$ were cut followed by cold rolling to have a final thickness of 1 mm. Tensile test was performed on the specimens parallel to the rolling direction. Heat treatment was carried out at different intercritical annealing temperatures (IAT) to obtain different martensitic phase fraction followed by water quenching. Mechanical properties of the investigated DP steels are shown in Table 2.1. After tensile test samples were prepared for metallography. The macroscopic mechanical properties can be interpreted by taking average over the microstructure volume element known as Representative Volume Element (RVE). RVE exhibits both phase composition and microstructural arrangement.

Table 2.1: Mechanical properties of the investigated DP steels. [Sodjit and Uthaisangsuk 2011]

| Material | IAT (°C) | Volume Fraction (%) | UTS (MPa) | Uniform Elongation (%) |
|---|---|---|---|---|
| S1 | 735 | 10 | 528 | 21.5 |
| | 750 | 20 | 601 | 22.6 |
| | 785 | 30 | 657 | 21.9 |
| | 800 | 40 | 708 | 20.8 |
| S2 | 750 | 30 | 794 | 18 |
| | 770 | 40 | 925 | 16 |
| | 790 | 50 | 1174 | 15.7 |

2D RVE simulation was carried out, for which precise model and material properties were prepared, a micrograph of real microstructure was converted to a 2D FEM model. Simulations for overall stress-strain curves were determined for different DP microstructures and the results were compared with experimental stress-strain curves. The comparisons were shown in Fig. 2.2 for the DP steel S1 and S2 containing different martensite contents, respectively.

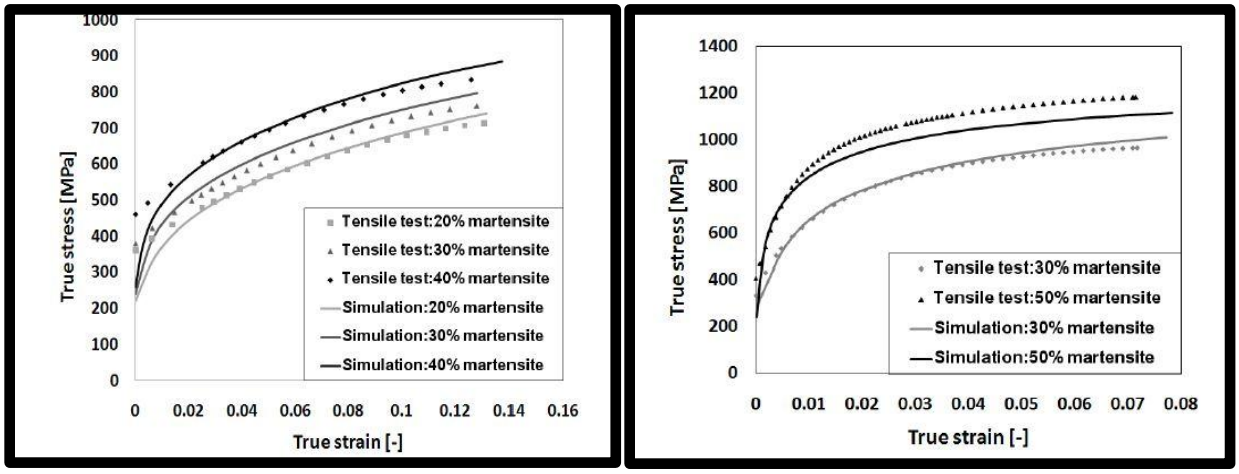


Figure 2.2: Comparison between experimental and numerical flow curves for the DP steel (a) S1 with 20, 30, and 40% MPF, and (b) S2 with 30 and 50% MPF. [Sodjit and Uthaisangsuk 2011]

Modeled flow curves for ferrite in DP steel S1 and S2 with different MPF values were depicted in Fig.2.3. Finer ferritic grains were observed with higher martensite fraction. They exhibited higher yield strength and strain hardening. Modeled martensite flow curves for the DP steel S1 and S2 are shown in Fig. 2.4.

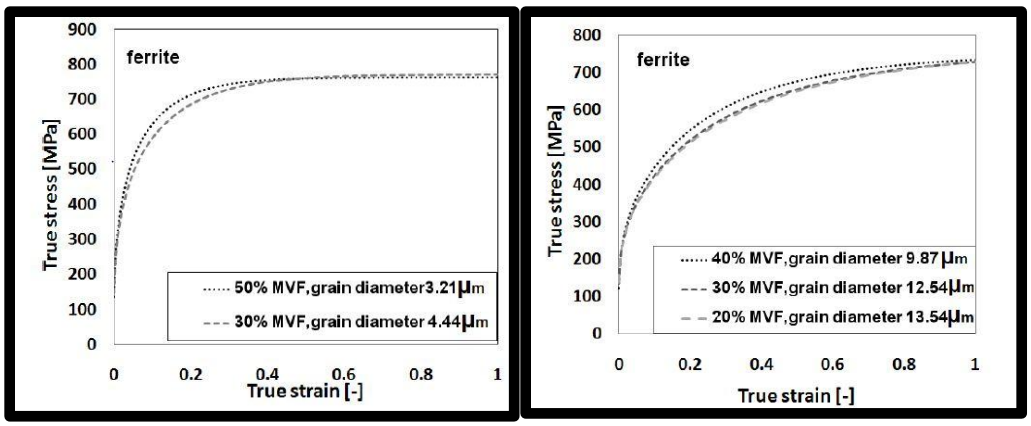


Figure 2.3: Modeled flow curves for ferrite in the DP steel (a) S1, and (b) S2 having different MPF values and ferritic grain sizes. [Sodjit and Uthaisangsuk 2011]

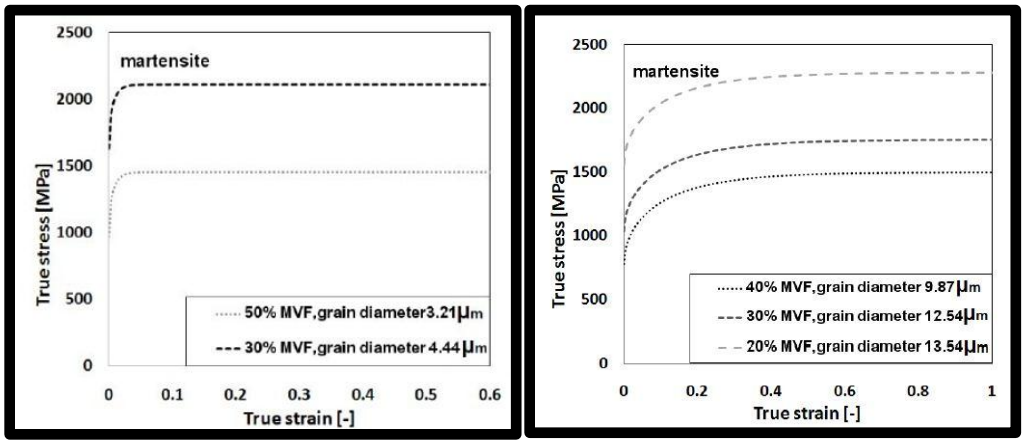


Figure 2.4: Modeled flow curves for martensite in the DP steel (a) S1, and (b) S2 having different MPF values and ferritic grain sizes [Sodjit and Uthaisangsuk 2011]

Martensite presented much higher stresses than the ferrite furthermore, all flow curves showed saturated stress characteristics at small strains. The stress-strain development of martensite clearly indicated its brittle behavior. The martensite in the DP steels S2 are more brittle than in the DP steel S1 therefore the martensite in S1 can sustain more deformation before failure as compared to S2. The results regarding the prediction of stress-strain responses were acceptable. Mechanical properties of DP steel are also influenced by morphology of the dispersed martensitic phase. This modeling approach can be further developed and used for describing deformation and failure behavior of multiphase steels.

**Wang et al. (2011)** presented the experimental results for the development of Ti-micro-alloyed bainite-ferrite multiphase steel with perfect comprehensive properties by Ti-micro-alloying

which had relative lower cost comparing with niobium and vanadium alloying. The experimental steel (C: 0.04–0.06; Si: 0.25–0.45; Mn: 1.4–1.6; Al: 0.02–0.04; Ti: 0.06–0.12; N: 0.003–0.005; Fe: balance; all in wt %age) was firstly melted in a vacuum induction furnace and casted into a 50 kg billet, this was then heated in reheating furnace to 1373 K. After that steel was rolled to a 5.5 mm-thick plate. Rolling finish temperature of plate was 1153-1103 K. Then steel was cooled to finish cooling temperature range of 903-863 K with cooling rate of 13-40 K/s and then quenched to room temperature. Authors revealed that microstructure obtained was composed mainly of lath bainite and some ferrites. Matrix of experimental steel was refined bainite laths, which showed 3–6 mm sheaves with interrupted or film type retained austenite between the laths. There was irregular granular bainite or acicular ferrite between the sheaves. These refined matrix structures had high strength and toughness. In addition, there were different volume fractions of polygonal ferrite distributed at original austenitic grain boundary or in the grain interior. With the increase of cooling rate after rolling (13–40 K/s), volume fraction of ferrite reduced gradually and the ferrite morphology turned from approximately polygonal to acicular which increased strength. In addition to this, Nano-sized cubic shape TiN and approximate spherical TiC precipitates existed in the experimental steel, which provided the strengthening effect by grain refinement, strengthening and precipitation hardening so as to increase the strength and toughness. The increase of cooling speed prevented or delayed the premature precipitation of titanium carbide during cooling, which was ready for formation of more dispersed precipitates, further improving strength and toughness of the steel. Through rational chemical composition design, control over rolling and rapid cooling, making full use of titanium precipitation hardening and grain refinement strengthening, Ti micro-alloyed bainite-ferrite multiphase steel was successfully developed with good comprehensive properties and relatively lower cost. Experimental steel had tensile strength up to 875 MPa, impact energy of 27 J at 253 K, showing a good balance of strength and toughness.

**Matlock et al. (2012)** studied the recent developments in advanced high strength steels (AHSS) and discussed the unique strength and ductility combinations for these steels. The authors argued that the on-going research in AHSS was focused on increasing strength and/or ductility to higher levels than exhibited by the first generation AHSS without significantly enriching the alloy compositions, or is aimed at reducing the alloying levels in second generation AHSS grades. These strategies for making third generation AHSS include: processing to enhance properties of

DP steels; development of high strength steels with ultrafine bainitic microstructures; implementation of new processing routes including quenching and partitioning (Q&P); and development of high Mn content TRIP steels. An increase in strength of Dual Phase steels could be readily obtained by increasing the martensite volume fraction by altering carbon content and/or inter-critical annealing temperature. A strength increase had also been obtained by microstructural refinement resulting from special hot deformation practices, one of which was referred to as Deformation Induced Ferrite Transformation (DIFT). The authors reported a recent work conducted to create ultrafine bainitic microstructures. The microstructure was obtained after a 15 day heat treatment, a time which may be too long for industrial purposes and thus further work had been done on increasing bainite kinetics, reducing heat treatment to hours rather than days by alloying with Al and/or Co. Quenching & Partitioning (Q&P) has been proposed recently as a new way of producing martensitic steels containing enhanced levels of retained austenite. The process consists of a two-step thermal treatment where the steel is quenched to a predetermined temperature (quench temperature, QT) in the $M_s$-$M_f$ range to produce a partially martensitic, partially austenitic microstructure. The second, so-called partitioning step, aimed at carbon enrichment of the austenite by (partial) carbon depletion of the martensite and carbon transport to the austenite. Thus, carbon stabilized austenite was retained in the microstructure after final quenching to room temperature. The addition of molybdenum retarded bainite transformation kinetics and increased the retained austenite volume fraction whereas aluminium substitution for silicon accelerated the bainite reaction and reduced the retained austenite fractions. High retained austenite fractions were believed to result in improved strength and ductility. An alternative process to produce fine grained or ultra-fine grained duplex ferrite-austenite microstructures based on “medium” manganese, low carbon (0.1 wt %) compositions is manganese enrichment of austenite during inter-critical annealing applied to a cold rolled 0.1-C, 7.1-Mn (wt %) steel to produce a range of microstructures with varying austenite fraction and stability. Based on equilibrium thermodynamic predictions, samples of the steel were annealed for 168 hours at temperatures between 575$^{o}$C and 675$^{o}$C. The long annealing times were employed to facilitate Mn partitioning. The resulting microstructures included between 2–43 % retained austenite in a fine grained ferrite matrix (between 0.9 and 1.5μm). It was important to note that alloy designs had been based primarily on low carbon steels due to welding considerations.

**Mohapatra et al. (2012)** investigated the different cooling processes for getting ultra-fast cooling rate for a hot static plain carbon steel plate. Additionally, process controlling parameters for UFC were investigated. Air assisted spray and conventional water spray experiments were conducted on 12 mm thick plate, which was heated in a muffle furnace to 1100$^{o}$C having K-type thermocouple inserted within the plate. After thermocouples were inserted, the strips were put inside the Muffle furnace. The thermocouple extensions were connected to the data acquisition system (DAS). After attaining the desired temperature in the muffle furnace, the pump (CP) and compressor (C) were switched on to make the spray system ready. The hot steel plate was brought out from the muffle furnace and put on the resting pad (RP); simultaneously, the temperature was recorded continuously in real time and saved in a file for further analysis. The flow rate of water was controlled by valves. The flow rate of air and water were set at a particular value by rotameters. The air pressure was controlled by valve (V1) and monitored by pressure gauge (G1). The data collected was analyzed for the heat flux was studied. From the experimental investigation, it was found that atomized spray could produce UFC cooling rates for both the early and late varieties for a hot steel plate. The maximum rate obtained by early UFC was 134$^{o}$C/sec, whereas that of late UFC was 155$^{o}$C/sec for 12mm thick plate. In addition to the above, the effect of water impingement density, air pressure and plate thickness on rate of cooling were also investigated. It was revealed that, on increasing the water impingement density, the cooling rate increased; also, on increasing air pressure, the cooling rate increased. On increasing plate thickness, the cooling rate decreased.

**Yong et al. (2012)** investigated the industrial applications of ultrafast cooling (UFC also known as NG-TMCP) and compared with the conventional thermo mechanical controlled processes (TMCP also ACC-accelerated cooling) for X70 pipeline. The authors revealed that the typical microstructure of X70 pipeline steel consisted of acicular ferrite and quasi polygonal ferrite. Ultra-fast cooling of plates immediately after the last finishing rolling pass led to ferrite grain refinement and finer precipitation of Nb (C, N). The nucleation rate increased with increasing cooling rate, which refined the acicular ferrite. Mechanical properties were improved by finer gain size and refined precipitates. It was also important for hot rolled steel to keep enough shape accuracy. The passing rate of shape of 17.2 mm X70 pipeline steel without UFC was only qualified by 10%. Also, severe plate warping occurred when conventional laminar cooling (ACC) was conducted. On the contrary, the passing rate of shape of the same X70 pipeline steel

as described above with UFC was qualified by 95%. It was very difficult to find plate warping phenomena for X70 pipeline steel after UFC. The control accuracy of red back temperature at UFC mode was much higher than that at ACC mode. The temperature uniformity in the longitudinal direction of X70 pipeline steel was improved significantly due to the UFC control systems, and this undoubtedly reduced cutting quantity of head and tail of the plate. The total cutting of head and tail got reduced from 900 mm (ACC) to 600 mm (UFC). Therefore, the UFC control system offered advantages of low cost and good performance, and they were suitable for X70 pipeline steel on production line.

**Li et al. (2013)** studied the effect of heating rate on ferrite recrystallization and austenite formation in a cold-rolled dual phase steel. For the experimental purpose industrially-manufactured cold-rolled dual phase (DP590) steel (0.1 C, 0.4 Si, 1.6 Mn, 0.013 P, 0.006 S, 0.017 Cr and balance Fe % weight) sheets of dimensions 160×15×1 $mm^3$ with the cold-rolled ratio of 70% were taken. For recrystallization and austenite formation, samples were heated to the desired annealing temperatures below 700 ℃ or intercritical temperatures with different heating rates of (5, 50 and 500 ℃/s) with holding time between (0–40 s) followed by water quenching. The microstructure of the specimens was observed using an optical microscope. Scanning electron microscopy (SEM) and transmission electron microscope (TEM) were used for the microstructure characterization. It was found out that ferrite grains and pearlite colonies where aligned in the rolling direction. The carbide phase was fragmented into small particles by cold-rolling, and distributed along the deformed ferrite grain boundary. Under the conventional continuous annealing conditions, ferrite recrystallization completed before sample were heated to the inter-critical temperature range, but at higher heating rates, ferrite recrystallization temperatures were delayed to above $Ac_1$. Austenite nucleation starts at the ferrite–cementite interfaces, first at the carbon containing colonies and later at the recrystallized ferrite grain boundaries. Austenite growth is mainly controlled by the rate of carbon diffusion. At low heating rates of 5 ℃/s, there was sufficient time for recrystallization of ferrite to take place before austenite formation started. The nucleation of austenite started at the ferrite-pearlite interface, and austenite grew until pearlite dissolution was completed. Then the austenite grew into the neighboring ferrite grains. For heating rate of 50 ℃/s, the recrystallization process declined. At 730 ℃, the microstructure consisted of a larger fraction of deformed ferrite grains. Austenite was unable to recrystallize at the moving ferrite grain boundaries, due to which, the number of

austenite nuclei formation at the ferrite grain boundaries decreased hence reducing austenite formation. With further increase in heating rate, the proportion of non-recrystallized ferrite grains increased. For heating rate of 500 ℃/s, the deformed ferrite was almost fully non-recrystallized before austenite formation began. Carbide particles were distributed along deformed ferrite grain boundary thus providing an increased nucleation density compared with the partly recrystallized samples. But after certain time the austenite grew rapidly until it covered almost all the deformed ferrite grain boundaries. Heating rate (5 ℃/s, 50 ℃/s and 500 ℃/s) resulted a variety of microstructures (fully recrystallized to almost totally non-recrystallized structures) for austenite nucleation temperature of 720 ℃. The steel heated at 50 ℃/s produced less volume fractions of austenite than the other two heating rates (5 and 500 ℃/s), as the nucleation of austenite is unfavorable at moving ferrite grain boundaries at low temperature.

**Armaki et al. (2014)** studied the deformation response of ferrite and martensite in a dual-phase (DP) steel (0.15 C, 1.45 Mn, 0.30 Si and balance Fe % wt.) sheet of thickness 2 mm. The steel was continuously annealed in the inter-critical region and was water quenched at 1000 ℃/s. The microstructure consisted of 60 % ferrite and 40 % martensite. Uniaxial tensile test specimens were cut parallel, perpendicular and at 45° to the rolling direction, tensile tests were interrupted to obtain different levels of plastic strain (0.5 %, 5% and 7%) respectively. After processing, nano-indentations were done at a load of 2500 μN. The indentations were then studied under scanning electron microscopy (SEM) and indentations were divided into various groups namely indentation in ferrite far from grain boundaries, ferrite close to martensite/ferrite interface and indentations located inside martensite. SEM of the as-received samples showed ferrite grain size of 4–15 μm enclosed by martensite which was less than 10 μm. TEM showed high dislocation density in ferrite and presence of fine Fe-carbide particles that help in pinning dislocations. Uniaxial tensile test showed that the yielding started at 350 MPa and UTS of 1050 MPa was achieved for a straining of 9.5% and fracture occurred at 15% straining. Indentations of as-received samples close to ferrite/martensite interface had hardness value of 5.8 GPa with indentation depth of approximately 80 nm. Indentations in ferrite far from grain boundaries were 120–130 nm deep with hardness values of 3.5 GPa. Indentations in martensite showed hardness value of 3–10 GPa for as-received and from 3–13 GPa for straining of 5% with indentation depth of 50–100 nm. For a pre-straining of 7 % indentations close to ferrite/martensite interface showed a hardness of 1.2–3.1 GPa while indentations in ferrite far from grain boundaries was 4.1

GPa. Thus, for 7 % pre-strain regions close to the ferrite/martensite interfaces are softer than the interior ferrite. Initially the ferrite close to the grain boundaries is harder but after a pre-straining of 7 % the ferrite close to grain boundaries softens and ferrite away from grain boundaries becomes hard.

**Cai et al. (2014)** studied the process design and evaluated the mechanical properties of dual phase (DP) steels with pre-positional ultra-fast cooling. The authors investigated the three-stage cooling process for DP steels with pre-positional ultra-fast cooling (UFC) equipment, which was different from the normal DP production line. DP steel strips (0.085 C, 0.62 Si, 0.92 Mn, 0.013 P, 0.008 S, 0.39 Cr, 0.08 Cu, 0.02 Nb, 0.02 Ti and balance Fe % weight) of dimensions 110×83×70 $mm^3$ were taken. Trials were conducted under both laboratory as well as industrial conditions. Laboratory samples were hot rolled on a two-high hot mill with provision for pre-positional UFC and laminar cooling. The mill was equipped with multi-functional cooling system (such as laminar cooling, water curtain, ultra-fast cooling, and spray cooling) and could realize a wide range cooling paths and cooling rates. The slab was reduced from 70 mm to 4 mm thickness. The cooling process involved air cooling, UFC, air cooling followed by laminar cooling. The cooling began at a temperature of 1050–1100 $^oC$ intermediate cooling temperature was kept between 740$^oC$–700 $^oC$ with a holding time of 6 s. The cooling rate of UFC was 120 $^oC/s$ and that for laminar cooling was 40 $^oC/s$. The industrial trials were carried out at the same conditions with the exception that the intermediate temperature was kept at 710 $^oC$ with a holding time of 5 s. For analysis purpose, a two-dimensional finite difference method (FEM) was employed to estimate temperature distribution across the cross-section and the CCT diagrams were prepared (for both conditions). The temperature field was simulated for various cross-sections. It was found that a higher cooling rate was achieved at the corners because of which there was more martensite in the final product. The biggest temperature difference across the cross-section was 7 ℃, 14 ℃, 22 ℃ and 45 ℃ for thickness of 2 mm, 3 mm, 4 mm, and 5 mm respectively. It was found that ferrite grain size was related to prior austenite grain size; the grain size distribution across the cross-section was obtained by coupling the temperature distribution and the grain size under different cooling routes. The microstructure varied a little from surface to centre (internal ferrite grain size was 5.2–5.4 μm but at the corner it was 4.5–5.2 μm). The stress–strain plot of each phase (ferrite and martensite respectively) was simulated and plotted. The laboratorial trial results were: 365–375 MPa (YS), 590–640 MPa (TS), and 0.57–0.78 (YR).

The industrial trial results were: 400–476 MPa (YS), 575–670 MPa (TS) and 0.57–0.79 (YR), which was a little better than laboratorial trial. In pre-positional UFC, the austenite transformation was inhibited (and there was suppression of pearlite and bainite formation), and the residual austenite transformed to martensite. The coil box was used for good temperature homogeneity. The finishing temperature was controlled precisely; UFC was mainly used to refine the grains. If the martensite fraction was to be increased then accordingly, the holding time should also be increased to obtain adequate austenite. The DP steels made by prepositional UFC had tensile strength and yield strength in excess of 590 MPa and 400 MPa respectively, the yield ratio was in the range 0.60–0.78 and the elongation was greater than 22%. Also by the combination of temperature field and phase field, the cooling process of DP steels could be simulated, and ferrite grain size and tensile behaviour could be predicted with reasonable accuracy. This simulation method, however, did not take into account precipitation effect of Nb, Ti and their compound.

**Meng et al. (2014)** studied the effect of fast-heating annealing of a cold-rolled dual-phase steel on the mechanical properties. For experiments, an industrial Dual Phase (DP590) steel (Fe, 0.07 C, 1.7 Mn, 0.429 Si, % weight) was taken. The $Ac_1$ and $Ac_3$ temperatures for pearlite-to-austenite transformation were taken as 1023 K and 1193 K. A heating rate of 500 K/s was performed on the specimen of dimension 300×260×1.5 $mm^3$ and was rapidly heated to 1133 K, on the self-designed fast-heating test bench, soaked for 2s and then cooled down to 323 K at a cooling rate of 100 K/s. The same DP590 steel commercially manufactured through continuous inter-critical annealing at a cooling rate of (3 to 5 K/s) was also studied for comparison. Two tensile samples were cut parallel to the rolling direction each for annealing routine and tensile testing. Quantitative phase measurements were conducted using a point counting method. Two typical tensile engineering stress–strain curves were obtained from the DP steel subjected to different annealing routines. Both curves showed clear discontinuous yielding characters of DP steel. It was found that the average yield strength of fast-heating samples increased from 277 MPa to 372 MPa (34.3% higher) and ultimate tensile strength improved from 625 MPa to 666 MPa (6.6% higher) as shown in Fig. 2.5, total elongation was improved from 23.3% to 26.6% (14.1% higher). Cold-rolled DP590 steel contained elongated ferrite grains and pearlite colonies, the average ferrite grain sizes in the fast-heating sample refined remarkably from about 11.2 to

4.3 µm, and the secondary phase changed from coarse lath-like martensite to fine fiber-like martensite.

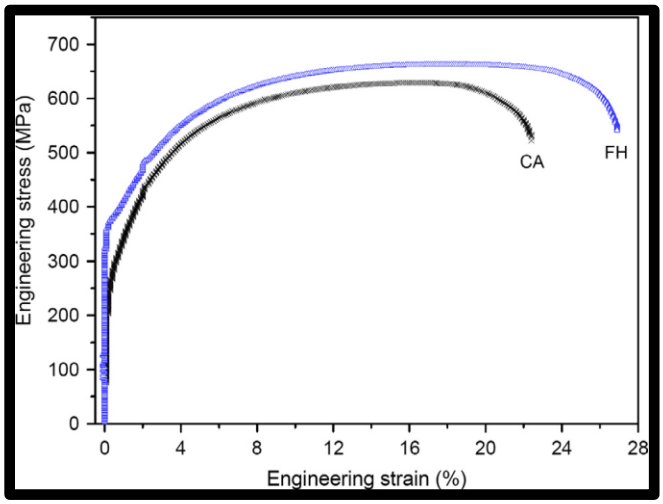


Figure 2.5: Engineering Stress–Strain Curves of DP590 Steel with Different Heating Routines. [Meng *et al.*, 2014]

The improvement of strength was thus related to the ferrite grain refinement. It was also noticed by quantitative measurement that the content of martensite increased slightly from 23 % (volume fraction) to 27 %, which also played a positive role on the strength in the fast-heating samples in addition to the grain refinement effect. In continuous annealing, ferrite matrix and the grain boundary dislocations were free and martensite had a coarse lath like structure. In the fast heating process, there was lesser time spent by steel above the $Ac_1$ temperature (only 3.3 s); so full austenite formation did not take place and a fine fibrous morphology of martensite was obtained. This improved the strength (some bainite may also be formed due to lack of carbon). During the conventional continuous annealing with slow heating rates, the ferrite recrystallization would have fully completed when heated to the inter-critical zone and then the austenite would have nucleated at the recrystallized ferrite grain boundaries and grew along them. However, under the fast-heating conditions, the recrystallization stage was strongly suppressed, during the heating stage; the austenite formation and its distribution were strongly influenced by the overlapping of the processes of recrystallization and austenization. This unique distribution of soft and hard microstructure was correlated with the improved strength and ductility, which implied that the simplified high-efficiency fast-heating process could be a promising alternative over the conventional continuous annealing process.

**Mittal (2014)** studied the effect of inter-critical annealing parameters on the recrystallization, austenite formation and stabilization in a dual phase steel. Experiments were performed on as-received cold rolled low carbon steel (0.08 C, 1.82 Mn, 0.40 Si, 0.042 Al, 0.017 P, 0.005 S, 0.0035 N and balance Fe %wt.). Metallography and SEM of as-received samples revealed presence of pearlite and pro-eutectoid ferrite. The annealing parameters viz. upper critical and lower critical temperatures were calculated using commercial software (JMat-Pro and Thermo-Calc). Thermo-Calc predicted the lower and upper critical temperatures to be 682.2 ℃ and 839.7 ℃ respectively and JMat-Pro predicted the TTT and CCT diagrams. To study the recrystallization kinetics, specimens (15×10×1.6 $mm^3$) were heated to different inter-critical temperature ranges of 700–850 ℃ (with a step size of 25 ℃) with holding time in the range of 30–180 s (with step size of 30 s) followed by air cooling. Activation energy and ferrite recrystallization was determined using JMAK analysis. Metallography and recrystallization study revealed that time period of 0–30 s was the recovery time of the specimens and this time was dependent upon the annealing temperature. TTT diagrams revealed that for temperatures lower than 775 ℃, austenite was not formed in an appreciable amount. However, increasing the holding time to 3 min, austenite volume fraction of 33.19% was observed. It was observed that with increase in annealing temperature, or holding time, or both, the fraction of austenite formed in the steel increased. The appropriate amount of austenite (40–50 %) was obtained at temperatures of 800 ℃ and 825 ℃ with soaking time periods of 5 min and 3 min respectively followed by water quenching. In annealing simulator for (3 min soaking at 825 ℃ followed by quenching with $N_2$+$H_2$), dual-phase microstructure with martensite fraction of 35 % was obtained which was less than that obtained by water quenching (cooling rate provided by water much higher than the gases used). Microstructure of the steel annealed in the simulator consisted of fine martensite phase dispersed in the recrystallized ferrite matrix. While for water quenching, a typical necklace type microstructure, in which martensite was observed on the ferrite grain boundaries was observed. As received specimen had a tensile strength of 810 MPa with elongation of 5.3%. However, the sample annealed under the optimum conditions in the simulator (having 35 % martensite) showed high total elongation of 26.5 % with a moderate ultimate strength of 610 MPa. Thus, by obtaining an appropriate microstructure through the selection of inter-critical annealing parameters, a good combination of strength and ductility was obtained in the given low carbon steel.

**Seyedrezai et al. (2014)** studied the effect of inter-critical annealing treatment on the final microstructure and work hardening behavior of a cold rolled dual phase (DP780) steel (0.09 C, 0.1 Mn, 0.012 P, 0.006 S, 0.02 Si, 0.03 Cu, 0.01 Ni, 0.26 Cr, 0.29 Mo, 0.004 N, 0.001 V, 0 B, 0.001 Ti, 0.002 Nb and balance Fe % wt.). Specimens of dimensions 100 × 20 × 0.95 $mm^3$ were taken. The specimens were cut in direction of rolling as well as in transverse direction. AT (Austempering) and QT (Quenching and Tempering) were performed on the samples. For AT, specimens were heated to a temperature of 920 ℃ for 30 min and then cooled to a temperature of 575 ℃, were soaked here to get bainite. QT was carried out at three different temperatures of 920, 970 and 1020 ℃. IC (inter-critical) annealing was performed on the pre-treated samples i.e. CR, AT and QT over the temperature range of 720–735 ℃ with an interval of 5 ℃. Microstructure characterization was done by using optical microscopy, scanning electron microscopy (SEM) and transmission electron microscopy (TEM). Microstructures of specimen before IC revealed that CR structures were highly deformed consisting of ferrite F, pearlite P and martensite M. AT specimens consisted of upper bainite and all three QT samples showed tempered martensite with uniform distribution; temperature increase only caused increase in austenite grain size. After IC annealing, the CR samples had uniformly distributed M with small size variation, F was fully recrystallized and no deformations were observed. AT samples after IC showed elongated martensite grains distributed along bainite grain boundaries and small amount was distributed along austenite grain boundaries. In QT after IC, large amount of M was present along austenite grain boundaries and a large martensite free region was present in ferrite matrix. Uniaxial tensile test revealed that all specimens had same ultimate tensile strength (UTS) but they varied in terms of yield strength (YS), uniform elongation and work hardening rates. The CR+IC samples showed the lowest YS, highest uniform elongation and highest work hardening rate, while OT+IC samples exhibited highest YS, lowest uniform elongation and lowest work hardening rate. Due to non-homogenous distribution of M in CR+IC samples, YS was low and good uniform elongation was achieved. Also as the M volume fraction increased, work hardening rate decreased, thus CR+IC showed highest and OT+IC showed the lowest work hardening rates.

**Shi et al. (2014)** improved the toughness and ductility of ferrite/acicular ferrite (F/AF) dual-phase steel through intercritical heat treatment. The steel specimens (0.14 C, 0.96 Mn, 0.44 Si, 0.32 Mo, 0.02 Nb, 1.14 Ni, 0.26 Cr, 0.62 Cu, 0.0074 N, 0.006 P, 0.003 S and balance Fe %

weight) 160 × 70 × 20 $mm^3$ were prepared from a steel plate. The samples were heated to 900 ℃ for 30 min and then air cooled (N) at a rate of 3 ℃/s to obtain F/AF dual phase microstructure. Two intercritical treatments were carried out namely step normalizing (SN) and intercritical normalizing (IN) the intercritical temperature of 780 ℃ was selected. For SN the specimens were heated to 900 ℃ for 30 min and then furnace cooled to 780 ℃ followed by a holding time of 50 min and then air cooled. For IN the specimens were heated to 900 ℃ for 30 min and then water quenched followed by reheating to 780 ℃ with holding time of 50 min followed by air cooling. All the specimens N, SN, IN were tempered (T) at 650 ℃ for 120 min NT, SNT, INT. Optical microscope, scanning electron microscopy and transmission electron microscopy were used for microstructure characterization. The N specimen consisted of acicular ferrite with irregular arrangement and a large grain size variation was observed. The SN specimens had large proportion of AF with small amount of polygonal ferrite and IN specimen revealed AF and lath ferrite. The N specimen revealed highest yield strength (YS) and ultimate tensile strength (UTS) followed by IN and SN respectively. IN had highest toughness (214 J) and SN had least toughness of (173 J) as shown in Fig. 2.6.

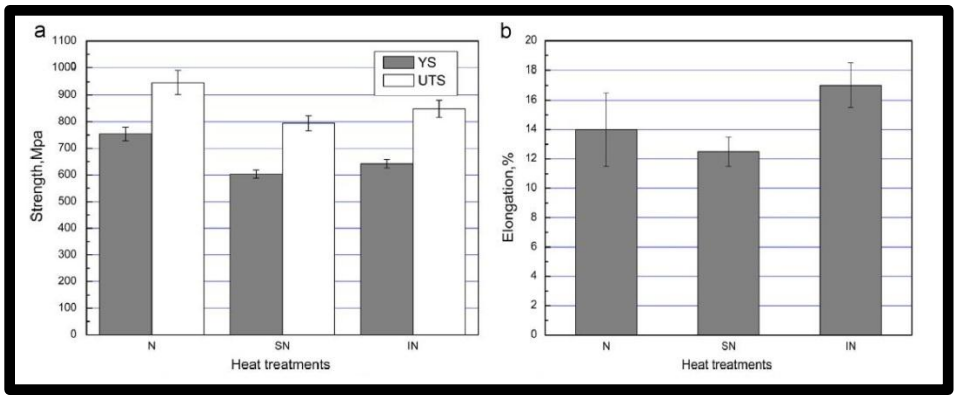


Figure 2.6: The tensile properties of specimens under different heat treatments (a) yield strength and ultimate tensile strength, and (b) elongation. [Shi *et al*., 2014]

After tempering T although N showed the highest hardness but the hardness value of NT, INT and SNT reduced by 19%, 15% and 18% respectively as compared to N, IN and SN specimen. NT specimen showed highest YS and UTS and SNT had the smallest value, however YS and UTS for NT reduced by 26% and 25% respectively and the UTS of INT decreased by 21% as shown in Fig. 2.7.

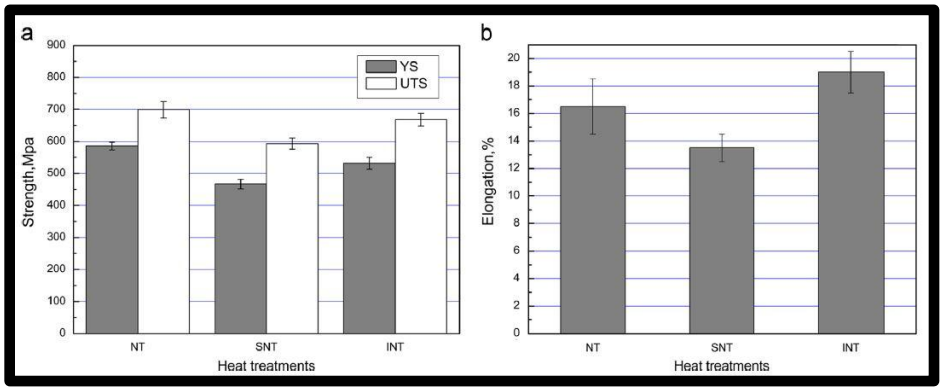


Figure 2.7: The tensile properties of tempered specimens under different heat treatments (a) yield strength and ultimate tensile strength, and (b) elongation. [Shi *et al*., 2014]

Thus IN specimen had greater tempering resistance to strength. Impact toughness of all the specimens increased after tempering. INT had the highest toughness (265 J) 24% higher. NT and SNT had a toughness increase of 19% and 14% respectively. IN treatment had a refined microstructure. IN specimen had lower strength and higher ductility and toughness while SN had the lowest strength, ductility and toughness. After tempering IN specimen had minimum loss in strength and maximum improvement in toughness.

**Mecozzi et al. (2015)** studied a mixed-mode model for the ferrite-to-austenite transformation in a ferrite/ pearlite microstructure. The authors proposed a semi-analytical mixed-mode model to describe the kinetics of ferrite-to-austenite transformation. The initial model of the microstructure was assumed to consist of ferrite matrix with supersaturated austenite grains. The super saturation of carbon grains was a result of the rapid dissolution of pearlite colonies present in the primary microstructure. Different mathematical models viz. semi-analytical, numerical, interface-controlled, and diffusion controlled model were described. It was observed that the diffusion-controlled model proved to be the least accurate for the whole process of transformation. The interface-controlled model predicted the faster austenite growth kinetics compared to numerical model (particularly at high interface mobility). The interface-controlled model overestimated the carbon percentage at the interface. This caused an increase in the deviation with respect to the equilibrium carbon percentage thus, the increasing the driving force of the transformation. At high interface mobility the diffusion-controlled model provided an acceptable description for the ferrite-austenite transformation kinetics while at lower interface mobility it overestimates the austenite growth kinetics. At the early stage of transformation there

is a development of a strong carbon percentage gradient in the austenite grains. Thus, the interface-controlled model leads to the faster transformation kinetics than the numerical model. The numerical solution of the differential equations showed that the semi-analytical mixed-mode model the authors developed gave the most accurate description of ferrite-austenite transformation for the entire process of transformation when compared to other classical models of ferrite-austenite transformation.

## 2.3 Summary of the Literature

- Most of the authors have reported on the formation of DP steels through the route of inter-critical annealing followed by water quenching. There are only a few studies in which the dual phase structure has been obtained from the fully austenitic state, followed by slow cooling and then finally followed by quenching [Adamczyk and Grajcar, 2006; Bhattacharya, 2006; Ahmad, 2007; Kuziak *et al*., 2008; Meng *et al*., 2009; Meng *et al*., 2014].
- Several authors have worked on the first generation DP steels and successfully achieved high strengths as compared to conventional counterparts but could not achieve good ductility. Several authors have worked to overcome this problem and substantially improved the ductility and strength by expensive alloy additions which made them expensive for use. Authors became successful in achieving good strength and ductility but because of alloying, however the weldability suffered. Finally, a few authors have reported their work on third generation DP steels where first generation Dual Phase steels have been modified through grain refinement and new process techniques to improve ductility, strength and toughness. Work has been reported on steels where carbon has been reduced to improve weldability [Patel *et al*., 2001; Erdogan and Tekeli, 2002; Bhattacharya, 2006; Kuziak *et al*., 2008; Wang *et al*., 2011; Matlock *et al*., 2012].
- A few authors have reported their work on making DP steels using NG-TMCP (ultra-fast cooling) process [Mohapatra *et al*., 2012; Yong *et al*., 2012; Cai *et al*., 2014].

## 2.4 Gaps in Literature

- Most of the literature reported on DP steels has focused mainly on *ferrite/martensite* microstructure. Very limited literature is available on dual phase steels with *ferrite/bainite* microstructure.
- Production of dual phase steels with a lean chemistry. There is a scope of work for processing dual phase steels through NG-TMCP route without the use of expensive grain refining elements viz. Ti, Nb, V, Cr etc. The NG-TMCP route offers advantages like fine grain structure, better dispersion of secondary phases etc.
- There is a scope of work to study the effect of carbon diffusion on austenite and to understand the kinetics for formation of carbon rich austenite (i.e. austenite phase obtained by dissolution of only pearlite and avoiding dissolution of pro-eutectoid ferrite present in the as-received steel) to facilitate formation of carbon rich martensite (of better hardness) during processing of dual phase steels (DP steels) for enhanced mechanical performance.
- Very limited literature has been reported on ferrite recrystallization kinetics, formation and stabilization of austenite phase during inter-critical annealing of low carbon steel.

# Chapter 3

# Design of the Study

## 3.1 General

This chapter discusses the detail of overall design of the study which includes objective of the research work, the key issues, methodology, simulations and the experimental procedure followed. The chapter also covers the details of machines, equipment and commercial software used for the experimental work.

## 3.2 Establishing the Objective Function

The main focus of the present work was to study the kinetics of formation and stabilization of austenite. The research work included studying the effect of different heating rates, isothermal temperatures, and holding periods (during isothermal annealing) on the formation of carbon rich austenite obtained through dissolution of pearlite only, in a low carbon steel. The main motive was to understand the kinetics of formation of carbon rich austenite (i.e. austenite obtained through dissolution of pearlite only; avoiding dissolution of pro-eutectoid ferrite present in the as-received steel) to facilitate formation of carbon rich martensite (of better hardness) during processing of dual phase steels (DP steels) for enhanced mechanical performance.

The main motive of the present research was to model the process of dissolution of pearlite (of as-received steel) into austenite to understand the kinetics of this process.

The key issues taken up during the research work are:

1. To investigate the microstructure of as-received hot band and cold rolled low carbon steel using optical microscopy and SEM.
2. To obtain the annealing parameters (annealing temperature, holding time, etc.) for the given alloy chemistry using DICTRA, Thermo-Calc, and JMat-Pro software.
3. To conduct simulations for isothermal annealing process of the given steel to obtain the holding time required for formation of austenite (from pearlite) in the steel as a function of annealing temperature and heating rate. In other words to model the effect of carbon

diffusion on austenite formation at different annealing temperatures and different heating rates (both equilibrium heating rates, as well as various non-equilibrium heating rates).

4. To perform experiments on annealing simulator (for conditions of equilibrium heating rate) and Gleeble 3800 (for conditions of non-equilibrium heating rate) to validate the simulation results.
5. To conduct microstructure characterization of the annealed specimens through optical microscopy, and SEM analysis. Also, to determine the **area** fractions and distributions of ferrite and martensite phases using 'analySIS FIVE Digital Imaging Solutions' software.
6. To perform tensile testing of specimens at a given heating rate and compare the microstructural variations and mechanical properties obtained in the hot rolled and cold rolled steels.

## 3.3 Experimental Procedure

The detail of experimental procedure followed in the present research work is described as follows:

### 3.3.1 Material and Processing

**Starting Material**

The as-received material was of lean chemical composition as shown in Table 3.1. This starting material was received in two forms subjected to two different conditions, viz. hot rolled with a final thickness of 2.8 mm, and cold rolled (57%) with a final thickness of 1.6 mm. A detailed microstructure characterization was carried out by using both optical microscopy and SEM analysis. The main focus of this characterization was to observe the phase fractions, and distribution of phases in the as received material.

Table 3.1: Chemical composition of the as-received steel specimens.

| C | Mn | P | S | Si | Al | N | Fe |
|---|---|---|---|---|---|---|---|
| 0.074 | 1.83 | 0.012 | 0.002 | 0.43 | 0.026 | 0.0032 | Balance |

Microstructure characterization of the as-received steel sheet followed the standard metallographic procedure (cutting, mounting, grinding, polishing and etching with 2% nital solution).

### 3.3.2 Simulations using Commercial Software

The next step was to determine the parameters for isothermal annealing process to be used for simulation of austenite formation. This included determination of intercritical annealing temperatures ($Ac_1$ and $Ac_3$), and holding time periods for various heating rate conditions. For this work, three main software viz. Thermo-Calc, DICTRA, and analySIS software were used. Thermo-Calc software was used to predict the annealing temperatures, and phase fraction details at various temperatures. DICTRA was used to determine the holding time periods (for given annealing temperature and heating rate) for formation of austenite. It was also used to predict the carbon diffusion from $Fe_3C$/ γ interface to γ/ α interface during the annealing process. Finally, 'analySIS FIVE software' was used to study the distribution and fractions of martensite and ferrite phases.

**A. Thermo-Calc**

Thermo-Calc software (*Thermo-Calc 3.0*; developed by *Thermo-Calc Software AB*, Stockholm, Sweden) was used to determine the inter-critical temperatures and phase fraction diagrams. For this purpose, equilibrium phase diagram and phase fraction diagram were plotted for the given alloy chemistry. Equilibrium phase diagram provided information about the inter-critical temperatures ($Ac_1$ and $Ac_3$), while phase fraction diagram provided information about the volume fraction of various phases at a given inter-critical temperature. Figure 3.1 shows the screen shot demonstration (inputs taken by the software) of the working of the software.

**B. DICTRA**

**D**iffusion **C**ontrolled **TRA**nsformations (DICTRA) software (DICTRA: version 27; developed by Thermo-Calc Software AB, Stockholm, Sweden) is a general software package for simulation of single and multicomponent systems. Any number of components may be treated (provided that necessary thermodynamic and kinetic data are available). DICTRA is particularly suitable for treating problems involving one-phase problems, moving boundary problems, diffusion in

multi-phase systems etc. The boundary conditions are given which enable the user to treat problems of practical interest. DICTRA is based on numerical solutions of multi-component diffusion equations in various regions of a material.


Figure 3.1: Screen Shot demonstration of the working of Thermo-Calc software.

In addition there is a post processor that enables the user to plot and list data from a simulation, e.g. concentration profiles, particle size as a function of time etc., and also a database module to handle thermodynamic and kinetic data.

DICTRA is console based software which has a specific syntax that needs to be followed. The steps are as follows:

1. Define the Thermo-Calc database. The database selection is dependent upon the type of alloy and base materials. For the steel of given alloy chemistry, the database TCFE7 (i.e. Thermo-Calc Iron Database, version 7) was used.

2. Define the mobility database. The mobility database provides information about the movement of interfaces and their velocities. For the given low carbon steel, MOBFE2 (i.e. Mobility Database of Iron version 2) database was used.
3. Set the conditions for simulation. The various conditions viz. annealing temperature, holding time periods (if any), required heating rates etc. need to be set.
4. Set-up the system for simulation:
    a. Define the region. Different regions which are present in the steel need to be defined. For the present study, cementite, austenite, and ferrite were defined.
    b. Define the grid points in the region. The grid points are points for which the simulation data is calculated. The grid points in the system can be defined as linear or geometric. For geometric distribution, geometric ratio ($r$) needs to be defined. If $r > 1$ the grid points are more towards lower interface and if $r < 1$, more grid points are towards upper interface. The width of the region also needs to be defined. Figure 3.2 shows a schematic representation of region grid points and width of the region.

       For the present work, linear system was considered.
    c. Define the phases and their nomenclature e.g. for cementite enter CEM; for ferrite enter BCC; and for austenite enter FCC.

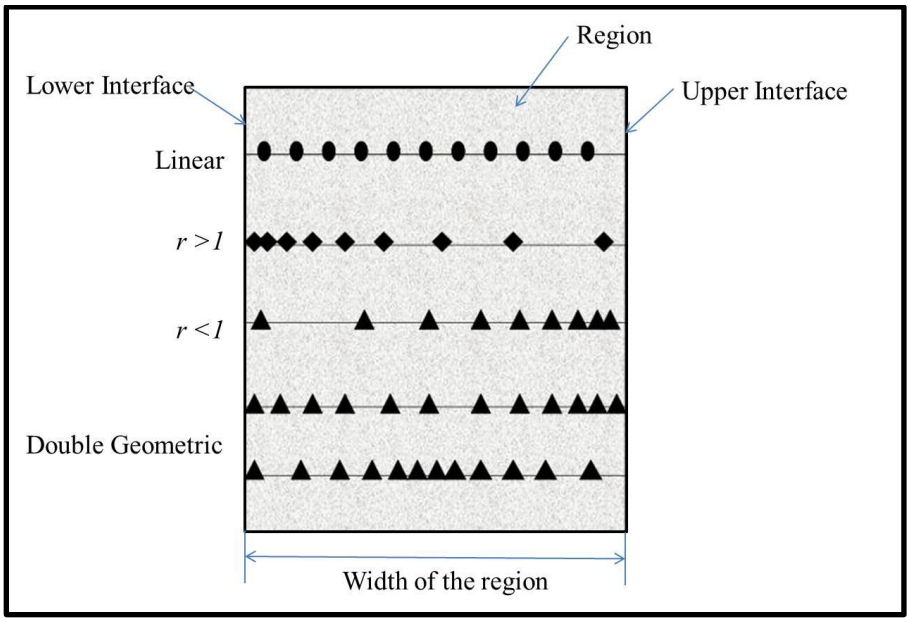


Figure 3.2: Schematic representation of a region, grid points, and width of the region.

5. Simulate for the above conditions for the desired time (any approximate time is considered for which it is anticipated that the simulation will complete). Figure 3.3 demonstrates the screen shots of input steps for simulations on DICTRA software.

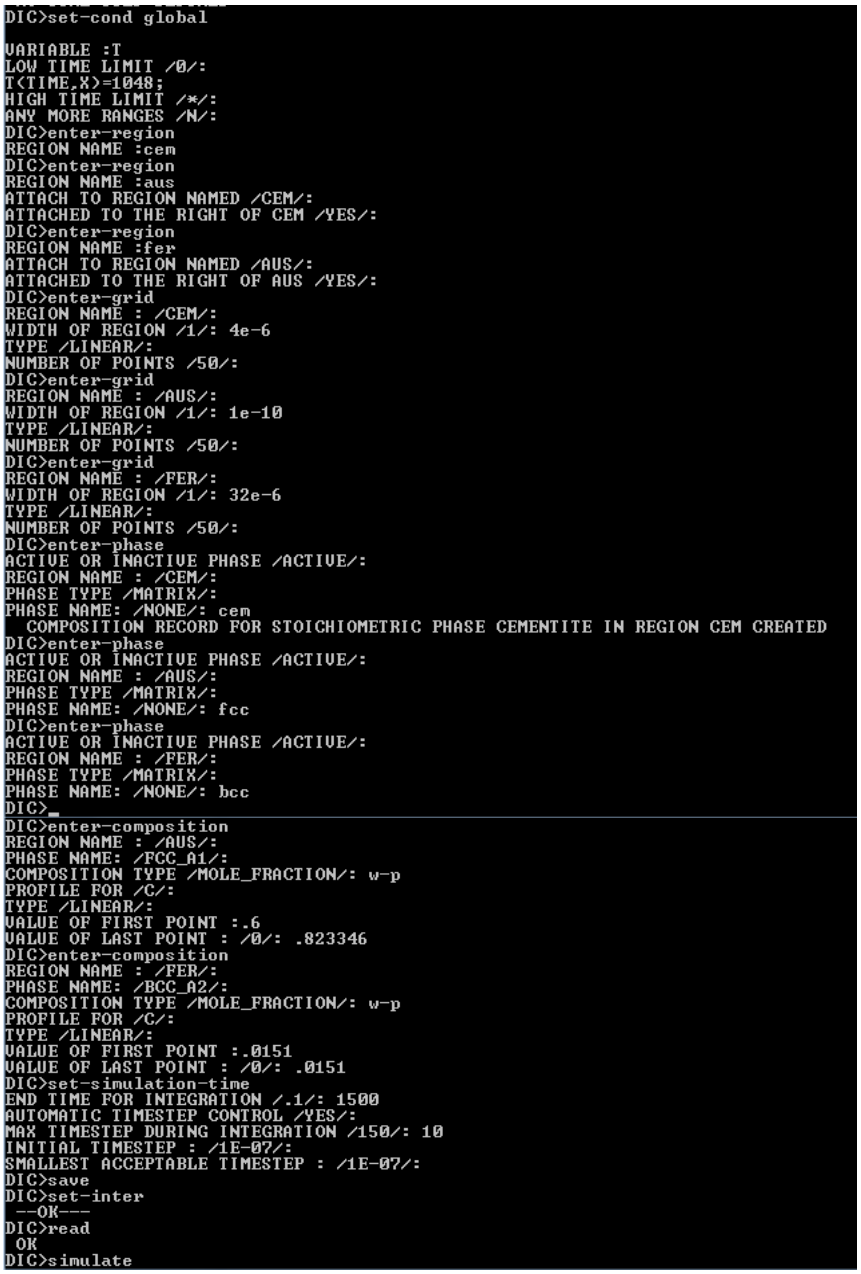


Figure 3.3: Screen Shot demonstration of input steps for the simulations on DICTRA software.

6. Finally, get the results in the output window. For this, a post-processor was used. This post processor is compatible with both Thermo-Calc and DICTRA. The various conditions were set up and the results were plotted. Figure 3.4 demonstrates the result output window for simulations on DICTRA software.

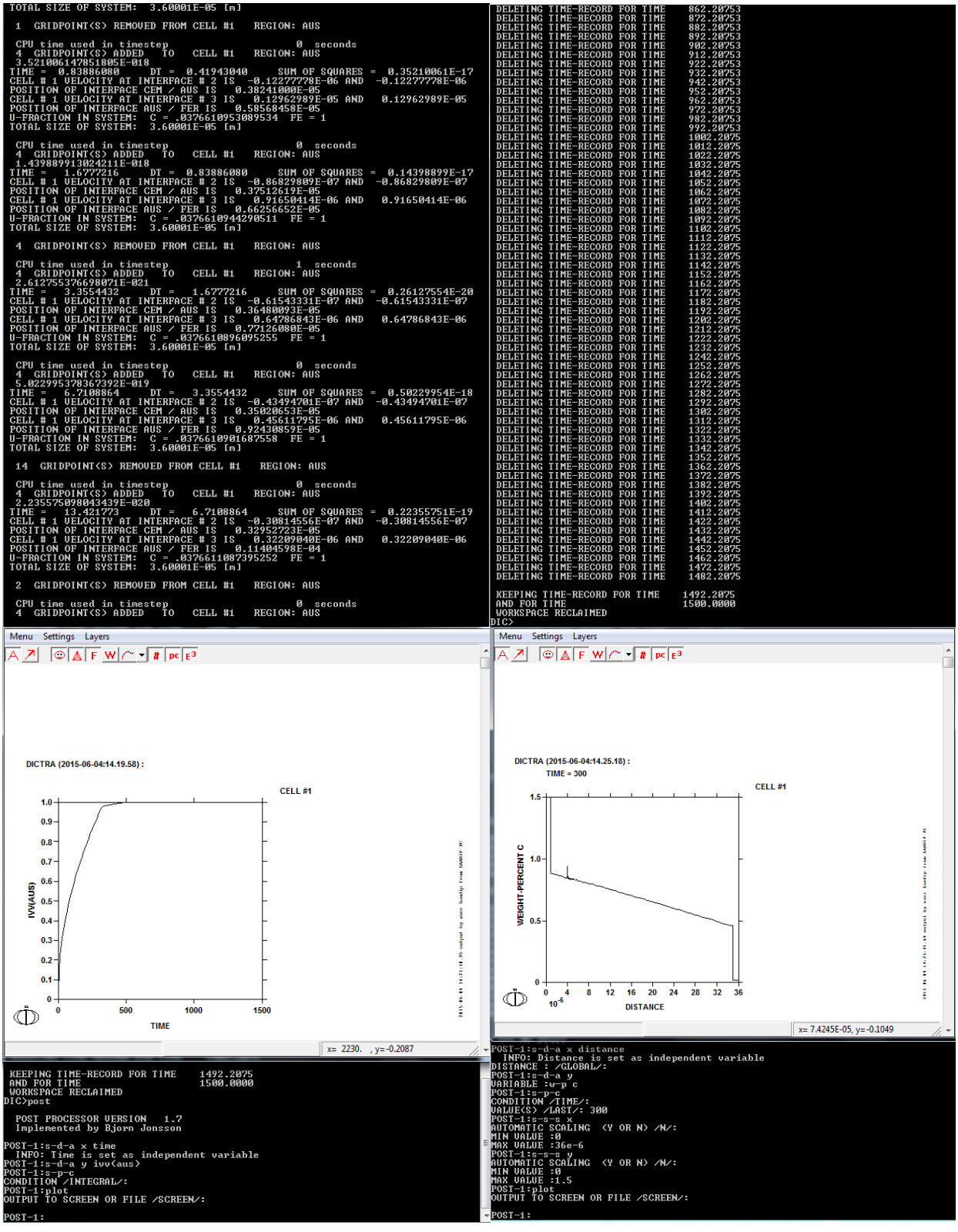


Figure 3.4: Screen shot demonstration for the result output window for simulations on DICTRA.

**C. ‘analySIS FIVE’ Digital Imaging Solutions**

The ‘analySIS FIVE Digital Imaging Solutions’ software (analySIS Five 5.05.07; developed by Olympus Soft Imaging Solutions, Notting Hill, Australia) is a leading software for image analysis and processing. It can analyze area and pixel value statistics of user-defined selections and intensity threshold objects. This software can display, edit, analyze, process, save, and print 8-bit color and gray scale, 16-bit integer and 32-bit floating point images. It can create density histograms and line profile plots and distribution plots for various phases. It supports standard image processing functions such as logical and arithmetical operations between images, contrast manipulation, convolution, Fourier analysis, sharpening, smoothing, edge detection and median filtering. For the present study, analySIS FIVE was used to measure the fraction and distribution of martensite and ferrite phases from the optical micrographs for the various cold and hot rolled steel samples. Figure 3.5 shows the microstructure characterization of a specimen using this software. Different colours in Fig. 3.5 represent the area fraction of martensite phase, each colour representing martensite of a specific grain size.

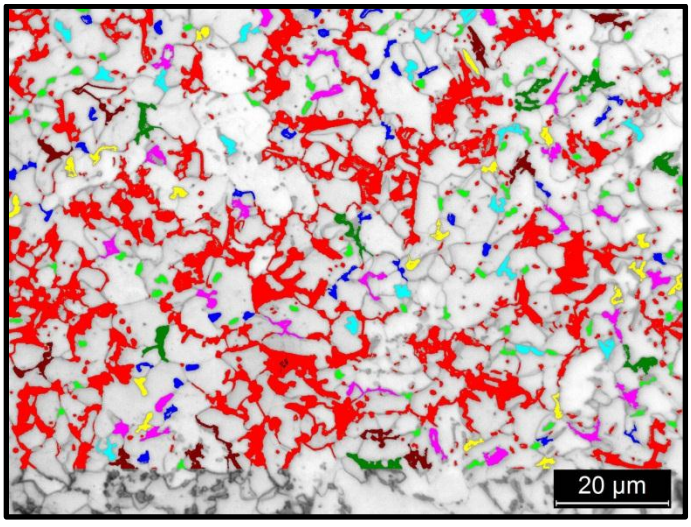


Figure 3.5: Microstructure characterization for phase fractions using analySIS.

### 3.3.3 Study of Austenite Formation

Theoretically, austenite formation can be studied by understanding the phase transformation kinetics of the given low carbon steel. Commercial software viz. DICTRA was used to simulate the time taken for austenite formation at a given annealing temperature. Experimentally, samples

were subjected to different annealing temperature-time combinations as predicted by DICTRA. After heat treatment, the samples were prepared for microstructural investigations. Finally, the simulation results obtained using DICTRA were compared with actual experimental results obtained both for hot rolled and cold rolled steel.

## 3.4 Machines and Equipment

This section describes the brief outline and characteristic features of various machines, equipment used for the present experimental work.

### 3.4.1 Precision Cutter

The precision cutter (Make: Micracut 125, *Metkon Instrumens Inc*., Bursa, Turkey) was used to cut the wide range of materials accurately. The specimen is mounted on aluminium vice. The specimen is placed in a position relative to the cutting wheel using a micrometer screw. The material is cut by lowering the specimen over the cutter using a dead weight mechanism. Figure 3.6 illustrates the precision cutter utilized in the present work.


Figure 3.6: Low speed precision cutter. (Courtesy: NML, Jamshedpur)

### 3.4.2 Annealing Simulator

An indigenously developed annealing simulator is equipment designed and developed jointly by CSIR-NML and Tata Steels, Jamshedpur (see Fig.3.7). In this simulator, the samples to be annealed can be heated in an inert environment ($N_2 + H_2$) and quenched under controlled cooling conditions. The different parts of the simulator are explained as below.

A. **Heating System**

The simulator is employed with a unique high speed heating method which has a capability of running 7–10 times faster than the conventional furnace. Heating rates of up to 100 ℃/min can be achieved. The thermocouples fitted in the chamber help in accurate control of specimen's and chamber's temperatures.

B. **Quenching System**

Quenching of the specimens is achieved by using a gas mixture of hydrogen ($H_2$) and nitrogen ($N_2$) at very high pressures. Quenching rates can be controlled by either changing the percentage of hydrogen gas in the gas mixture or the inlet gas mixture pressure or both.

C. **PLC based Digital Control System**

PLC based Digital Control System is the heart of the system. It provides a versatile control over the annealing simulator. The system can be operated manually or with a combination of computer and manual control. Various operations can be controlled by using the PLC control viz. furnace heating rate, furnace temperature, furnace door opening and closing, cooling rates, etc.

D. **Process Simulation of Annealing Simulator**

Metallurgical simulation requires precise control over the process environment, temperatures, heating rates, and cooling rates.

- **Heating Mode:** Heating is caused by radiation heat transfer. A maximum operating temperature of 1050 ℃ is achievable in the annealing simulator at controlled heating rates are achievable.

- **Process Environment:** A gas mixing system is required to maintain an inert environment to prevent oxidation of specimens and also for the purpose of quenching. A ($H_2$ + $N_2$) gas mixture with 5–30% $H_2$ for adjusting the dew point, which is desired for bright annealing of steels, could be maintained in the annealing simulator. Pure $N_2$ gas medium could also be used in the system.

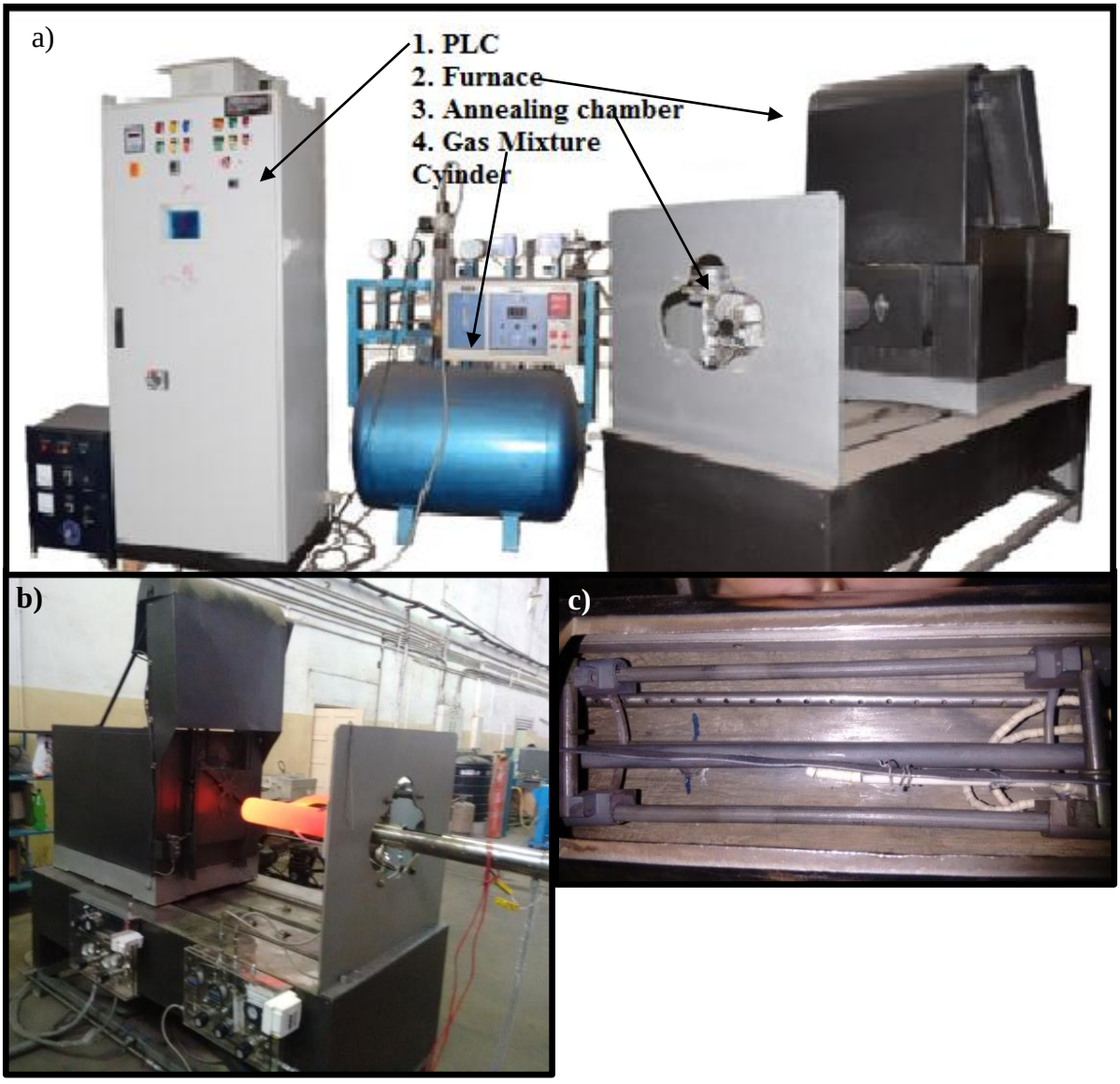


Figure 3.7: (a) Annealing simulator, (b) furnace and specimen chamber, and (c) mechanism for holding and inserting the specimen into the furnace. (Courtesy: NML, Jamshedpur)

- **Cooling Medium**

Controlled cooling rates (>100 ℃/s) of specimens can be obtained by using high pressure gas jet. Cooling can be done using hydrogen, nitrogen, or mixture of these. Cooling rates were varied by changing either the percentage of hydrogen gas in the gas mixture, or the inlet gas mixture, pressure or both.

In the present work, annealing simulator was used to validate the results of DICTRA simulations for pearlite dissolution time at equilibrium heating conditions and to prepare specimens for tensile testing.

### 3.4.3 Gleeble 3800 Simulator

The Gleeble 3800 (Make: Dynamic System Inc, *Poestenkill,* New York, USA) is a fully automated thermal and mechanical testing system. It uses Windows based computer software and provides a friendly interface to create, run and analyze data from thermal-mechanical tests and physical simulation programs. The direct resistance heating system Gleeble has a capacity to heat the specimens at heating rates of up to 10,000 $℃/s$ , or even hold at a steady-state equilibrium temperature. The grips are highly conductive which enable the simulator to achieve high cooling rates up to 10,000 $℃/s$ . The mechanical system of Gleeble 3800 is a hydraulic servo system with a capacity of 20 tons in compression and 10 tons in tension. Displacement rates, as fast as 2000 mm/s can be achieved. The mechanical system is capable of allowing changes from one control mode to another during any given test; this provides the flexibility necessary to simulate many thermal-mechanical processes necessary during the test.

A Windows based workstation and a powerful embedded processor is used. The Gleeble 3800 provides a number of programming options including QuikSim Software, a spreadsheet-like, fill-in-the-blanks software that describes each action in a test sequence in order and duration. Once the simulation has been finished, the results are automatically loaded into Origin software, a flexible and powerful data analysis package included with every Gleeble 3800 System. Figure 3.8 shows a Gleeble 3800 simulator. In the present work, Gleeble simulator was used to validate the results of DICTRA simulations for pearlite dissolution during non-equilibrium heating conditions.

### 3.4.4 Tensile Testing Machine

The tensile testing machine (Make: Instron 8501 System, *Instron Engineering Corporation*, Norwood, USA) with a loading capacity of 100 kN was used for stress-strain analysis in the present work. The machine provides data in form of values of stress corresponding to respective strains. The data when plotted can be used to calculate the yield strength, ultimate tensile strength and total elongation.


Figure 3.8: Gleeble 3800 simulator. (Courtesy: NML, Jamshedpur)

Figure 3.9 shows the tensile testing machine used in the present work. An extensometer (gauge length of 25 mm) was used to measure the elongation.

Flat dog-bone shaped tensile specimens with gauge length of 35 mm were prepared as per the ASTM standard E-8M to test the specimens. Figure 3.10 shows the schematic of tensile specimens used for the experimental work.


Figure 3.9: Tensile testing machine. (Courtesy: NML, Jamshedpur)

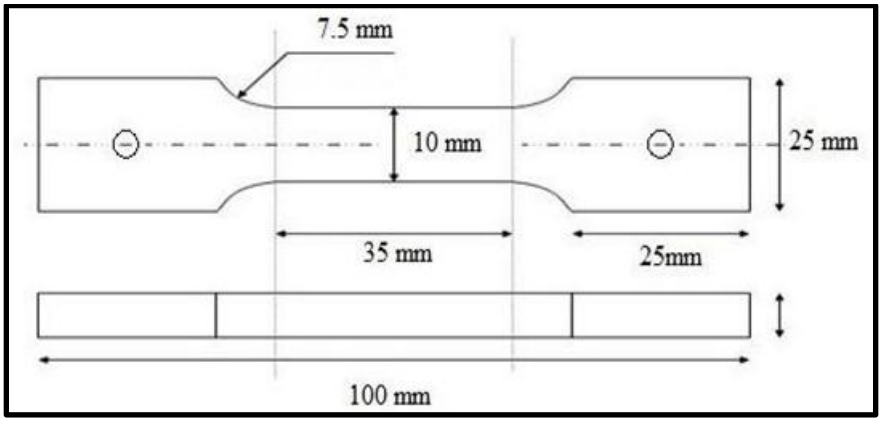


Figure3.10: Schematic of flat dog-bone shaped specimens for tensile testing.

### 3.4.5 Sample Preparation for Metallography

In order to prepare samples for metallography, some basic steps need to be followed carefully. These include mounting, planar grinding, rough polishing, final polishing, etching and microscopic analysis. These steps are discussed in brief as follows:

A. **Mounting**

The use of mounting of samples is to facilitate their easy handling. Mounting is done either with copper or with bakelite. Copper is used for mounting when specimen is to be used for SEM analysis. Specimens are hot mounted at a temperature of 160 ℃ by following the procedure of powder metallurgy. The edges of the mounted samples are rounded to minimize the damage to grinding/polishing discs. The mounting press (Make: BAINMOUNT METCO, *Chennai Metco Pvt. Ltd.*, Chennai, India) was used in the presented work and is shown in Fig. 3.11.


Figure 3.11: Mounting press. (Courtesy: NML, Jamshedpur)

B. **Grinding**

The surface to be examined by microscope is polished with abrasive papers of successive finer grades such as 80, 120, 220, 320, 400, 600, 800, 1000, 1200, 1500 and 2000 mesh abrasive paper (shown in Fig. 3.12). Each time the sample is rubbed on SiC paper, scratch marks are introduced, therefore polishing is continued till all the scratches are in one direction. Then, the next paper with finer grade is used with direction of rubbing switched perpendicular to previous scratches. Similar process is repeated from the coarse grade paper (80 grit size) up to fine grade paper (2000 grit size). Over-heating of sample is avoided so that no modification in the microstructure occurs. Pressure needs to be adjusted, as high pressures can introduce deep scratches whereas low pressures result in long time consumption.

Figure 3.12: Abrasive papers. (Courtesy: NML, Jamshedpur)

C. **Polishing**

The next step is polishing on a horizontal rotating wheel. Polishing wheels are covered with a soft cloth (velvet, canvas, suede or selvet etc.) which need to be soaked with a polishing medium (alumina or colloidal). The polishing cloth is washed thoroughly with water before the start of polishing to remove any chances of introduction of contaminants which may cause deep scratches on surfaces. Polishing medium is spread on to a well washed cloth and as soon as the specimen starts to stick or friction starts to act between the specimen and cloth, water is poured on to the rotating wheel. The specimen is held on the rotating disc in order to obtain a scratch free surface with mirror like finish. Polishing machine (Make: BANIPOL METCO, Model No: PMV018, *Chennai Metco Pvt. Ltd.*, Chennai, India) of 0.37 kW capacity was used in the present work. Polishing machine has been shown in Fig. 3.13.

D. **Etching**

Etching is done in order to reveal the microstructure of the metal/alloy system through selective chemical attack. The sample must be thoroughly cleaned before etching. Etchant must be selected and prepared accurately. Etchant may be applied using a cotton bud wiped over the surface for a few times (necessary precautions must be taken while etching, as very small difference occurs between etching and over-etching). Nital (2% nitric acid ($HNO_3$) in ethanol) and Picral (pre etched in 0.4 g picric acid in 10 ml ethanol for 60 s and finally etched in solution of 1 g sodium meta sulphate ($Na_2S_3O_5$) in 10 ml distilled water) were used as etchants in the

present work. The specimens were immediately washed with alcohol after applying the etchant and were then dried.


Figure 3.13: Polishing machine. (Courtesy: NML, Jamshedpur)

E. **Levelling**

The surface to be examined optically should be perfectly flat and levelled. If not, then the viewing area would be out of focus i.e. if the centre is focused, the sides would go out of focus and vice versa. By using a specimen levelling press, this problem can be avoided, as it presses the mounted specimen into clay on a microscope slide, making it levelled. A small piece of paper or cloth covers the surface of the specimen to avoid scratching. In the present work, a levelling machine as shown in Fig. 3.14 was used.

### 3.4.6 Microstructural Evaluation

Mechanical properties are strongly influenced by the microstructure, so microstructural evaluation is important. The present research work utilized optical microscopy and scanning electron microscopy (SEM).

Figure 3.14: Levelling machine. (Courtesy: NML, Jamshedpur)

A. **Optical Microscope**

Optical microscope is used for the purpose of magnifying small samples with the help of visible light and a system of lenses. Metallic materials are usually opaque and therefore investigations of plane cross-sections by incident light prevail in metallography. Due to the difference in the refractive indices, there appear different grey or colour shades. Starting from the sample preparation, to etching of the specimen, and setting up of microscope, all steps should be carefully optimized in order to get maximum information from a microscopic study. The optical microscope (Make: Leica DM2500 M; *Lieca Microsystems*, Wetzlar, Germany) was used in the present work (see Fig. 3.15).

Figure 3.15: Optical microscope. (Courtesy: NML, Jamshedpur)

B. **Scanning Electron Microscope**

A scanning electron microscope (SEM) is a type of electron microscope that images a sample by scanning it with a high-energy beam of electrons. The electrons interact with the atoms that make up the sample and produce signals that contain information about the sample's surface topography, composition, and other properties such as electrical conductivity etc. SEM can produce very high-resolution images of the sample's surface, revealing details less than 1 nm in size. Due to the very narrow electron beam, SEM micrographs have a large depth of field yielding a characteristic three-dimensional appearance useful for understanding the surface structure of a sample. Figure 3.16 shows the scanning electron microscope (Make: Nova Nano SEM 430; *Field Emission Inc.,* Hillsboro, USA) used in the present study.

Figure 3.16: Scanning electron microscope. (Courtesy: NML, Jamshedpur)

## 3.5 Summary of the Chapter

This chapter describes the design of the study that was adopted for the present work. In this chapter of the report, the objective function with key issues has been discussed. An overview of the commercial software used for simulation and experimental procedure followed has been discussed. The details of various machines and equipment have been provided. This chapter also includes the procedure for sample preparation for metallography, microstructural analysis and mechanical properties evaluation etc.

# Chapter 4

# Results and Discussion

## 4.1 General

This chapter presents the main results and discussions with regards to the research carried out for the dissertation work. The chapter deals with results of simulations and subsequent predictions made by the software viz. Thermo-Calc, DICTRA, and analySIS FIVE. The chapter also discusses the results of experimental work carried out to validate the simulation results.

## 4.2 Characterization of the As-received Material

The initial microstructure of the as-received steel (both hot rolled and cold rolled) typically comprised of ferrite and pearlite structure as shown in Fig. 4.1. Figure 4.1a–b shows the micrograph for hot rolled steel and cold rolled steel respectively. By using linear intercept method, the average grain size (for hot rolled steel specimen) was determined as 9.13 µm. The volume fraction of pearlite was calculated as 16.78 % using 'analySIS FIVE' software. The ferrite and pearlite distribution (for hot rolled steel specimen) was calculated using analySIS FIVE software (see Fig. 4.2 a–b).

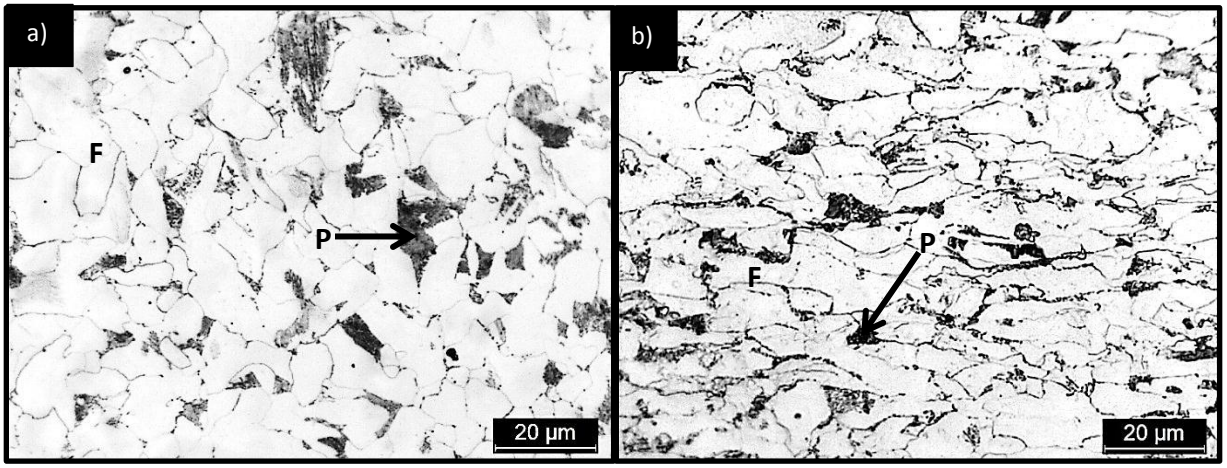


Figure 4.1: Optical micrographs of the as-received material (a) hot rolled, and (b) cold rolled. P= pearlite and F= ferrite

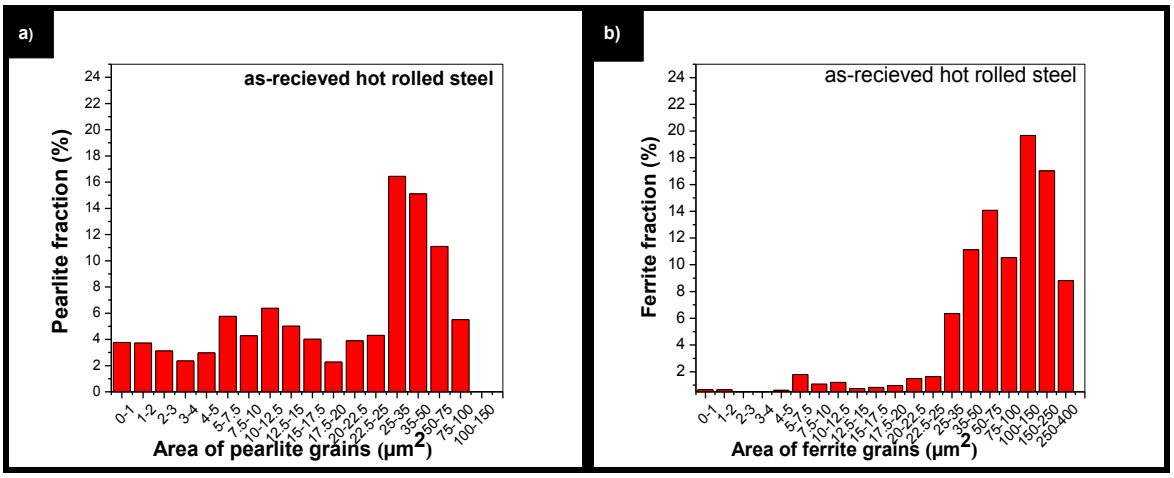


Figure 4.2: Size distribution of phases in as-received hot rolled steel for (a) pearlite, and (b) ferrite

## 4.3 Prediction of Annealing Parameters using Thermo-Calc

The annealing temperature ranges (lower critical temperature, $Ac_1$ and upper critical temperature, $Ac_3$ were predicted using Thermo-Calc 3.0 software. Thermo-Calc was used for constructing the equilibrium phase diagram, and the phase fraction diagram for the given hot rolled steel. Figure 4.3a–b shows these diagrams for the given steel. The equilibrium diagram predicted the intercritical temperatures as 682.2 ℃ and 839.7 ℃ respectively**.** Hence, the temperature range for the experimental study was determined.

## 4.4 DICTRA Simulations

DICTRA was used to predict the holding time at a given annealing temperature for complete pearlite dissolution in the given hot rolled steel. For the simulation work, pearlite present in the steel was assumed to be completely lamellar with a constant volume ratio of constituent phases (ferrite and cementite phases were assumed to be present in pearlite in volume ratio of 8:1). Thus, a linear system was chosen to represent the $Fe_3C$/ γ and γ/ α interfacial regions (see Fig. 4.4a). Figure 4.4b shows that austenite phase grows both in the $Fe_3C$/ γ and γ/ α interfacial regions (γ grows towards the left in $Fe_3C$/ γ and towards the right in the γ/ α interfacial regions respectively). The system considered for simulation was assumed to have a total lamellar width (for one lamella each ferrite and cementite) of 36 μm (width of ferrite lamella: 32 μm; and width of cementite lamella: 4 μm).

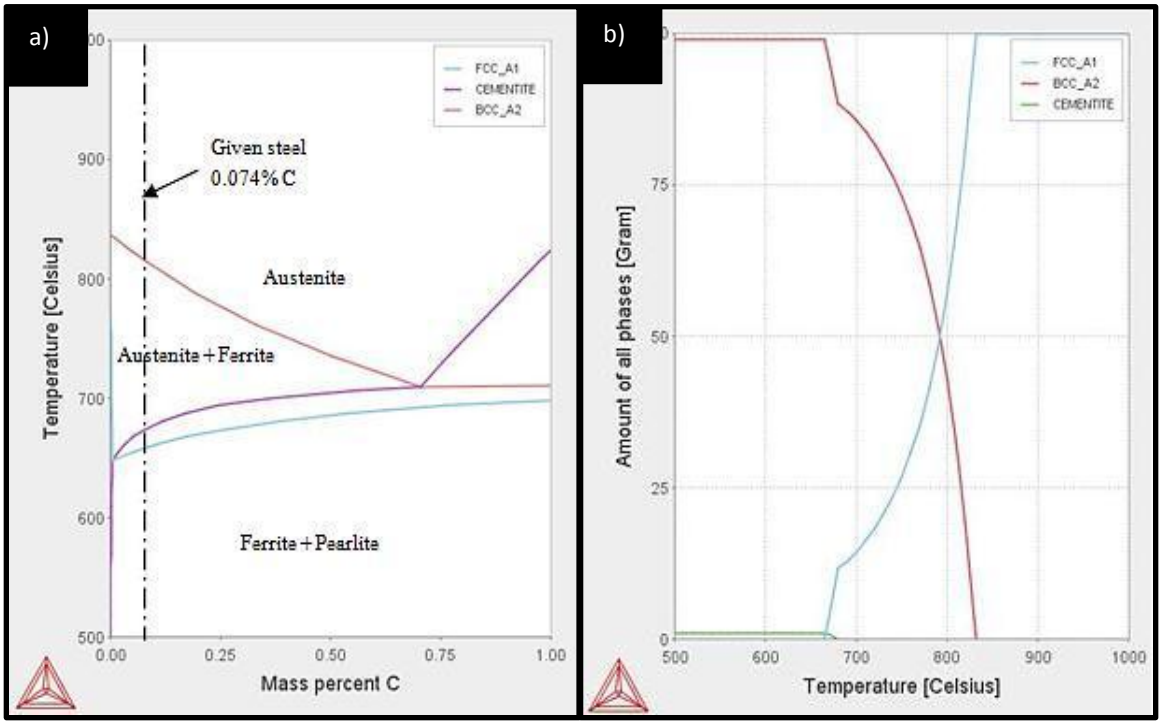


Figure 4.3: Result window of Thermo-Calc (a) equilibrium diagram, and (b) phase fraction diagram.

Thermo-Calc software was used to calculate the percent weight of carbon available at $Fe_3C$/ γ and γ/ α interfaces, the mean percentage weight of carbon in austenite etc.; the results of which are presented in Table 4.1.

Table 4.1: Percent weight of carbon at various interfaces for different annealing temperatures.

| **Annealing temperature (℃)** | **Percent weight of carbon at $Fe_3C$/ γ interface (%)** | **Percent weight of carbon at γ/ α interface (%)** | **Mean percent weight of carbon in γ (%)** |
|---|---|---|---|
| 750 | 0.82334 | 0.60058 | 0.71196 |
| 775 | 0.88599 | 0.45857 | 0.67228 |
| 800 | 0.94865 | 0.45857 | 0.64513 |
| 825 | 1.01687 | 0.23719 | 0.62703 |
| 850 | 1.08927 | 0.15644 | 0.62285 |

DICTRA simulations were carried out at different inter-critical annealing temperatures (750, 775, 800, 825 ℃ respectively) and also a temperature above $Ac_3$ (850 ℃) assuming lamellar pearlite with ferrite and cementite phases in the ratio of 8:1.

The first step in DICTRA simulation included the determination of time required for formation of austenite from pearlite during isothermal holding at a given annealing temperature (assuming that the temperature is being reached through equilibrium heating).

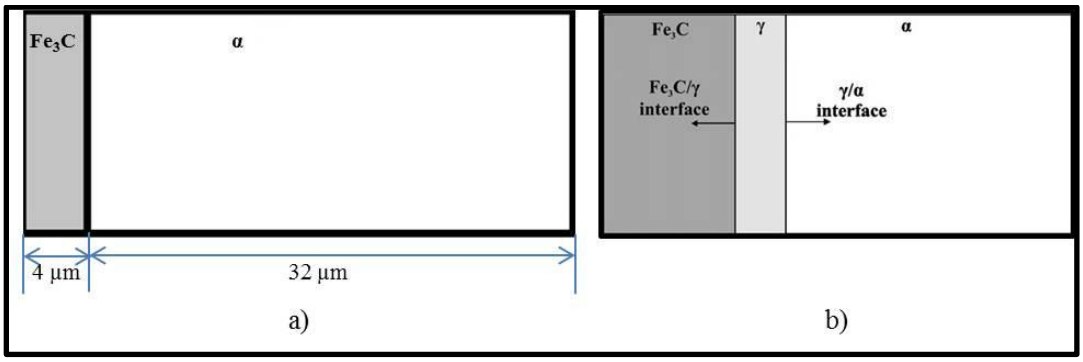


Figure 4.4: Schematic representation of (a) lamellar pearlite assumed for simulation, and (b) the growth of austenite at $Fe_3C$/ γ and γ/ α interfaces.

Further, DICTRA simulations also provided the information on interface movement. Figure 4.5 presents a schematic for showing the interface movement.

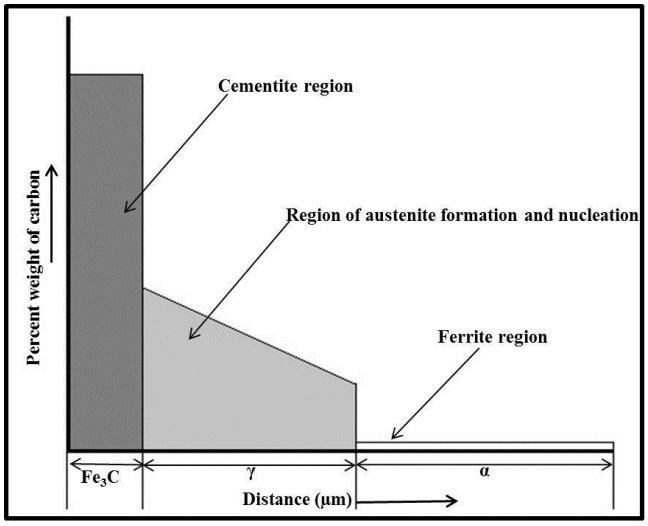


Figure 4.5 Schematic for interface movement during dissolution of pearlite for formation of austenite.

The second step included investigations with regards to (i) the effect of heating rates on formation of austenite followed by isothermal holding, and (ii) the effect of holding time on the formation of austenite.

### 4.4.1 DICTRA Simulations for Pearlite Dissolution under Equilibrium Heating Conditions

This section discusses the determination of time required for the nucleation and formation of austenite from pearlite during isothermal holding at a given annealing temperature (under equilibrium heating conditions). Isothermal annealing at different annealing temperatures were simulated assuming equilibrium heating. The time for formation of austenite (from just pearlite and not from proeutectoid ferrite) was calculated using the simulation results. The key inputs for DICTRA software were taken from Table 4.1.

Figure 4.6 shows the results obtained from DICTRA simulations. The figures bring forth the isothermal annealing time required for complete conversion of pearlite to austenite at a given annealing temperature under equilibrium conditions. Figure (4.6 a, c, e, g, i) shows the austenite volume fraction as a function of holding time during the conversion process (pearlite to austenite). Figure (4.6 b, d, f, h, j) shows the carbon (% wt.) variation across the growing austenite phase (in-between the cementite and ferrite lamellae i.e. as a function of distance from the start of original cementite lamella in the initial pearlite structure).

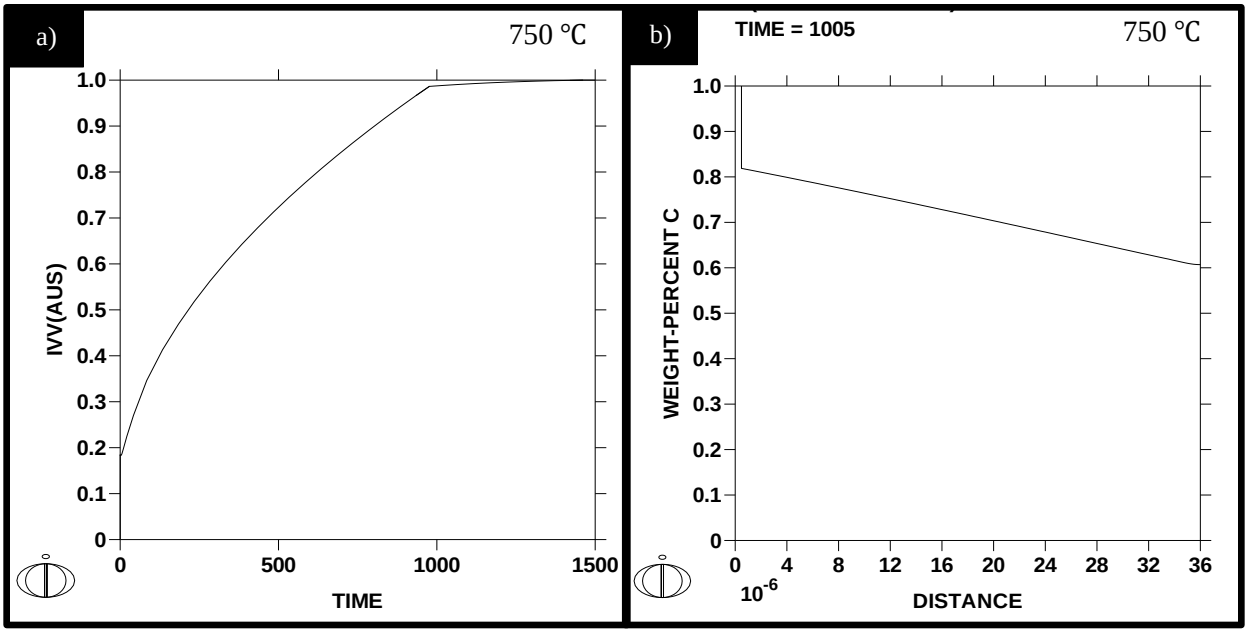

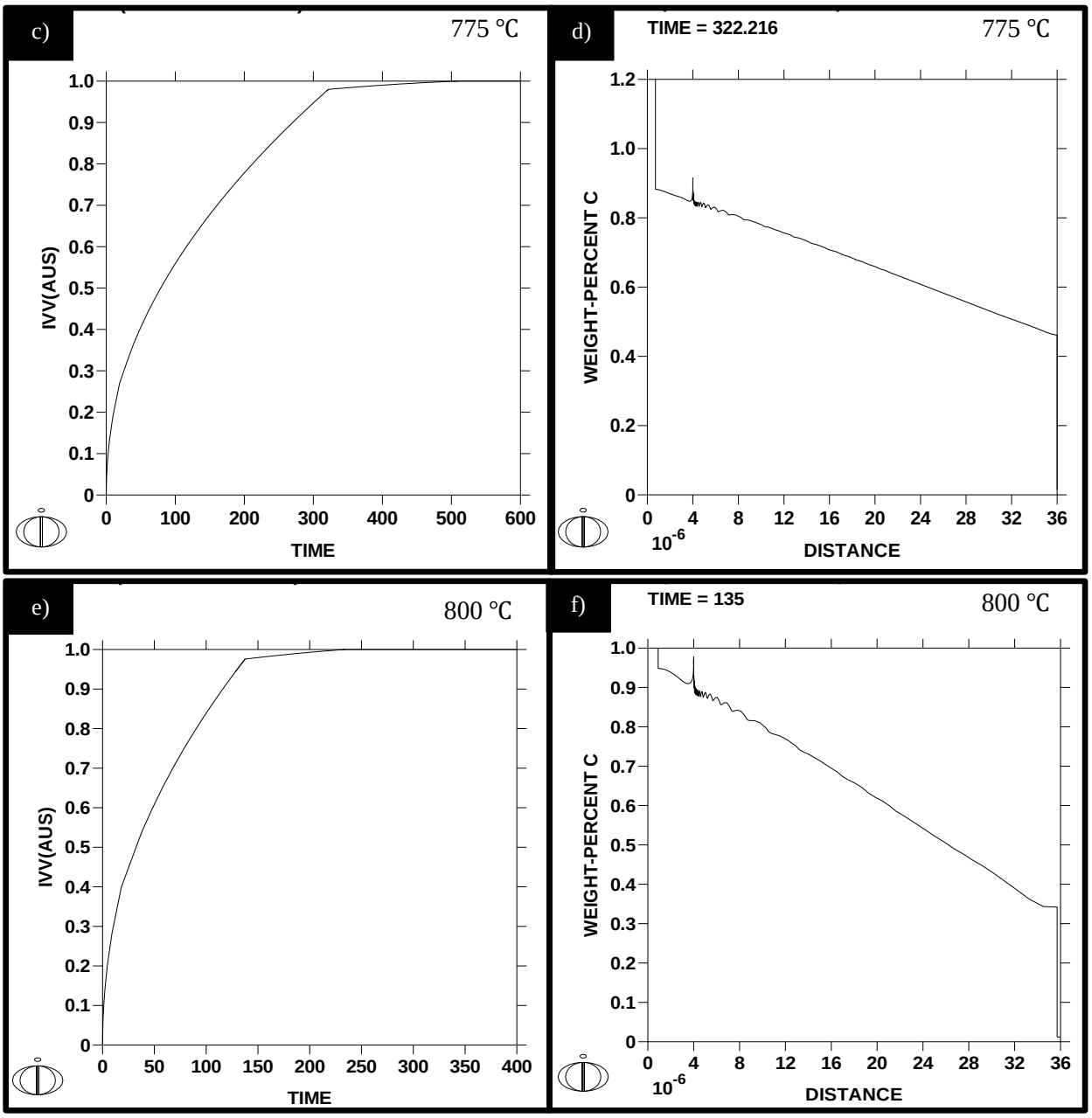
c)
775 ℃
IVV(AUS)
TIME
d)
TIME = 322.216
775 ℃
WEIGHT-PERCENT C
10-6
DISTANCE
e)
800 ℃
IVV(AUS)
TIME
f)
TIME = 135
800 ℃
WEIGHT-PERCENT C
10-6
DISTANCE

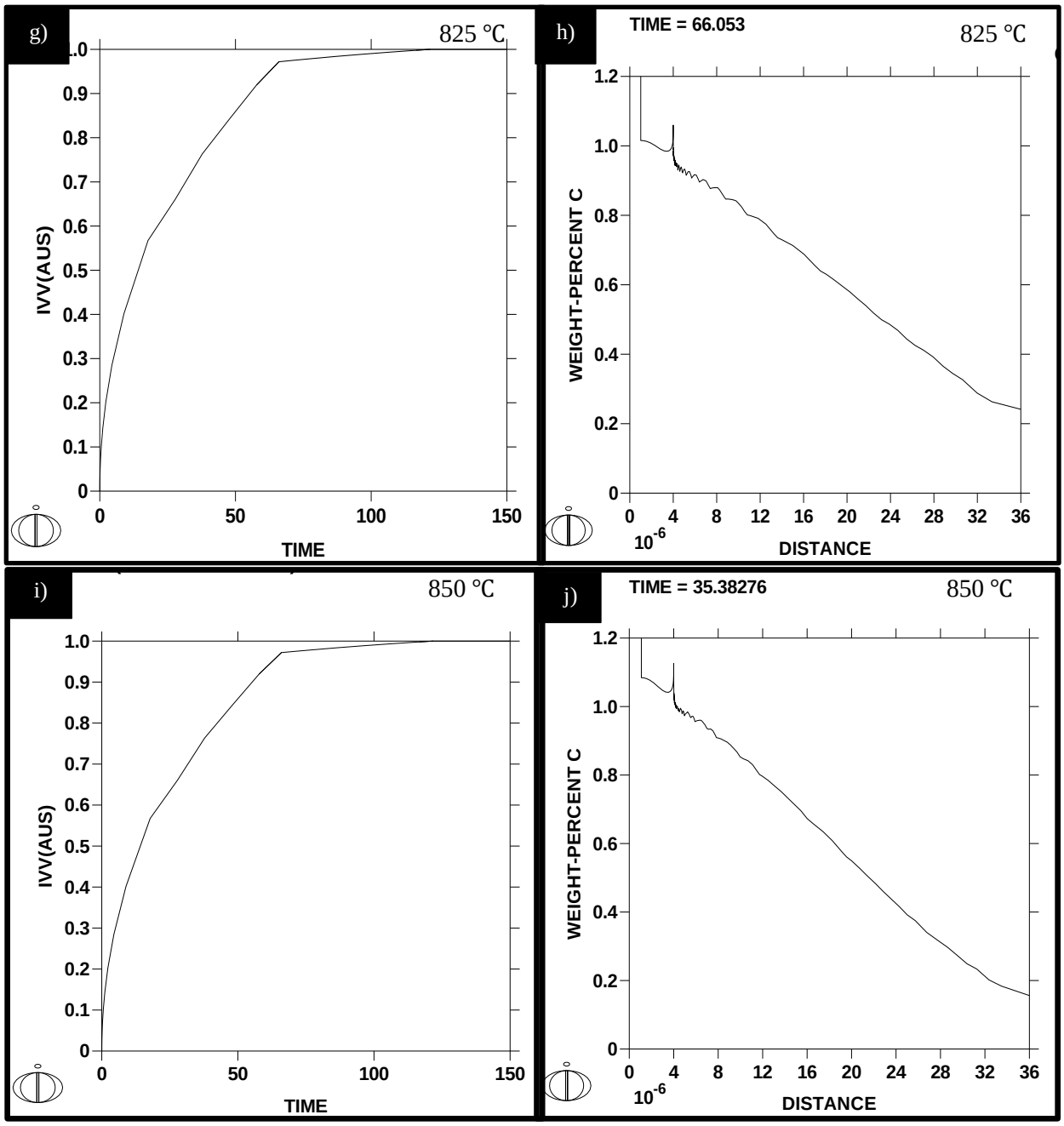


Figure 4.6: Result window of DICTRA simulations for different annealing temperatures showing (a, c, e, g, i) austenite volume faction as a function of holding time, and (b, d, f, h, j) weight percent of carbon in austenite as a function of distance. IVV(AUS) = austenite volume fraction, TIME = holding period in seconds, DISTANCE = distance from start of original cementite lamella of pearlite mixture in microns.

Table 4.2 presents the main results of the DICTRA simulations with regards to isothermal annealing at different temperatures. The table summarizes the results of Fig. 4.6 i.e. provides details of austenite volume fraction and percent weight carbon in austenite at $Fe_3C/\gamma$ and $\gamma/\alpha$ interfaces.

Table 4.2: Results of DICTRA simulations to predict isothermal holding periods and carbon concentration at interfaces during conversion of pearlite to austenite under equilibrium heating.

| **Annealing temperature (℃)** | **Percent weight of carbon at the interface** | | **Isothermal annealing time for conversion of pearlite to austenite (s)** |
|---|---|---|---|
| | **$Fe_3C/\gamma$** | **$\gamma/\alpha$** | |
| 750 | 0.82334 | 0.60058 | 1005 |
| 775 | 0.88599 | 0.45857 | 323 |
| 800 | 0.94865 | 0.45857 | 135 |
| 825 | 1.01687 | 0.23719 | 66 |
| 850 | 1.08927 | 0.15644 | 36 |

Further, the DICTRA simulation results also presented the interface movements i.e. depletion of ferrite and cementite phases with progressive holding at a given annealing temperature and thereby representing growth in the region of austenite phase (see Fig. 4.7; at annealing temperature of 775 ℃, comparing Fig. 4.7a and Fig.4.7g, it can be noted that for more holding, cementite and ferrite lamellae width has considerably decreased and that of austenite has considerable increased). Further, simulation results also revealed that with progressive holding, the slope of weight percent carbon in the austenite region continuously decreased, indicating decrease in heterogeneity of carbon in austenite phase with increase in holding time periods (again comparing Fig. 4.7a and Fig.4.7g, it can be noted that for more holding, the slope of curve in the growing austenite region has considerably decreased, representing lesser heterogeneity) (see Fig. 4.7 for illustrated case at 775 ℃; see Appendix-I for other annealing temperatures).

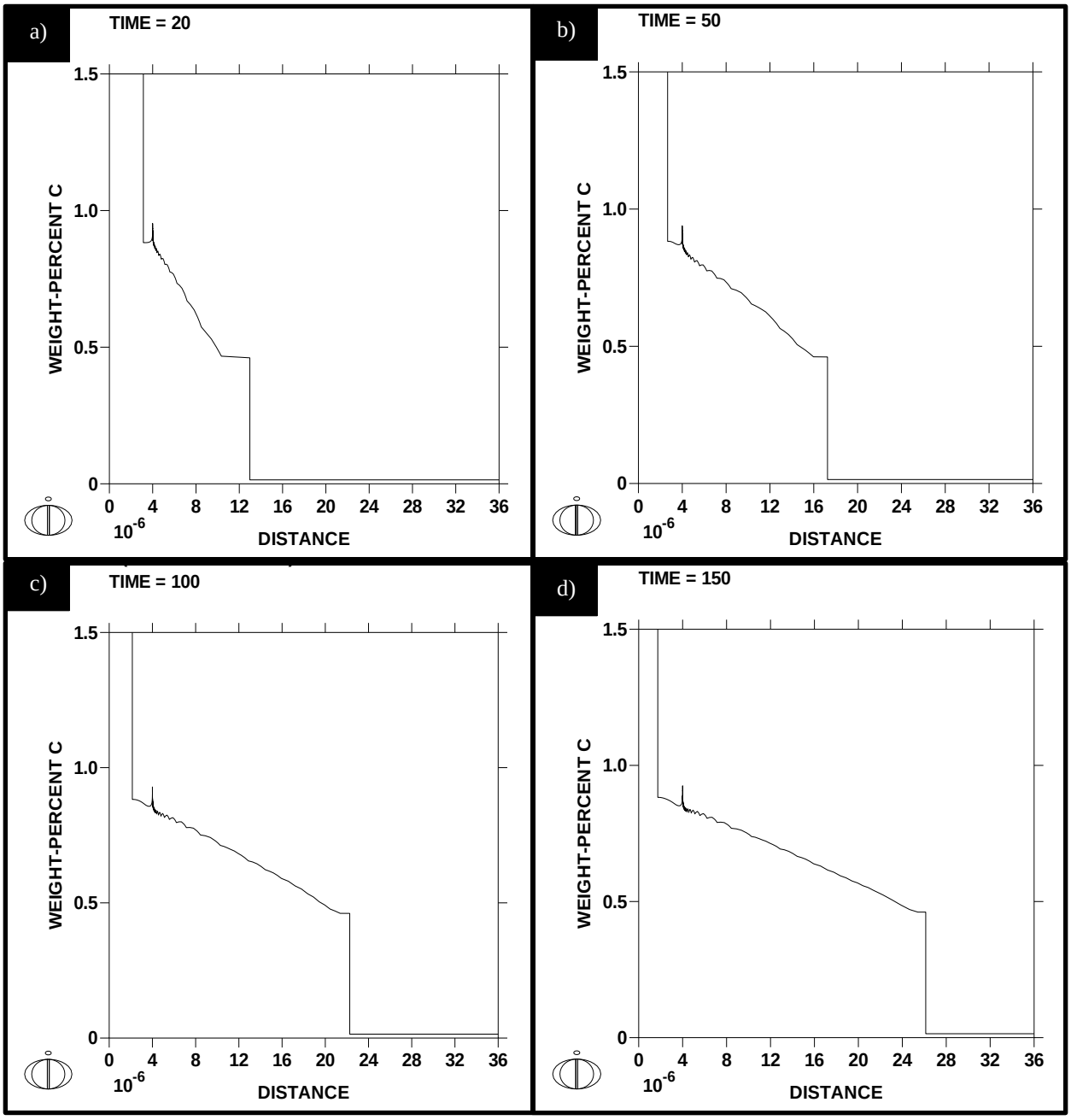
a)
TIME = 20
WEIGHT-PERCENT C
1.5
1.0
0.5
0
0 4 8 12 16 20 24 28 32 36
10-6
DISTANCE
b)
TIME = 50
WEIGHT-PERCENT C
1.5
1.0
0.5
0
0 4 8 12 16 20 24 28 32 36
10-6
DISTANCE
c)
TIME = 100
WEIGHT-PERCENT C
1.5
1.0
0.5
0
0 4 8 12 16 20 24 28 32 36
10-6
DISTANCE
d)
TIME = 150
WEIGHT-PERCENT C
1.5
1.0
0.5
0
0 4 8 12 16 20 24 28 32 36
10-6
DISTANCE

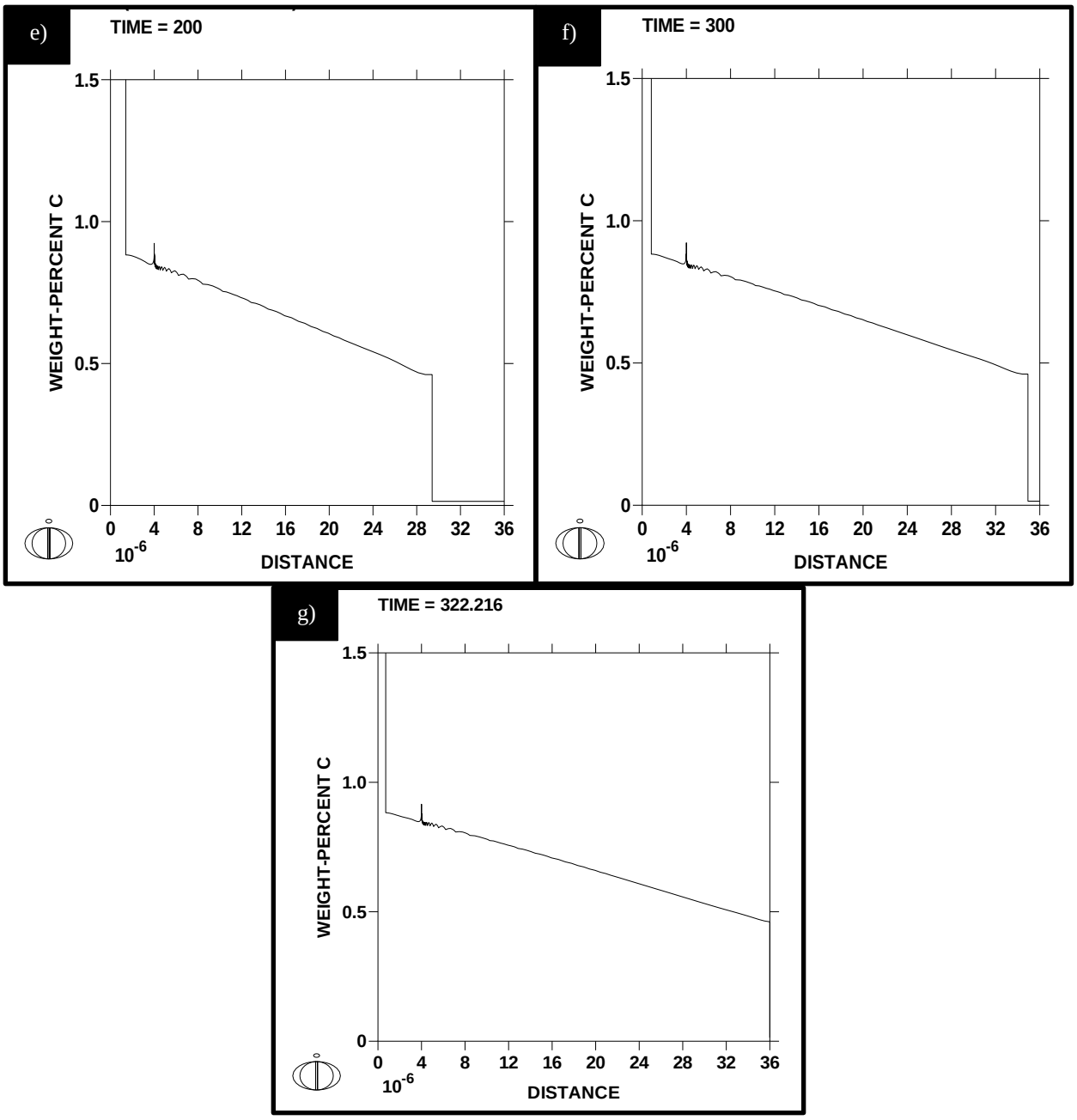


Figure 4.7: Result window DICTRA simulation for the interface movement of carbon for different time periods at 775 ℃ as a function of distance.

From the above simulations, it was observed that with increase in austenization temperature, the holding time required for transformation of pearlite into austenite decreases. Figure 4.8a presents the temperature-time relation for transformation of pearlite into austenite.

Figure 4.8b presents the difference between maximum and minimum carbon concentrations ($C_{max} - C_{min}$) of austenite at a given annealing temperature after complete dissolution of pearlite

into austenite. The plot reveals that as the annealing temperature increases, the mean variation of carbon in austenite also increases i.e. heterogeneity of carbon in austenite increases.

Similarly Fig. 4.8c represents the change in slope of the curve; where slope is defined as the ratio of maximum difference in carbon concentration of austenite to the distance from the start of original cementite lamella in the initial pearlite structure i.e. slope = $(C_{max} - C_{min})$/ distance. A similar trend, as shown in Fig.4.8b was observed showing increase in slope with increase in annealing temperature.

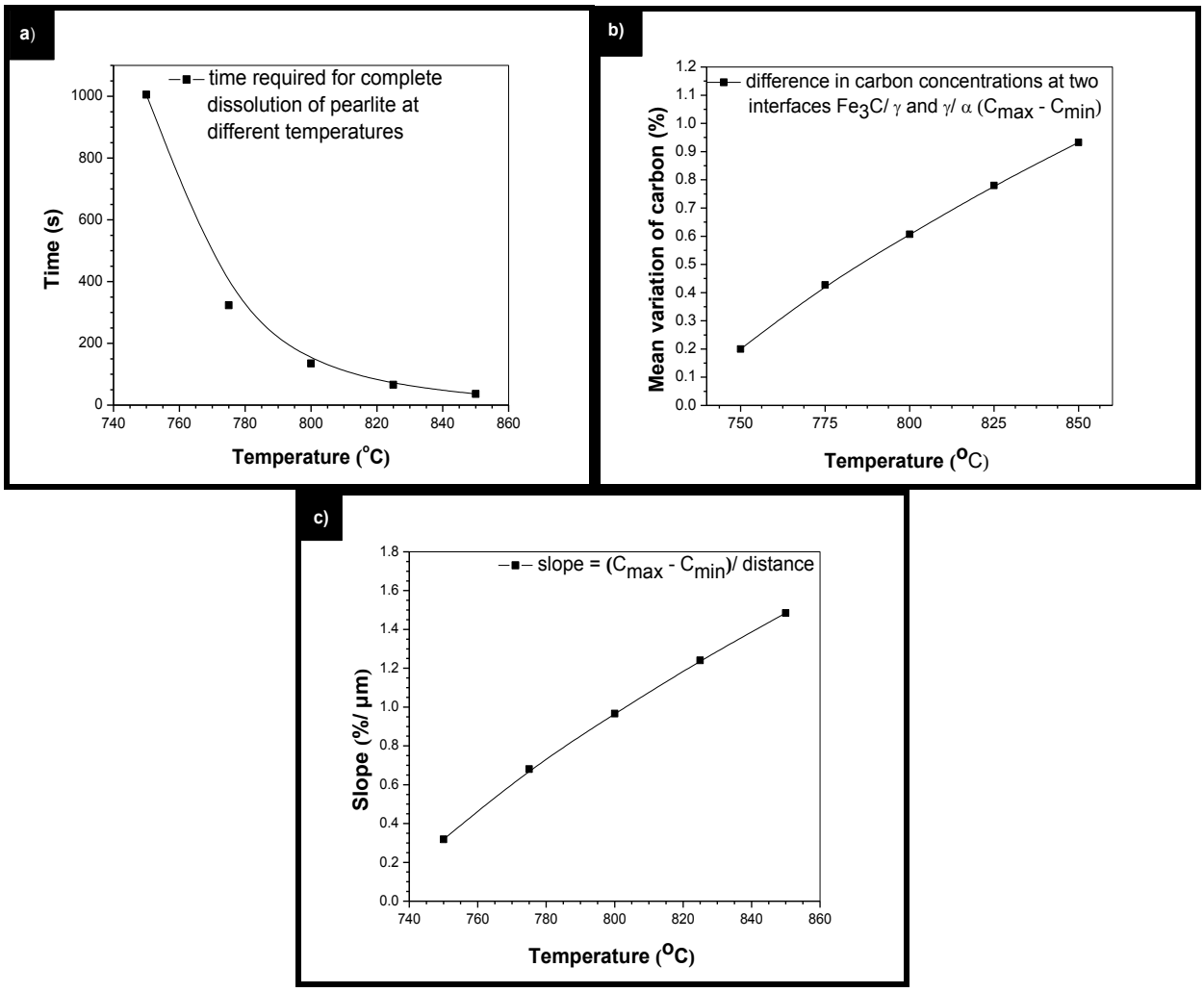


Figure 4.8: (a) Temperature-time relationship for transformation of pearlite into austenite, (b) mean variation of carbon in austenite as a function of annealing temperature, and (c) slope representing carbon variation in austenite as a function of annealing temperature.

### 4.4.2 DICTRA Simulations for Effect of Heating Rates on Pearlite Dissolution

The previous section discussed the results of DICTRA simulations for pearlite dissolution for formation of austenite under equilibrium heating conditions. This section describes the results of DICTRA simulations for pearlite dissolution under non-equilibrium heating conditions i.e. effect of heating rates on pearlite dissolution.

DICTRA simulations were performed for different heating rates viz. 10, 20, 50, 100, 200, 300, 400, and 500 ℃/s followed by isothermal holding for a time period in which full pearlite transformed to austenite. Simulations were carried out assuming the initial system to be at room temperature of 27 ℃ (300 K).

Simulations, in this section were carried out in two different steps. The first step (Step-I) included simulations to investigate the effect of only heating rates on the nucleation and formation of austenite, without considering the effect of holding periods at a given annealing temperature i.e. considering changes occurring only during the time required to heat the sample to the desired annealing temperature. The second step (Step-II) included simulations to investigate the effect of holding periods at a given annealing temperature on the nucleation and formation of austenite.

Simulations (Step-I) were done for each annealing temperature with different heating rates viz. 10, 20, 50, 100, 200, 300, 400, 500 ℃/s. In this section, the simulation results (Step-I) for the annealing temperature of 800 ℃ have been discussed (see Fig. 4.9a–h for results obtained at 800 ℃; see Appendix-II for other annealing temperatures). Here, it may be noted that for the simulation at any given anealing temperature, two main inputs were needed viz. the heating rate to be followed, and time required to reach the annealing temperature following the given heating rate.

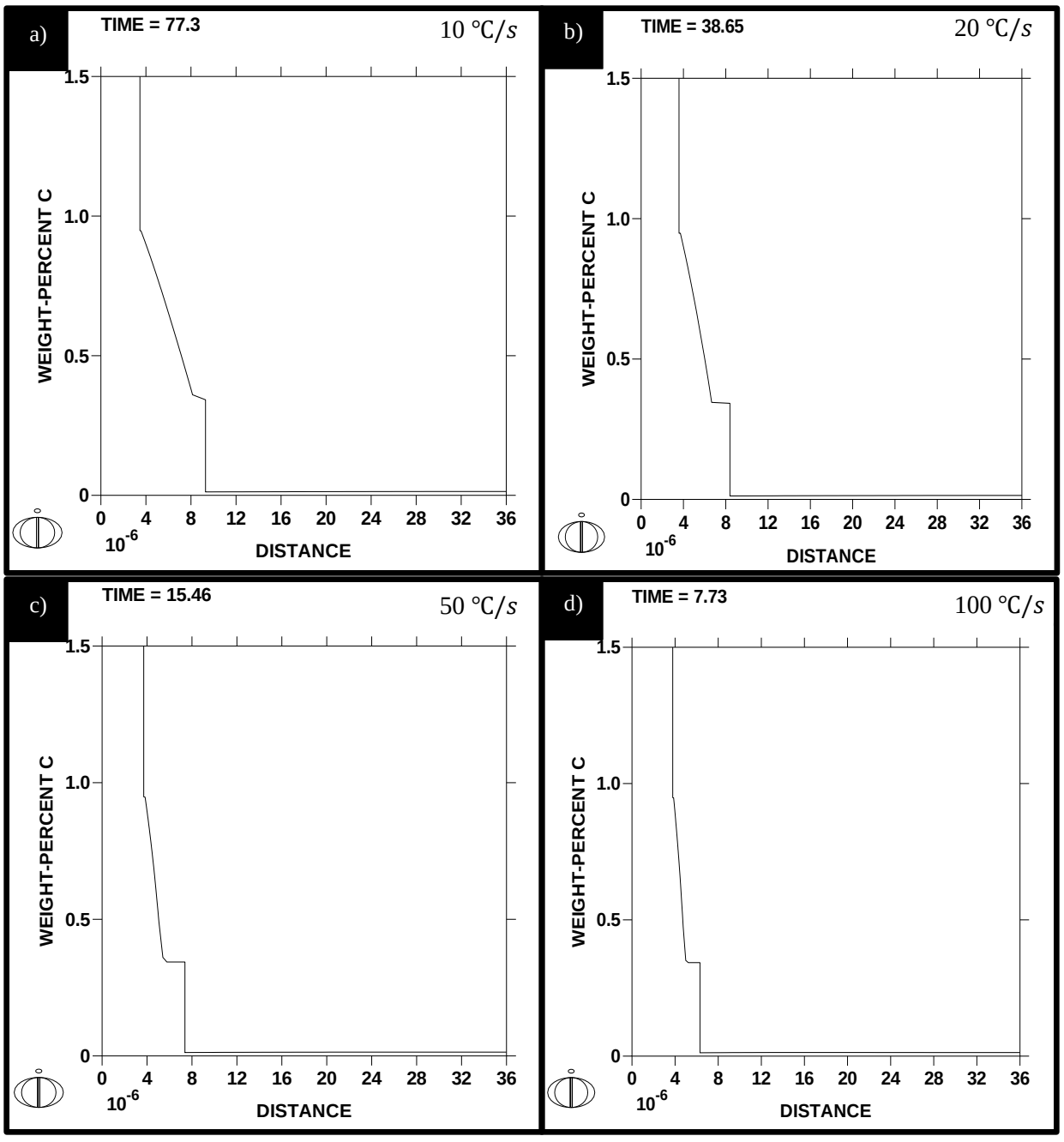
a)
TIME = 77.3
10 ℃/s
WEIGHT-PERCENT C
1.5
1.0
0.5
0
0 4 8 12 16 20 24 28 32 36
10-6
DISTANCE
b)
TIME = 38.65
20 ℃/s
WEIGHT-PERCENT C
1.5
1.0
0.5
0
0 4 8 12 16 20 24 28 32 36
10-6
DISTANCE
c)
TIME = 15.46
50 ℃/s
WEIGHT-PERCENT C
1.5
1.0
0.5
0
0 4 8 12 16 20 24 28 32 36
10-6
DISTANCE
d)
TIME = 7.73
100 ℃/s
WEIGHT-PERCENT C
1.5
1.0
0.5
0
0 4 8 12 16 20 24 28 32 36
10-6
DISTANCE

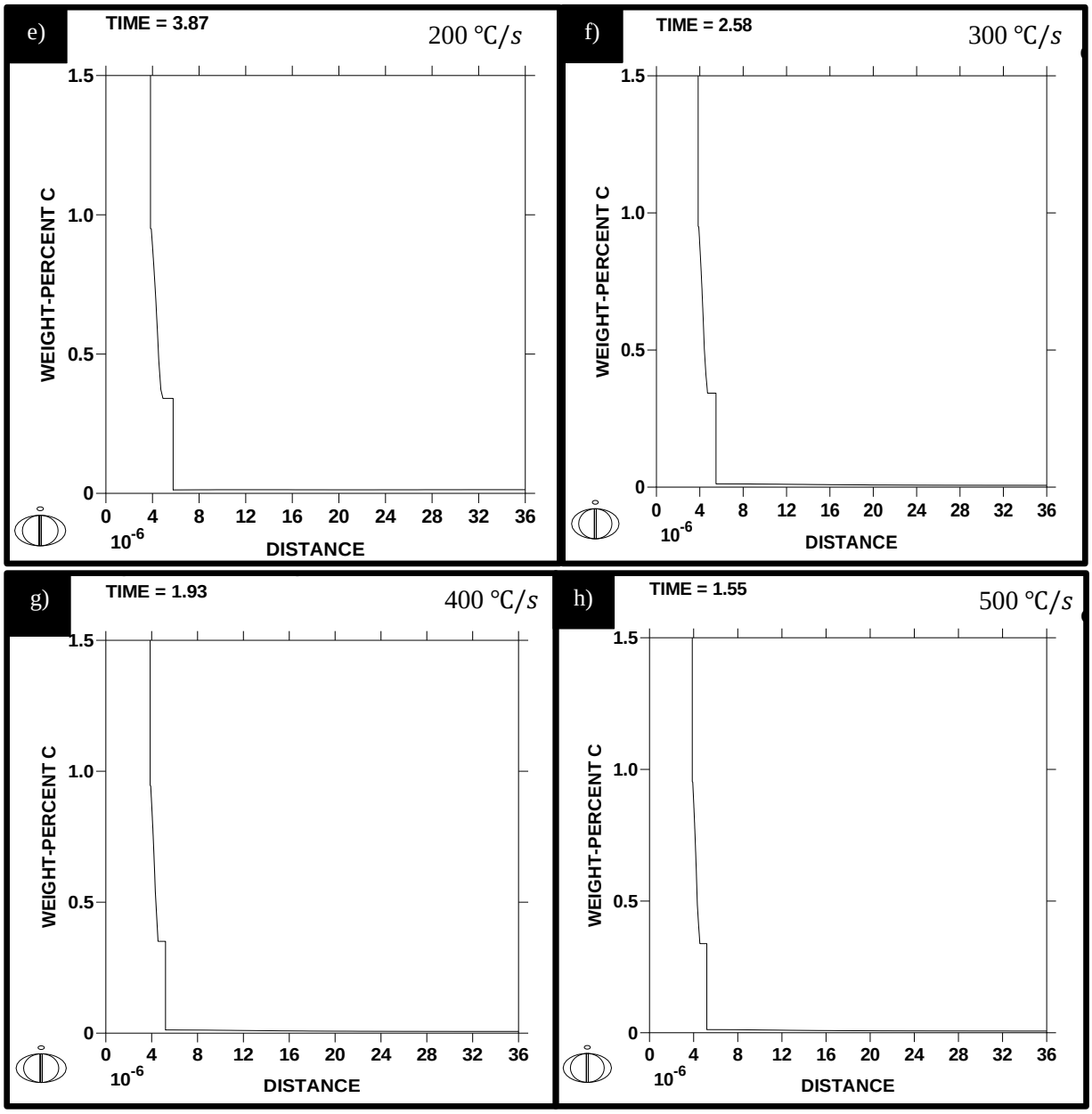


Figure 4.9: Result window of DICTRA simulations showing weight percent carbon in austenite as a function of distance, at different heating rates at the given annealing temperature of 800 ℃. DISTANCE = distance from original cementite lamella of initial pearlite mixture, in microns.

Step-I simulation results provided the variation of carbon in austenite at a given annealing temperature as a function of heating rate. Figure 4.9a–h presents the weight percentages of carbon in austenite as a function of distance, at different heating rates at the given annealing temperature of 800 ℃. The results of Step-I simulation were further utilized to find the amount

of austenite volume fraction at the given annealing temperature as a function of heating rate. For this, for each heating rate at a given annealing temperature, the ratio of the width of austenite region to the total lamellar width provided the austenite fraction formed during heating following that heating rate. For example, at annealing temperature of 800 ℃, for a heating rate of 10 ℃/s, the austenite fraction can be calculated using Fig. 4.9a. From Fig.4.9a, it is observed that austenite region extends from 3.45 μm to 9.31 μm providing width of the austenite region as 5.86 μm. Further, Fig. 4.9a provides the total lamellar width as 36 μm. Therefore, the austenite fraction formed at the given annealing temperature following the given heating rate comes out to be 0.1627 (i.e. 5.86/ 36 × 100 = 16.27 %). Similarly, for all the annealing temperatures, the austenite fraction obtained following different heating rates was obtained and is summarized in Table 4.3.

Table 4.3: Austenite fractions obtained at a given annealing temperature as a function of heating rate.

| **Heating rate (**℃/$s$) | **Fraction of austenite formed at annealing temperature of** | | | | |
|---|---|---|---|---|---|
| | **750** ℃ | **775** ℃ | **800** ℃ | **825** ℃ | **850** ℃ |
| 10 | 1.83 | 9.25 | 16.27 | 25.50 | 37.80 |
| 20 | 1.22 | 4.94 | 13.55 | 21.22 | 29.81 |
| 50 | 1.22 | 3.39 | 10.47 | 18.60 | 25.20 |
| 100 | 0.92 | 2.44 | 7.06 | 13.56 | 19.06 |
| 200 | 0.88 | 2.44 | 5.83 | 9.83 | 14.75 |
| 300 | 0.94 | 2.14 | 4.61 | 8.00 | 9.22 |
| 400 | 0.94 | 1.83 | 4.00 | 7.69 | 8.94 |
| 500 | 0.02 | 1.83 | 4.00 | 6.75 | 7.69 |

It can be observed from Table 4.3 that as the heating rate for a given annealing temperature is increased, the austenite volume fraction decreases this is because, at higher heating rates, the number of austenite nuclei formed at the ferrite grain boundaries decrease which results in less austenite formation at high heating rates at a given annealing temperature [Li *et al.,* 2013]. However, for constant heating rate followed for different annealing temperatures, it was observed that increase in annealing temperature led to increase in austenite volume fraction [Katsamas 2007]. These two main observations are also clear from Fig. 4.10 shown as follows.

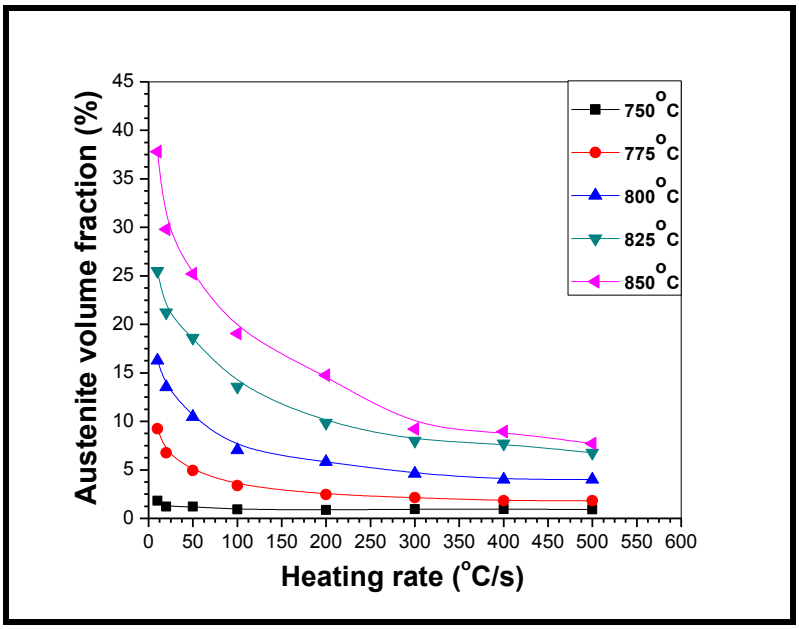


Figure 4.10: Effect of annealing temperature and heating rate on austenite volume fraction.

The second step (Step-II) included simulations to investigate the effect of holding periods at a given annealing temperature on the nucleation and formation of austenite. The input data for simulations was taken from the Step-I simulation results viz. width of cementite, austenite, and ferrite lamellae at a given annealing temperature reached through a particular heating rate.

Simulations (Step-II) were done for each annealing temperature reached through a specific heating rate and then subjected to different holding time periods. In this section, the simulation results (Step-II) for the annealing temperature of 800 ℃ reached through two specific heating rates (10 ℃/s and 20 ℃/s respectively) have been discussed (see Fig.4.10a–d for results obtained at 800 ℃; see Appendix-III for other conditions). Step-II simulation results provided the holding time periods required for complete dissolution of pearlite into austenite (i.e. 100 % transformation of all available pearlite to austenite) at a given annealing temperature reached through a given heating rate. Figure 4.11 (a, c) shows the austenite volume fraction as a function of holding time during the conversion process (pearlite to austenite). Figure 4.11 (b, d) shows the carbon (% wt.) variation across the growing austenite phase (in-between the cementite and ferrite lamellae) as a function of distance (from the start of original cementite lamella in the initial pearlite structure).

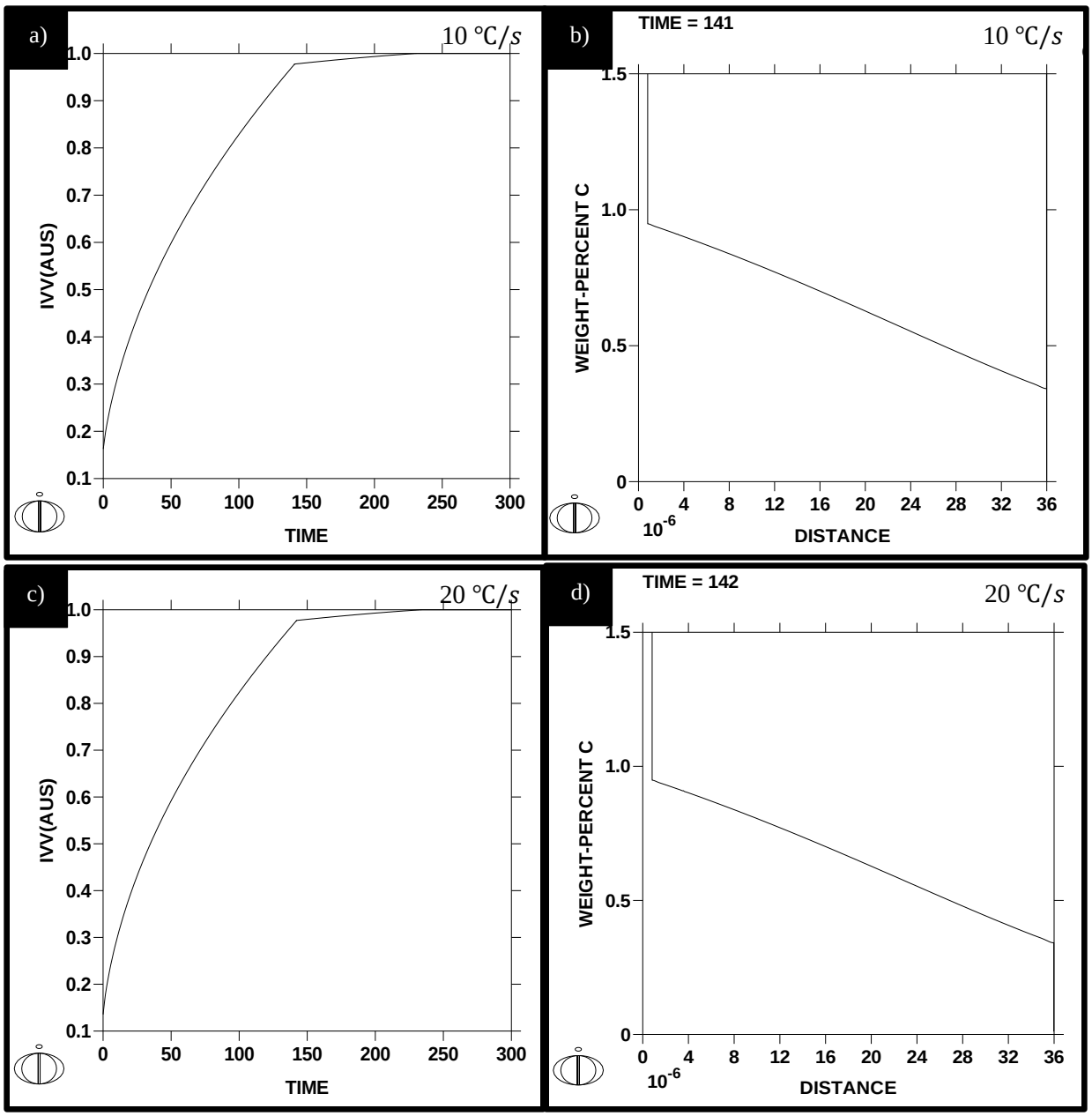


Figure 4.11: Result window of DICTRA simulations showing (a, c) austenite volume faction as a function of holding time, and (b, d) weight percent carbon in austenite as a function of distance, at different heating rates. IVV(AUS) = austenite volume fraction, TIME = holding period in seconds, DISTANCE = distance from original cementite lamella of the initial pearlite mixture, in microns.

Further, Step-II simulation results also revealed interface movements with progressive holding for a given heating rate at a given annealing temperature. The DICTRA simulations in this step presented the interface movements i.e. depletion of ferrite and cementite phases with progressive holding at a given annealing temperature and heating rate and thereby representing growth in the

region of austenite phase (see Fig. 4.12; for annealing temperature of 800 ℃ reached at a heating rate of 50℃/$s$). Comparing Fig. 4.12a and Fig. 4.12f, it can be noted that for more holding, cementite and ferrite lamellae width has considerably decreased and that of austenite has considerable increased. Further, simulation results also revealed that with progressive holding, the slope of weight percent carbon in the austenite region continuously decreased, indicating decrease in heterogeneity of carbon in austenite phase with increase in holding time periods (again comparing Fig. 4.12a and Fig.4.7f, it can be noted that for more holding, the slope of curve in the growing austenite region has considerably decreased, representing lesser heterogeneity) (see Fig. 4.12 for 800 ℃ for the heating rate of 50 ℃/$s$; see Appendix-IV for other annealing temperature-heating rate combinations).

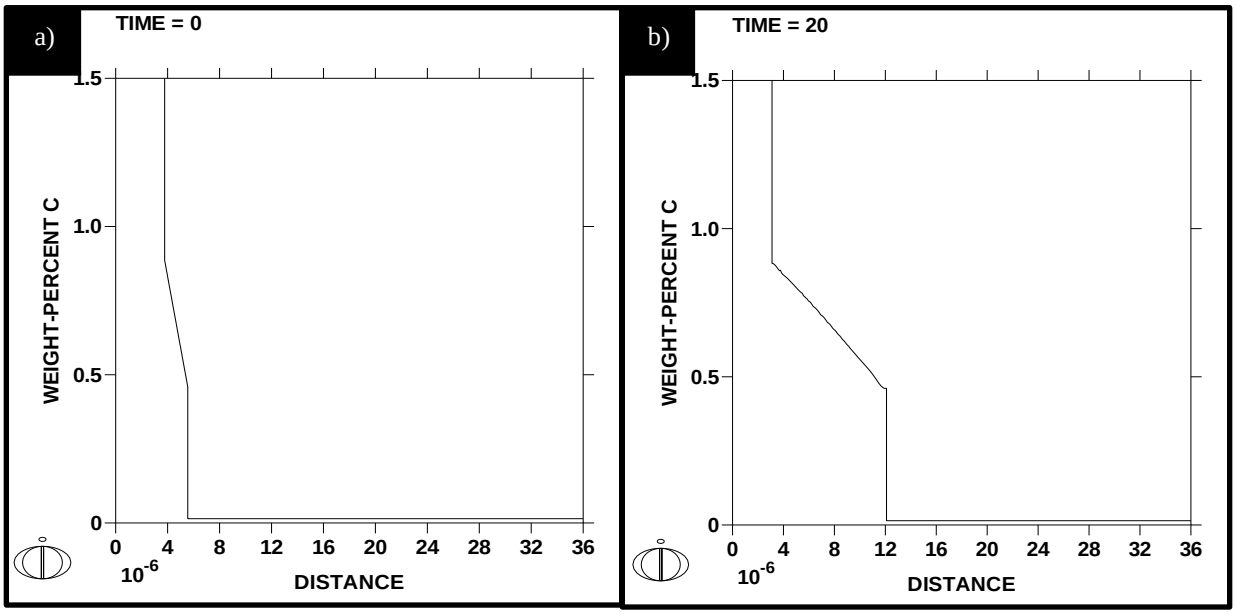

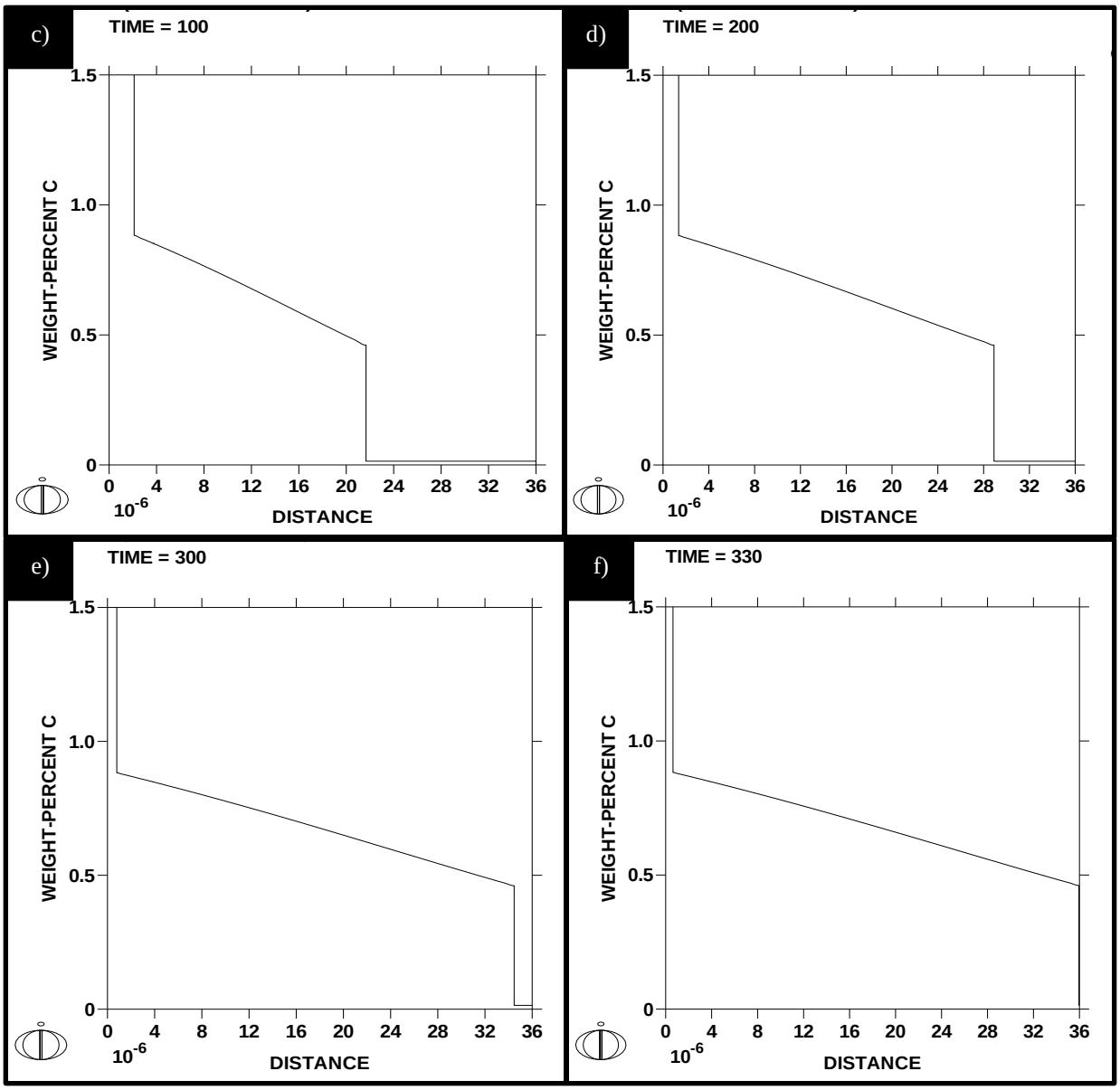


Figure 4.12: (a–f) Result window of DICTRA simulations showing weight percent carbon as a function of distance, at a given annealing temperature of 800 ℃ and heating rate of 50 ℃/s. DISTANCE = distance from original cementite lamella of initial pearlite mixture, in micron.

Table 4.4 presents the results of holding time periods predicted for complete dissolution of pearlite to austenite at a given annealing temperature and heating rate (see Appendix-V for actual distance of austenite formed by DICTRA simulations at different annealing temperatures for different heating rates).

Table 4.4: Holding time periods for complete transformation of pearlite to austenite at a given annealing temperature and heating rate.

| Heating rate (℃/*s*) | Holding time period (s) at annealing temperature of | | | | | | | | | |
|---|---|---|---|---|---|---|---|---|---|---|
| | 750 ℃ | | 775 ℃ | | 800 ℃ | | 825 ℃ | | 850 ℃ | |
| | Step1* | Step 2# | Step 1* | Step 2# | Step 1* | Step 2# | Step 1* | Step 2# | Step 1* | Step 2# |
| 10 | 72.3 | 1038 | 74.8 | 327 | 77.3 | 141 | 79.8 | 67 | 82.3 | 32 |
| 20 | 36.15 | 1043 | 37.4 | 328 | 38.65 | 142 | 39.9 | 68 | 41.15 | 33 |
| 50 | 14.46 | 1043 | 14.96 | 330 | 15.46 | 143 | 15.96 | 67 | 16.46 | 31 |
| 100 | 7.23 | 1043 | 7.48 | 329 | 7.73 | 144 | 7.98 | 70 | 8.23 | 36 |
| 200 | 3.62 | 1043 | 3.74 | 331 | 3.87 | 144 | 4 | 71 | 4.12 | 37 |
| 300 | 2.41 | 1043 | 2.49 | 330 | 2.58 | 144 | 2.66 | 71 | 2.74 | 38 |
| 400 | 1.81 | 1043 | 1.87 | 330 | 1.93 | 144 | 2 | 71 | 2.06 | 38 |
| 500 | 1.45 | 1043 | 1.5 | 330 | 1.55 | 144 | 1.6 | 71 | 1.65 | 38 |
| • Time required to reach the annealing temperature from room temperature (300 K) following a given heating rate.<br># Holding time required at a given annealing temperature for complete (100 %) dissolution of pearlite into austenite. | | | | | | | | | | |

# 4.5 Experiments to Validate the Simulation Results

Experiments were performed to validate the results obtained through DICTRA simulations. The simulations in the earlier sections were carried out for two different isothermal holding conditions. In the first type of conditions, the specimens reached a given annealing temperature through equilibrium heating and were then subjected to holding for complete dissolution of pearlite into austenite. In the second condition, the specimens reached a given annealing temperature through a specific heating rate (non-equilibrium conditions) and were then subjected to holding for complete dissolution of pearlite into austenite. For validating the former case, experiments were conducted in the annealing simulator, where for the latter case, experiments were conducted in a commercial simulator (Gleeble 3800).

## 4.5.1 Experiments to Validate DICTRA Simulations under Equilibrium Heating Conditions

Experiments were performed at annealing temperatures of 775, 800, 825, 850 ℃ respectively on the annealing simulator. For the annealing experiments, samples were heated to the desired annealing temperature at a very slow heating rate. They were held at this temperature for the holding time periods (323, 135, 66, and 36 s for annealing temperatures of 775, 800, 825, 850 ℃ respectively) as obtained from the DICTRA simulation results, and were finally quenched using nitrogen ($N_2$) + hydrogen ($H_2$). The samples were then prepared (etched with 2 % nital) for microstructural analysis using optical microscopy. SEM analysis was also conducted at the selected annealing temperatures to confirm the results of optical microscopy.

Figure 4.1**3** presents the optical micrographs of specimens annealed at various annealing temperatures.

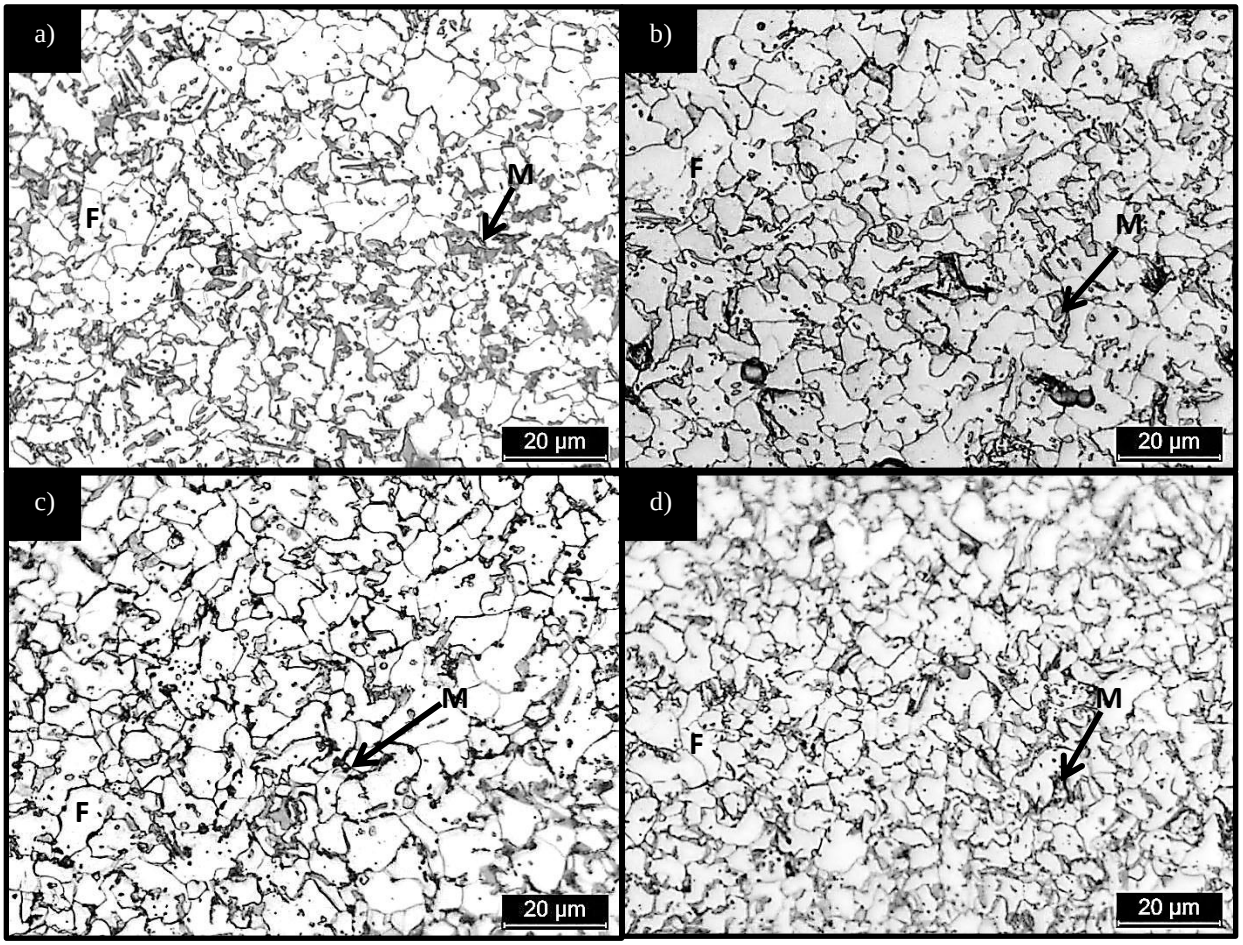


Figure 4.13: Optical micrographs of specimens subjected to isothermal holding in annealing simulator at temperatures of (a) 775, (b) 800, (c) 825, and (d) 850 ℃. F= ferrite and M= martensite

Figure 4.14 presents the SEM micrographs of specimens subjected to annealing at temperatures of 775 ℃ and 800 ℃ respectively. SEM images clearly show the presence of martensite in the microstructure.

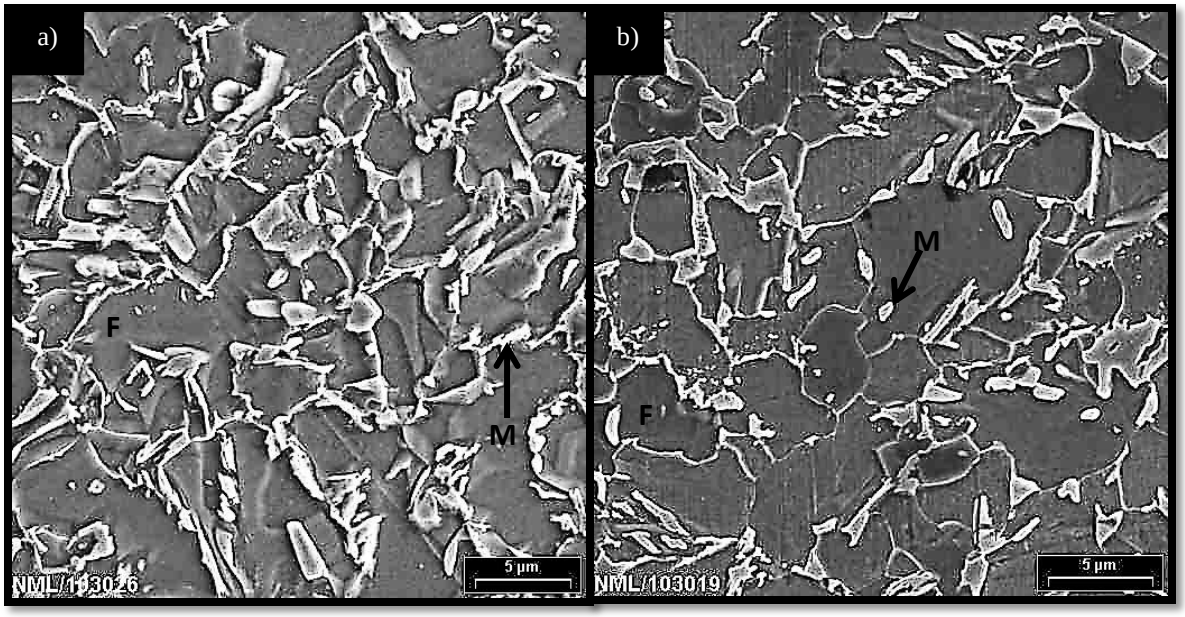


Figure 4.14: SEM micrographs of specimens subjected to isothermal holding at annealing temperatures of (a) 775 ℃, and (b) 800 ℃. F= ferrite and M= martensite

Martensite volume fraction (MVF) was calculated using 'analySIS FIVE' software for each annealing temperature. Table 4.5 presents volume fraction of martensite obtained at various annealing temperatures. The experimental results (with annealing for holding periods as provided by simulation results) gave almost similar microstructures (Fig. 4.13–4.14) showing complete dissolution of pearlite into austenite (as indicated by martensite volume fraction which is nearly same for all annealing temperatures, and is close the original pearlite volume fraction of 16.7 %. Thus, the experimental results show that if the as-received steel is annealed at a given annealing temperature with holding period (as obtained through simulation results), only pearlite dissolution into austenite occurs. Thus, this time period can be utilized for annealing the steel at a given annealing temperature. This time period will ensure that austenite is obtained just from pearlite dissolution. This austenite is always carbon rich (consequently leading to formation of martensite of better hardness).

### 4.5.2 Experiments to Validate DICTRA Simulations under Non-equilibrium Heating Conditions

Simulations for non-equilibrium conditions had been carried out in two different steps (see Section 4.4.2). The first step (Step-I) included simulations to investigate the effect of only

heating rates on the nucleation and formation of austenite, without considering the effect of holding periods at a given annealing temperature i.e. considering changes occurring only during the time required to heat the sample to the desired annealing temperature. The second step (Step-II) included simulations to investigate the effect of holding periods at a given annealing temperature on the nucleation and formation of austenite.

Table 4.5: Martensite volume fraction in steel at different annealing temperatures under equilibrium conditions.

| **Annealing temperature (℃)** | **Martensite volume fraction (%)** |
|---|---|
| 775 | 19 |
| 800 | 21 |
| 825 | 22 |
| 850 | 21 |

Experiments were initially performed at annealing temperatures of 775, 800, 825, 850 ℃ respectively on the Gleeble 3800 simulator, to validate the results of Step-I simulations. Though DICTRA simulations were carried out at various heating rates for each annealing temperature, the experimental validation was carried out for one of the heating rates only i.e. 20 $℃/s$. For the annealing experiments, samples were heated to the desired annealing temperature at a heating rate of 20 $℃/s$ (representing non-equilibrium heating conditions) followed by water quenching. Figure 4.15 and Figure 4.16 present the time-temperature profiles and optical micrographs respectively for different annealing temperatures reached by following the heating rate of 20 $℃/s$. Simulation results had predicted the austenite fraction (fraction of available pearlite, and not the fraction of total microstructure) in steel when heated to various temperatures with a specific heating rate. Table 4.3 showed the austenite fraction (fraction of available pearlite that transformed to austenite) as 4.94, 13.55, 21.22, and 29.81 % (i.e.0.83, 2.27, 3.56, and 5.00 % of the total microstructure) for annealing temperatures of 775, 800, 825, and 850 ℃ respectively for heating rate of 20 $℃/s$. Optical micrographs (see Fig. 4.16) showed presence of pearlite, ferrite, and martensite (martensite obtained through quenching of freshly formed austenite) in the microstructure of steel. This confirmed the simulation results that during heating of steel (for all annealing temperatures and heating rates), pearlite dissolution into austenite had started (confirmed by presence of martensite in all the micrographs).

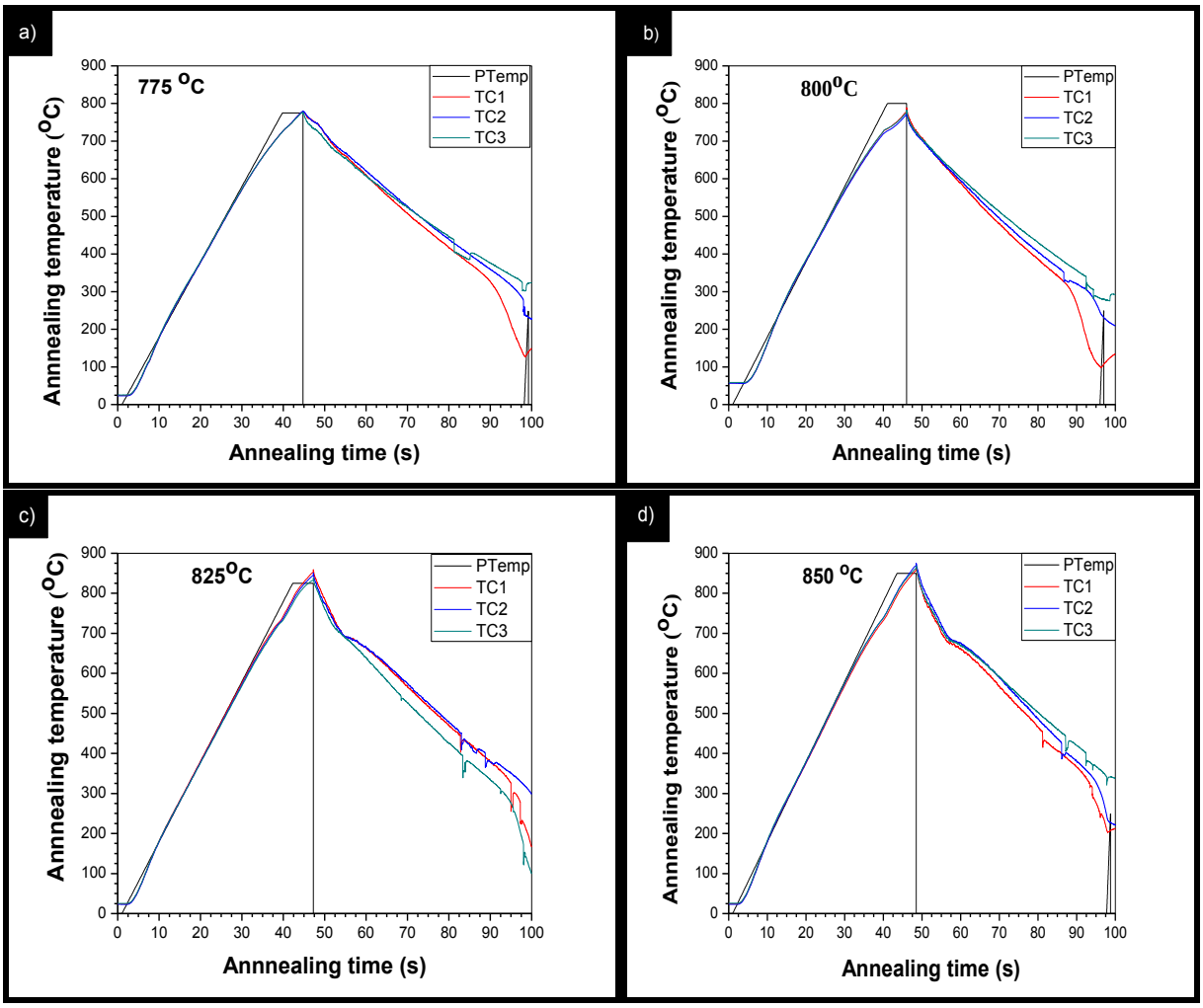


Figure 4.15: Time-temperature profiles with heating rate of 20 ℃/$s$ for annealing temperature of (a) 775, (b) 800, (c) 825, and (d) 850 ℃.

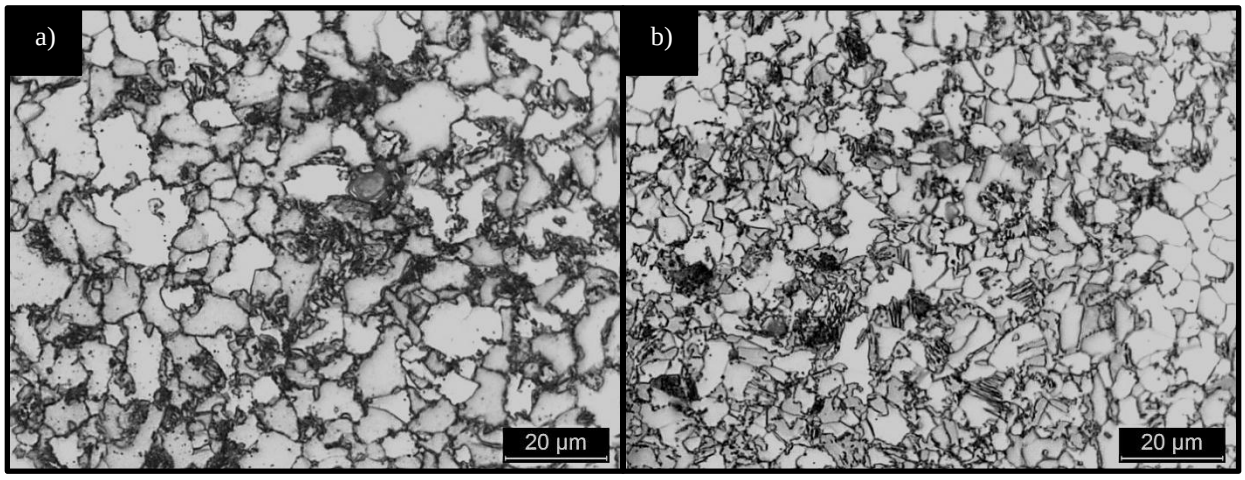

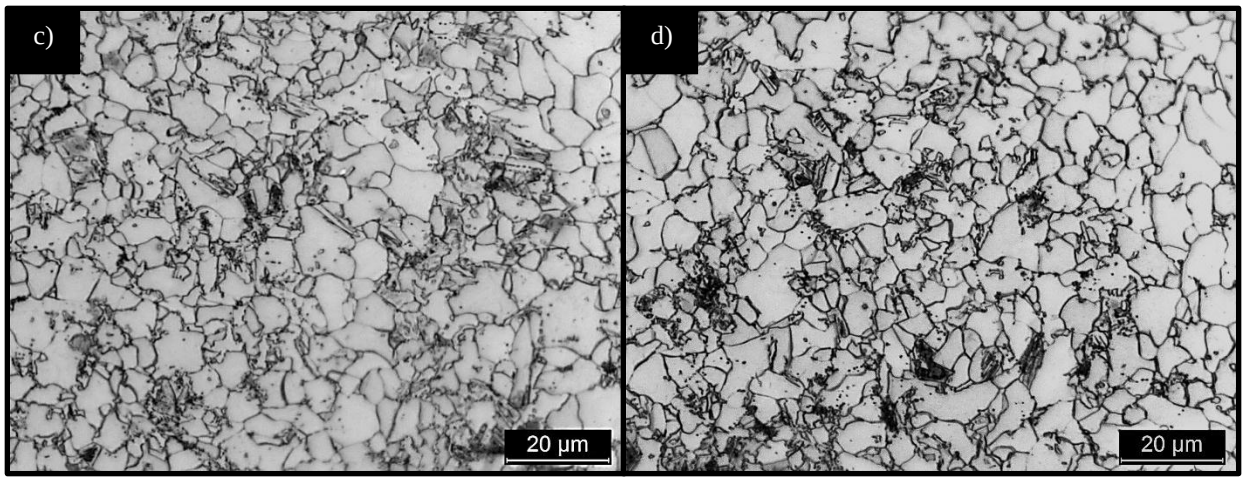


Figure 4.16: Optical micrographs of specimens for heating rate of 20 ℃/$s$ subjected to annealing temperatures of (a) 775, (b) 800, (c) 825, and (d) 850 ℃.

Since the austenite fraction was too low (< 5%) for all annealing temperature-heating rate conditions, the optical microscopy results were confirmed by SEM analysis (conducted for temperatures of 825 ℃ and 850 ℃ respectively; see Fig. 4.17).

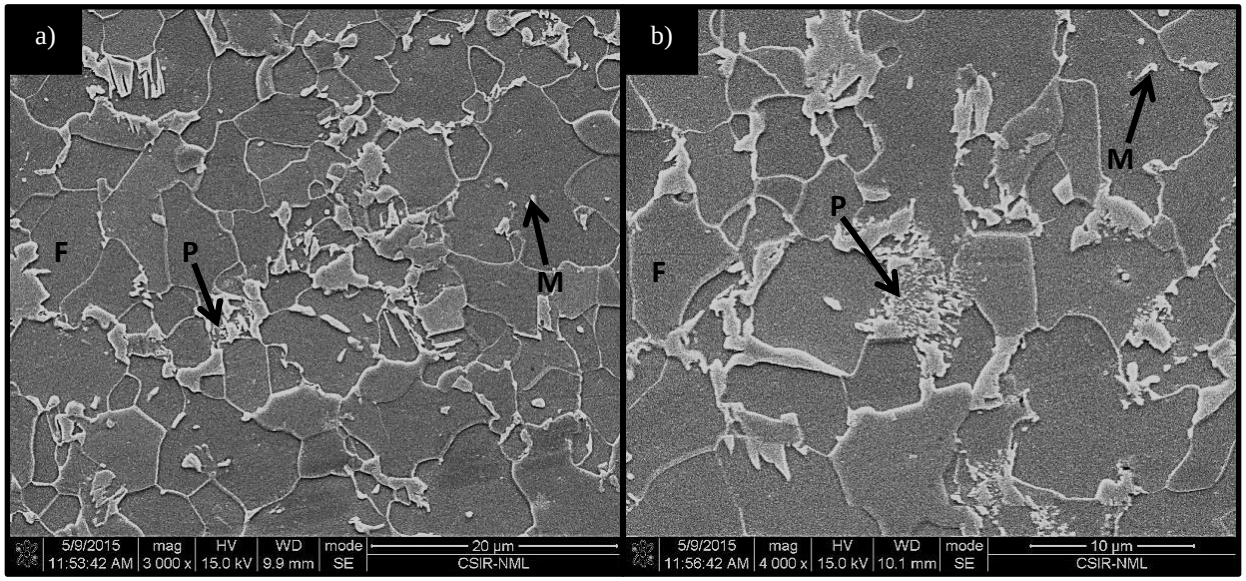


Figure 4.17: SEM micrographs of specimens for heating rate of 20 ℃/$s$ subjected to annealing temperatures of (a) 825, and (b) 850 ℃. F= ferrite, M= martensite and P= pearlite

Further, the experiments were performed at annealing temperatures of 800 ℃ and 825 ℃ respectively on the Gleeble 3800 simulator, to validate the results of Step-II simulations. Though DICTRA simulations were carried out at various temperatures and heating rates for each

annealing temperature, the experimental validation was carried out only for two temperatures (800 ℃ and 825 ℃) and one heating rate only (20 ℃/$s$). For the annealing experiments, samples were heated to the desired annealing temperature at a heating rate of 20 ℃/$s$ (representing non-equilibrium heating conditions), were held at the annealing temperature for a holding period (provided by the simulation results), and followed by water quenching. The samples were then prepared (etched with 2 % nital) for microstructural analysis using optical microscopy. Figure 4.18 and Figure 4.19 present the time-temperature profiles and optical micrographs respectively f or the selected annealing temperatures reached by following the heating rate of 20 ℃/$s$.

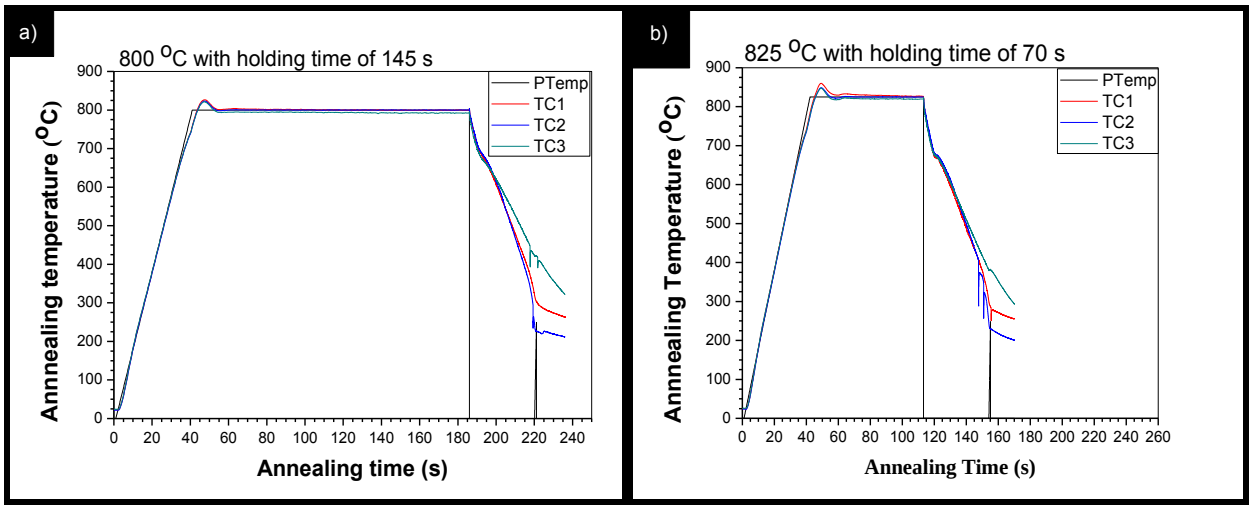


Figure 4.18: Time-temperature profiles of specimens for heating rate of 20 ℃/$s$ subjected to annealing temperatures of (a) 800 with holding time of 142 s, and (b) 825 ℃ with holding time of 68 $s$.

Table 4.4 showed the holding time periods for complete transformation of pearlite to austenite at a given annealing temperature and heating rate. For annealing temperatures of 800 ℃ and 825 ℃ with heating rate of 20 ℃/$s$, simulation results provided holding periods of 142 s and 68 s respectively for complete dissolution of pearlite into austenite phase. Optical micrographs (see Fig. 4.19) showed presence of ferrite, and martensite in the microstructure of steel, without presence any pearlite. This showed that with the given holding at the annealing temperatures, complete dissolution of pearlite to austenite had occurred, thus validating that the soaking period obtained through simulations was correct. Also, phase fraction measurements through analySIS provided martensite volume fractions in the two samples as 19.61% and 20.15% respectively,

which matched closely with initial pearlite content (16.78 %) in the as-received steel, thus further validating the simulation results.

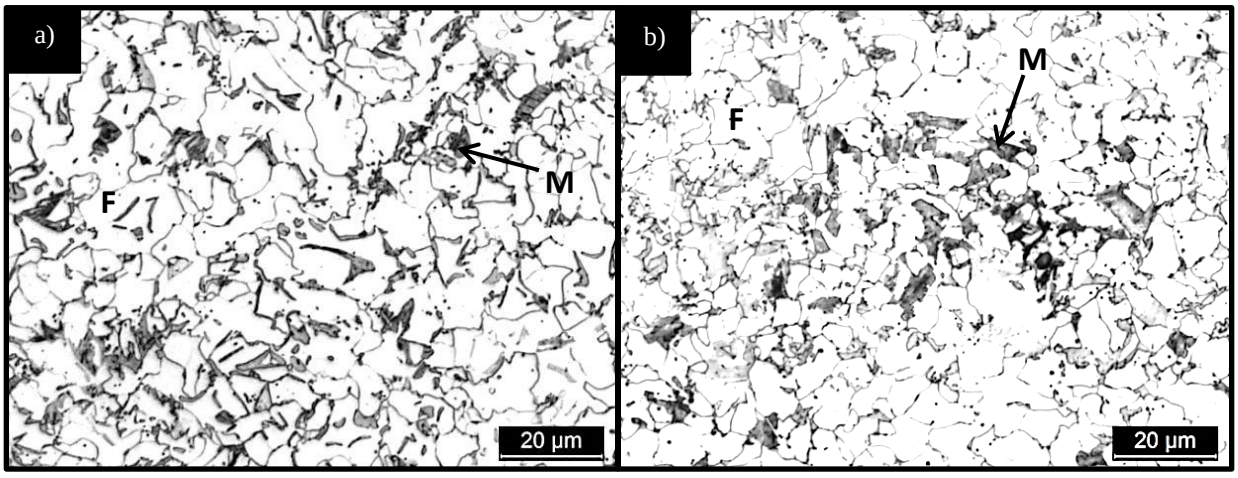


Figure 4.19: Optical micrographs of specimens for heating rate of 20 ℃/$s$ subjected to annealing temperatures of (a) 800 with holding time of 142 s, and (b) 825 ℃ with holding time of 68 $s$. F= ferrite and M= martensite

## 4.6 Experiments to Compare Simulation Results for Hot and Cold Rolled Steel

In the previous sections, experiments were conducted on hot rolled (as-received steel) specimens and it was observed that DICTRA simulation results (pertaining to holding time periods) hold good both under equilibrium and non-equilibrium heating conditions. In this section, experiments were performed to investigate if the simulation results hold good for cold rolled specimens also (or not). For this purpose, experiments were now conducted separately for the hot rolled and cold rolled steel specimens (in the annealing simulator) for different annealing temperatures following one of the heating rates (here, 10 ℃/$s$). The specimens were heated at 10 ℃/$s$ to the desired heat treatment temperature, were soaked here for a holding period obtained through simulation results (Table 4.4) and were finally quenched (through a gas mixture of $H_2$ + $N_2$) to room temperature. Annealing experiments were performed at 775, 800, 825, and 840 ℃ with holding periods of 330, 130, 65, and 40 s respectively, for both hot rolled and cold rolled steel specimens. After the treatment, the specimens were etched with nital (2% $HNO_3$ in 10 ml ethanol). To confirm the presence of phases identified through nital etching, colour etching was

done using picral (pre-etched in 0.4 g picric acid in 10 ml ethanol for 60 s and finally etched in solution of 1 g sodium meta bisulphate ($Na_2S_3O_5$) in 10 ml distilled water). Optical micrographs were analyzed to compare the volume fraction of austenite obtained in the hot rolled and cold rolled specimens treated at various temperatures for the case of 10 ℃/$s$ heating rate. Further, the size distribution of constituent phases, for both cold rolled and hot rolled steel specimens at different annealing temperatures (with heating rate of 10 ℃/$s$) was compared.

Figure 4.20 shows the optical micrographs of hot rolled steel specimens (etched with nital and picral respectively) for 775, 800, 825, and 840 ℃ respectively.

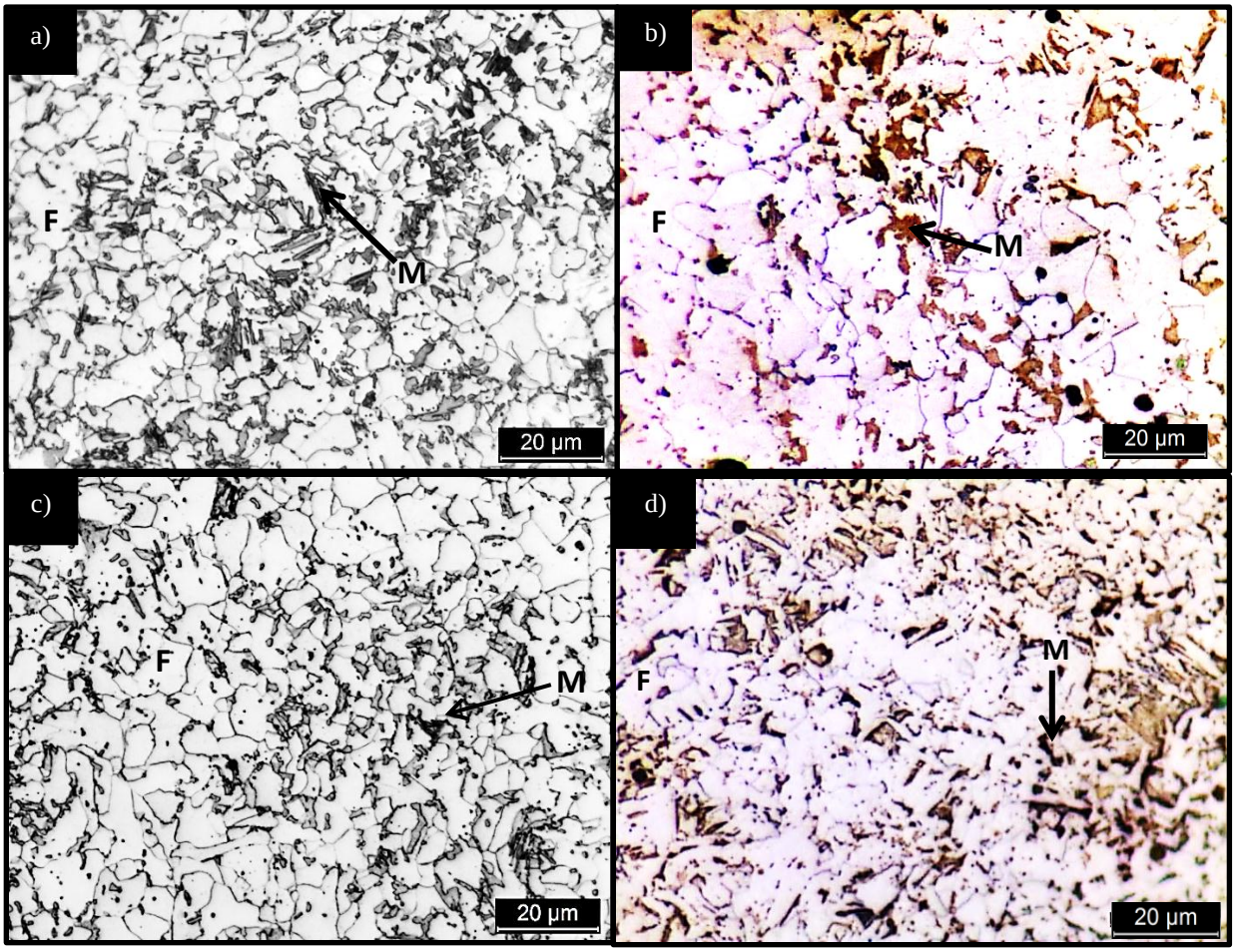

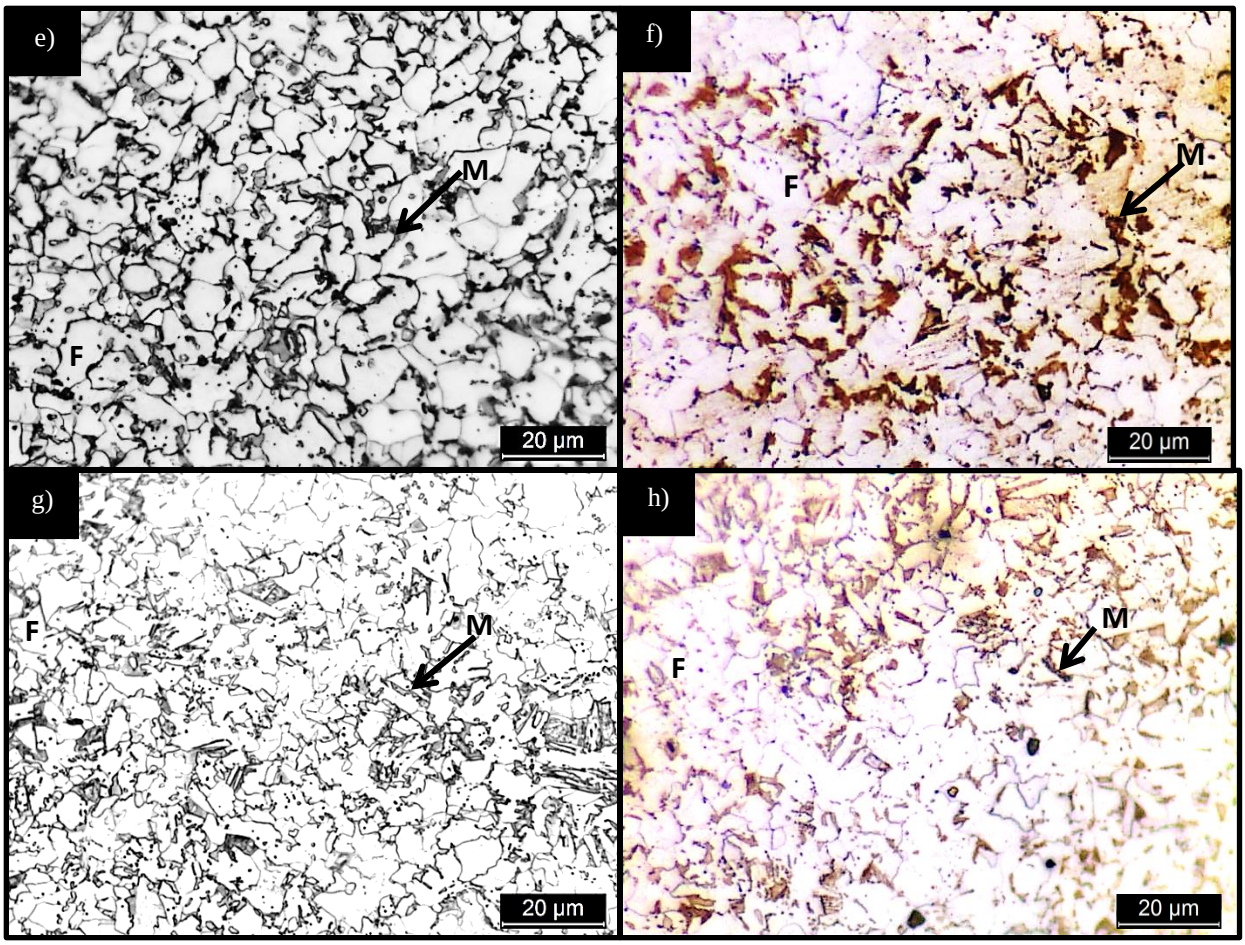


Figure 4.20: Optical micrographs of hot rolled steel specimens for 775, 800, 825, and 840 ℃ etched with (a, c, e, g) nital, and (b, d, f, h) picral. F= ferrite and M= martensite

Figure 4.21 shows the optical micrographs of cold rolled steel specimens (etched with nital and picral respectively) for 775, 800, 825, and 840 ℃ respectively.

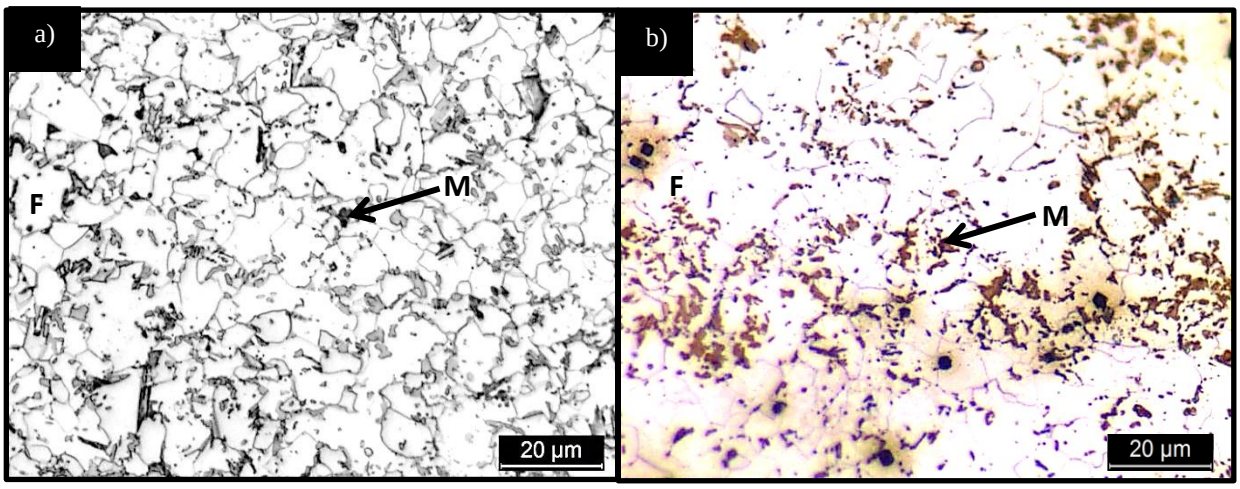

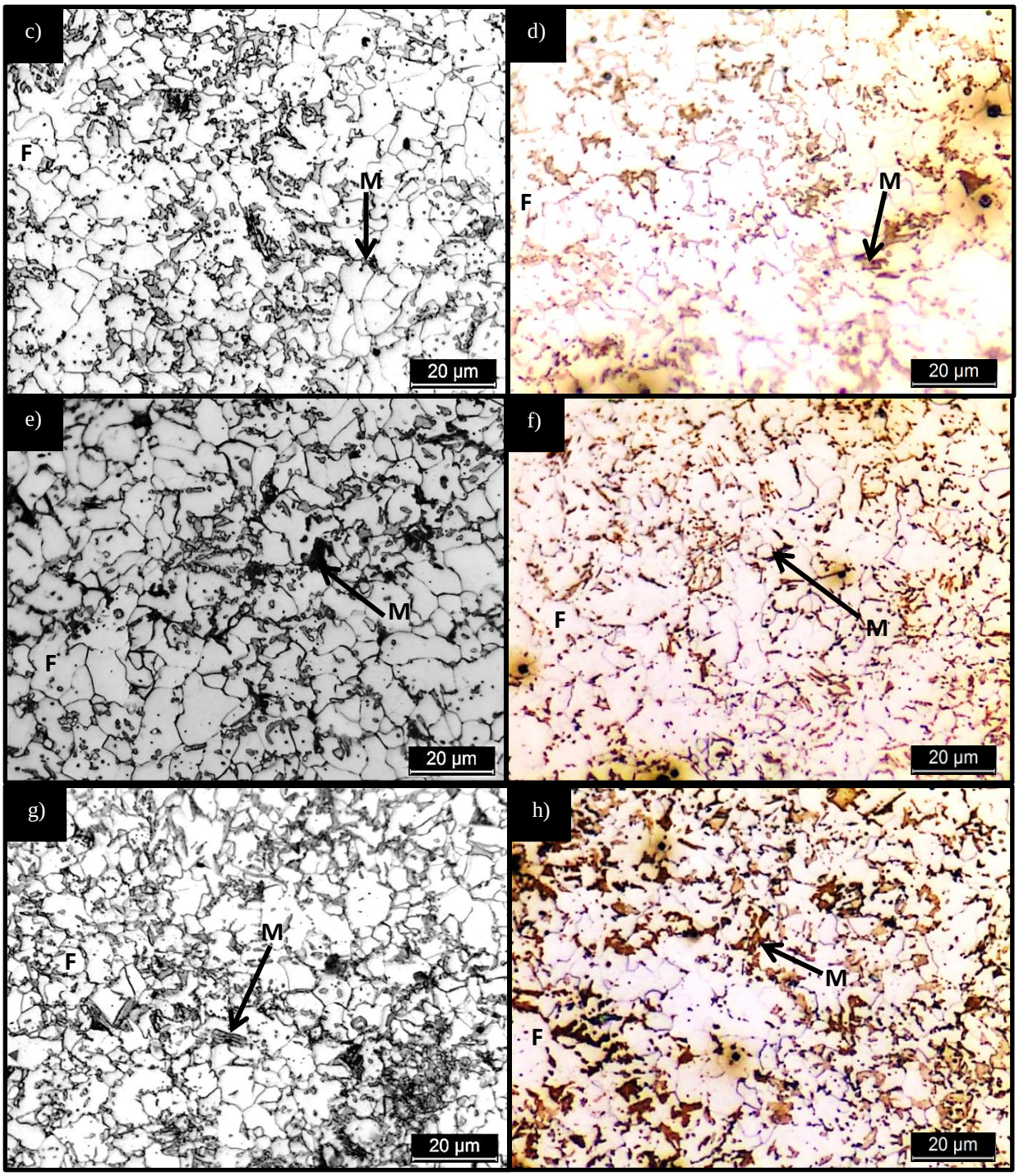


Figure 4.21: Optical micrographs of cold rolled steel specimens for 775, 800, 825, and 840 ℃ etched with (a, c, e, g) nital, and (b, d, f, h) picral. F= ferrite and M= martensite

Table 4.6 summarizes and compares the results with regards to volume fraction of austenite obtained in the hot rolled and cold rolled specimens treated at various temperatures for the case of 10 ℃/$s$ heating rate.

Table 4.6: Comparison of austenite fraction in hot rolled and cold rolled steel specimens.

| **Annealing temperature (℃)** | **Heating Rate (℃/$s$)** | **Holding time obtained from simulation ($s$)** | **Volume fraction of austenite in steel (%)** | | |
|---|---|---|---|---|---|
| | | | **Simulation** | **Hot rolled** | **Cold rolled** |
| 775 | 10 | 330 | 16.78 | 20.18 | 23.58 |
| 800 | 10 | 130 | 16.78 | 21.86 | 26.62 |
| 825 | 10 | 65 | 16.78 | 19.24 | 28.17 |
| 840 | 10 | 40 | 16.78 | 20.24 | 30.24 |

It can be noted again that volume fractions of austenite in steel obtained through simulation results and obtained through experiments in hot rolled steel show a good agreement. However, the austenite fraction in cold rolled specimens (obtained through experiments), for a given condition is considerably different (higher) as compared to hot rolled steel (and simulation results). This is because the recrystallization kinetics in case of cold rolled steel is much faster than that in hot rolled steel [Zheng and Raabe 2013].

Figure 4.22 compares the size distributions of constituent phases for the hot and cold rolled specimens annealed at 840 ℃ (for other annealing temperatures, see Appendix VI).

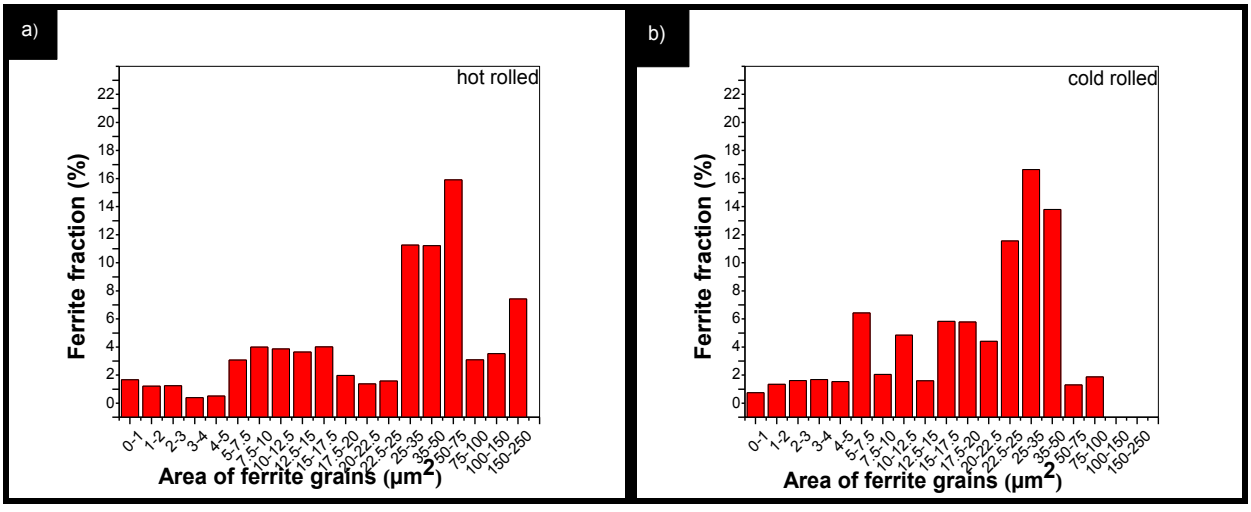

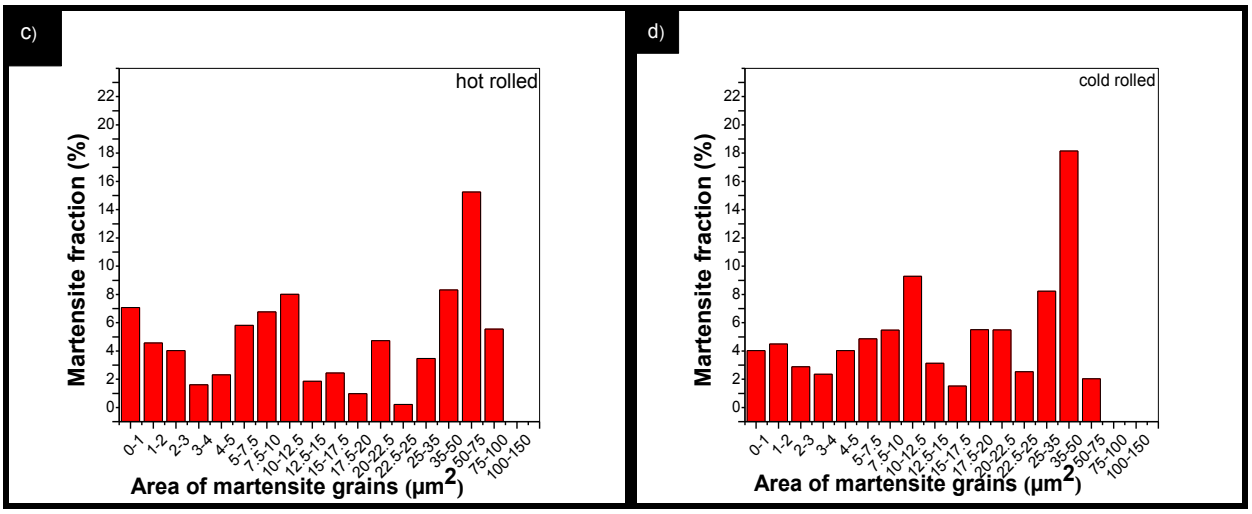


Figure 4.22: Size distribution of phases for annealing temperature of 840 ℃ in (a, b) hot rolled, and (c, d) cold rolled.

Ferrite phase in the as-received hot rolled steel specimen showed a distribution skewed towards relatively coarse grained size (most of the grains were in the size range of 25–400 μm$^2$; see Fig. 4.2b) while that for the annealed (hot rolled) specimens, the grains obtained were relatively finer (shifted towards smaller size ranges; see Fig. 4.22c and Appendix-VI). Further, it was observed that the size distribution of ferrite phase in the cold rolled annealed specimens was still finer (compared to both as-received and hot rolled annealed). Similarly, comparing the size distributions for martensite phase, it was observed that relatively finer grains were observed with cold rolled annealed specimens. This is because the recrystallization kinetics in case of cold rolled steel is much faster than that in hot rolled steel [Zheng and Raabe 2013].

## 4.7 Effect of Ferrite and Martensite Distribution on Tensile Properties

Tensile tests were performed for the as-received as well as annealed (both hot and cold rolled) specimens. Figure 4.23 and Table 4.7 present the results of tensile testing. In the present work, it was observed that the simulation results accurately predicted the holding time periods required for complete pearlite dissolution during annealing of the hot rolled steel.

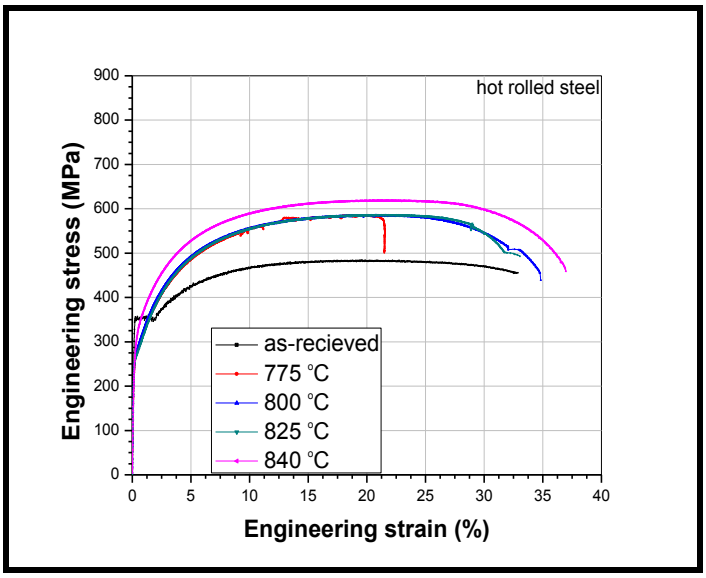


Figure 4.23: Engineering stress strain plots for specimens under different conditions (a) hot rolled, and (b) cold rolled.

This section discusses the results of tensile testing to establish that annealing of the hot rolled as-received steel leading to complete dissolution of pearlite (of the initial microstructure) results in improved combinations of strength and ductility in the annealed steel (by formation of carbon rich austenite and hence martensite).

Table 4.7: Results of tensile tests for hot rolled steel at different annealing temperatures.

| **Annealing Temperature (℃)** | **Hot rolled steel** | |
|---|---|---|
| | **TE (%)** | **UTS (MPa)** |
| 775 | 22 | 590 |
| 800 | 33 | 590 |
| 825 | 33 | 590 |
| 840 | 35 | 610 |

The as-received hot rolled steel showed a moderate strength-percent elongation combination with a UTS and percent elongation of 490 MPa and 33 % respectively. For the hot rolled specimens annealed at various temperatures (with holding time periods as predicted through simulation results), a considerable improvement in strength-percent elongation combinations were observed. The best combination of properties was achieved at an annealing temperature of 840 ℃ (UTS ~ 610 MPa; total elongation, TE ~ 35%).

# Chapter 5

# Conclusions

## 5.1 General

DP steels play a vital role in industrial applications e.g. automobile industry. In DP steels, strength is provided by martensite phase and ductility is provided by ferrite phase. In the present work, DICTRA simulations were performed for calculating the holding time for complete pearlite dissolution (formation of carbon rich austenite) during inter-critical annealing of a hot rolled steel. Time is an important parameter when dealing with industrial applications. Industries are always searching for a annealing path where heating rates are as high as possible and the holding times are as short as possible. So, the predictions for pearlite dissolution time can help in determining various processing parameters (annealing temperature, holding time etc.) for industry. This, in turn, could make the continuous annealing process short and efficient. Simulation results were validated through actual annealing experiments at various annealing temperatures with holding periods as predicted through simulations. Simulation results were found to be correct and the holding time periods predicted improved the mechanical properties appreciably.

## 5.2 Results and Conclusions

The main results and conclusions from the present experimental work are as follows:

**As-received material**

- The microstructure of the hot rolled as-received steel comprised of lamellar pearlite colonies (16.78 %) and pro-eutectoid ferrite (no deformed ferrite).
- The microstructure of the cold rolled as-received steel had distorted pearlite colonies. The ferrite present in the steel was highly deformed.

**DICTRA simulations for pearlite dissolution under equilibrium heating conditions**

- Complete pearlite dissolution time (soaking time at the annealing temperature) for the hot band steel was calculated for equilibrium conditions using DICTRA software. It was

observed that holding time required at a given annealing temperature decreases with increase in annealing temperature (for increase in annealing temperature from 750 to 850 ℃, the holding time predicted decreased from 1005 to 36 s).

- As the annealing temperature increased, the difference of carbon concentrations at the two interfaces $Fe_3C$ /γ and γ /α also increased. Also, the austenite formed near the $Fe_3C$ /γ interface was of higher carbon concentration as compared to that present at γ /α interface.

**DICTRA simulations for effect of heating rates on pearlite dissolution**

- DICTRA simulations were performed for different heating rates viz. 10, 20, 50, 100, 200, 300, 400, and 500 $℃/s$. Simulations results showed that a small amount of pearlite transformed to austenite when the specimens were subjected to different annealing temperature-heating rate combinations. For a given heating rate, the austenite fraction formed during heating was dependent upon the annealing temperature. As the annealing temperature increased, for a given heating rate, the austenite fraction also increased. For example, at a heating rate of 20 $℃/s$, for increase in annealing temperature from 750 to 850 ℃, the austenite fraction (predicted) increased from 1.22 to 29.81% (fraction of pearlite transformed to austenite).
- DICTRA simulation results showed that at a given annealing temperature, the austenite fraction formed during heating was dependent upon the heating rate. As the heating rate increased, for a given annealing temperature, the austenite fraction decreased. For example, at a annealing temperature of 800 ℃, for increase in the heating rate from 10 to 500 $℃/s$, the austenite fraction (predicted) decreased from 16.27 to 4.00 % (fraction of pearlite transformed to austenite).
- DICTRA simulations also predicted that irrespective of the heating rate followed for a given annealing temperature, the holding time required for complete pearlite dissolution was approximately the same.

**Experiments to validate DICTRA simulations (equilibrium/ non-equilibrium conditions)**

- Optical micrographs revealed that volume fraction of austenite obtained through simulation results and that through actual annealing experiments for the hot rolled steel showed a good

agreement (for annealing temperature of 800 ℃, the volume fraction of martensite observed in the annealed steel was 21% which was close to the 16.78% fraction of pearlite in the as-received steel).

- SEM microscopy revealed the presence of both martensite and pearlite (at annealing temperature of 825 ℃; heating rate of 20 $℃/s$), validating the simulations that a small amount of pearlite transformed to austenite when the specimens were subjected to different annealing temperature-heating rate combinations.

**Experiments to compare simulation results for hot and cold rolled steel**

- Optical micrographs revealed that volume fractions of austenite obtained through experiments and obtained through simulation results in hot rolled steel showed a good agreement. However, the austenite fraction in cold rolled specimens (obtained through experiments), for a given condition was considerably higher, as compared to hot rolled steel (and simulation results).
- The size distribution of ferrite phase in the cold rolled annealed specimens was finer as compared to the hot rolled steel. Similarly, for martensite phase, finer grains were observed with cold rolled annealed specimens.
- The simulation results accurately predicted the holding time periods required for complete pearlite dissolution during annealing of the hot rolled steel. However, for the cold rolled steel, simulation results over estimated the holding time. With the predicted time, the cold rolled steel developed more volume fraction of austenite than could be obtained by complete dissolution of pearlite.

**Effect of ferrite and martensite distribution on Tensile Properties evaluation**

- The as-received hot rolled steel showed a moderate strength-percent elongation combination (490 MPa, 33 %) while for hot rolled specimens annealed at various temperatures (with holding time periods as predicted through simulation results), a considerable improvement in strength-percent elongation combinations was observed for most of the annealing temperatures (590–610 MPa, 33-35 %).
- The best combination of properties was achieved at an annealing temperature of 840 ℃ (UTS ~ 610 MPa; total elongation, TE ~ 35%) for the hot rolled annealed steel.

## 5.3 Major Conclusions and Recommendations

- The simulations could establish correctly the time required for complete dissolution of pearlite; this is important for continuous annealing processes which run at very small isothermal holding times.
- The simulations could establish the effect of heating rate, annealing temperature and holding time periods on pearlite dissolution and austenite formation in a hot rolled steel which in turn governs the volume fraction of martensite, its size and distribution.

## 5.4 Scope of Future Work

In the present work, the holding time taken for pearlite dissolution at a given annealing temperature and heating rate has been calculated by DICTRA simulations. Simulation results were validated by subsequent annealing experiments for the hot rolled steel. However, the effect of cold deformation in the as-received steel on pearlite dissolution has not been studied. The cold rolled material has deformed structure and broken pearlite colonies. The initial strain in the cold rolled material increases the kinetics pearlite dissolution i.e. deformation accelerates the kinetics of austenite formation, and thus, for the same time periods at a given temperature and heating rate, the fraction of austenite formed in the cold rolled material is more as compared to that of hot rolled. For DICTRA simulations of cold rolled materials, the effect of deformation behaviour on pearlite dissolution needs to be studied and incorporated in the simulation module. The advanced techniques viz. TEM, EBSD etc. can be utilized further to study the effect of martensite distribution and shape etc. on mechanical properties of steels.

# References


- Adamczyk, J., Grajcar, A. (2006), 'Effect of heat treatment conditions on the structure and mechanical properties of DP-type steel', *Journal of Achievements in Materials and Manufacturing Engineering*, Vol. *17*, pp. 305–308.
- Ahmad, E., Manzoor, T., Hussain, N., Qazi, N.K. (2008), 'Effect of thermo-mechanical processing on hardenability and tensile fracture of dual-phase steel', *Materials and Design*, Vol. *29*, pp. 450–457.
- Armaki, H. G., Maab, R., Bhat, S.P., Sriram, S., Greer, J.R. and Kumar K.S. (2014), 'Deformation response of ferrite and martensite in a dual-phase steel', *Acta Materialia*, Vol. 62, pp. 197–211.
- Bhattacharya, D. (2006) Developments in advanced high strength steels. *Presented at Advanced High Strength Steel Workshop*, Arlington, Virginia, USA, pp. 22–23.
- Cai, X., Liu, C., and Liu, Z. (2014), 'Process design and prediction of mechanical properties of dual phase steels with prepositional ultra-fast cooling', *Material and Design*, Vol. *53*, pp. 998–1004.
- Calcagnotto, M., Ponge, D., and Rabbe, D. (2010), 'Effect of grain refinement to 1μm on strength and toughness of dual-phase steels', *Materials Science and Engineering A*, Vol. *527*, pp. 7832–7840.
- Cornet, X. and Herman, J. C. 'Method for making a multiphase hot-rolled steel strip',*U.S. Patent 0041933 A1*, March 6, 2003.
- Demir, B. and Erdogan, M. (2008), 'The hardenability of austenite with different alloy content and dispersion in dual-phase steels', *Journal of Materials Processing Technology*, Vol. 208, pp. 75–84.
- Dziedzic, M. and Turczyn, S. (2010), 'Experimental and numerical investigation of strip rolling from dual phase steel', *Archives of Civil and Mechanical Engineering*, Vol. *10*, pp. 21–30.
- Erdogan, M. and Tekeli, S. (2002), 'The effect of martensite particle size on tensile fracture of surface-carburized AISI 8620 steel with dual phase core microstructure',*Materials and Design*, Vol. 23, pp. 597–604.
- Hairer, F., Karelova, A., Krempaszky, C., Werner, E., Hebesberger, T. and Pichler, A.

(2010), 'Etching techniques for the microstructural characterization of complex phase steels by light microscopy', *Mechanics of High Performance Alloys,* pp. 50–54.

- Han, Q., Kang Y., Zhao X., Stanford, N. and Cai, M. (2013), 'Suppression of Ms temperature by carbon partitioning from carbon-supersaturated ferrite to metastable austenite during intercritical annealing', *Materials and Design,* Vol. 51, pp.409–414.
- Homberg, D., Krumbiegel, K. and Togobytska, N. 'Modelling, simulation and control of multiphase steel production', presented at *19th International Congress on Modeling and Simulation, Perth, Australia,* 12–16 December, 2011.
- Katsamas, A. I. (2007), 'A computational study of austenite formation kinetics in rapidly heated steels', *Surface & Coatings Technology,* Vol. 201, pp.6414–6422.
- Kumar, A., Singh, S.B. and Ray, K.K. (2008), 'Influence of bainite/martensite-content on the tensile properties of low carbon dual-phase steels', *Materials Science and Engineering: A,* Vol. 474, pp. 270–282.
- Kuziak, R., Kawalla, R. and Waengler, S. (2008), 'Advanced high strength steels for automotive industry', *Archives of Civil and Mechanical Engineering,* Vol. 8, pp.103–117.
- Li, P., Li, J., Meng, Q., Hu, W.; Xu, D. (2013), 'Effect of heating rate on ferrite recrystallization and austenite formation of cold-roll dual phase steel', Journal of Alloys and Compounds, Vol. 578, pp. 320–327.
- Lorusso H, Burgueno A, Egidi D, Svoboda H. (2011) Application of dual phase steels in wires for reinforcement of concrete structures. *Proceedings of 11th International Congress on Metallurgy & Materials SAM/CONAMET*, Argentina.
- Matlock, D. K., Speer, J. G., Moor, E. D. and Gibbs, P. J. (2012), 'Recent developments in advanced high strength sheet steels for automotive applications: an overview', *JESTECH,* Vol. *15(1),* pp. 1–12.
- Mecozzi, M.G., Bosb, C. and Sietsmaa, J. (2015), 'A mixed-mode model for the ferrite-to-austenite transformation in a ferrite/pearlite microstructure', *Acta Materialia,* Vol. 88, pp. 302–313.
- Meng, Q., Li, J., Wang, J., Zhang, Z. and Zhang, L. (2009), 'Effect of water quenching process on microstructure and tensile properties of alloy cold rolled dual-phase steel', *Material and Design,* Vol. 30, pp. 2379–2385.

- Meng, Q., Li, J., Zheng, H. (2014), 'High-efficiency fast-heating annealing of a cold rolled dual-phase steel', *Materials and Design*, Vol. *58*, pp. 194-197.
- Mittal, M. (2014), 'Effect of Inter-critical Annealing Parameters on the Recrystallization, Austenite Formation and Stabilization in a Dual Phase Steel' , ME Thesis, Thapar University, Patiala.
- Mohapatra, S. S., Chakraborty, S. and Pal, S. K. (2012), 'Experimental studies on different cooling processes to achieve ultra-fast cooling rate for hot steel plate', *Experimental Heat Transfer,* Vol. 25, pp. 111–126.
- Mohrbacher, H. (2005), 'Modern steel grades and advanced steel semi-products for automotive body applications', *METAL*, Vol. 24.
- Parkes, D., Westerbaan, D., Nayak, S.S., Zhou, Y., Goodwin, F., Bhole, S. and Chen, D.L. (2014), 'Tensile properties of fiber laser welded joints of high strength low alloy and dual-phase steels at warm and low temperatures', *Materials and Design*, Vol. 56, pp. 193–199.
- Patel, J., Klinkenberg, C. and Hulka, K. (2001), 'Hot rolled HSLA strip steels for automotive and construction applications', *International symposium, Niobium; science & technology*, pp. 647-674.
- Ramazani, A., Bruehl, S., Gerber, T., Bleck, W. and Prahl, U. (2014), 'Quantification of bake hardening effect in DP600 and TRIP700 steels', *Materials and Design*, Vol. 57, pp.479–486.
- Saleh, M. H. and Priestner, R. (2001), 'Retained austenite in dual-phase silicon steels and its effect on mechanical properties', *Journal of Materials Processing Technology,* Vol. 113, pp. 587–593.
- Sayed, A.A. and Kheirandish, Sh. (2012), 'Affect of the tempering temperature on the microstructure and mechanical properties of dual phase steels', *Materials Science and Engineering: A*, Vol. 532, pp. 21–25.
- Seyedrezai, H., Pilkey, A.K. and Boyd, J.D. (2014), 'Effect of pre-IC annealing treatments on the final microstructure and work hardening behavior of a dual-phase steel', *Materials Science & Engineering A*, Vol. 594, pp.178–188.

- Shi, L., Yan, Z., Liu, Y., Zhang, C., Ning, B., Li, H. and Qiao, Z. (2014), 'Improved toughness and ductility in ferrite/acicular ferrite dual-phase steel through intercritical heat treatment', *Materials Science and Engineering A*, Vol. 590, pp.7–15.
- Sodjit, S. and Uthaisangsuk, V. (2011), 'High Strength Dual Phase Steels and Flow Curve Modeling Approach', The Second TSME International Conference on Mechanical Engineering, Krabi.
- Tan, W., Han, B., Wang, S. H., Yang, Y., Zhang, C. and Zhang Y. K. (2012), 'Effects of TMCP parameters on microstructure and mechanical properties of hot rolled economical dual phase steel in CSP', Journal of Iron and Steel Research, International, Vol. 19(6), pp. 37–41.
- Wang, J., Li, G. and Xiao, A. (2011), 'A Bainite-Ferrite Multi-Phase Steel Strengthened by Ti-Micro alloying', *Materials Transactions,* Vol. 52, pp. 2027–2031.
- Wang, W. and Wei, X. (2013), 'The effect of martensite volume and distribution on shear fracture propagation of 600–1000 MPa dual phase steels in the process of deep drawing', *International Journal of Mechanical Sciences,* Vol. *67*, pp. 100–107.
- Yong, T., Shuai, T., Bingxing, W., Zhaodong, W. and Guodong, W. (2012), 'Development and industrial application of ultra-fast cooling technology', *Science China Technological Science,* Vol. 55, pp. 1566–1571.
- Zakerinia, H., Kermanpur, A. and Najafizadeh, A. (2009), 'Color metallography: a suitable method for charecterization of martensite and bainite in multiphase steels', *International Journal of ISSI,* Vol. 6, pp. 14–18.
- Zheng, C. and Raabe, D. (2013), 'Interaction between recrystallization and phase transformation during intercritical annealing in a cold-rolled dual-phase steel: A cellular automaton model', *Acta Materialia,* Vol. 61, pp. 5504–5517.

# APPENDIX-I

Carbon percentages of $Fe_3C$/ γ and γ/ α interface during the conversion process at a given annealing temperature as a function of distance.

**A) 750** ℃

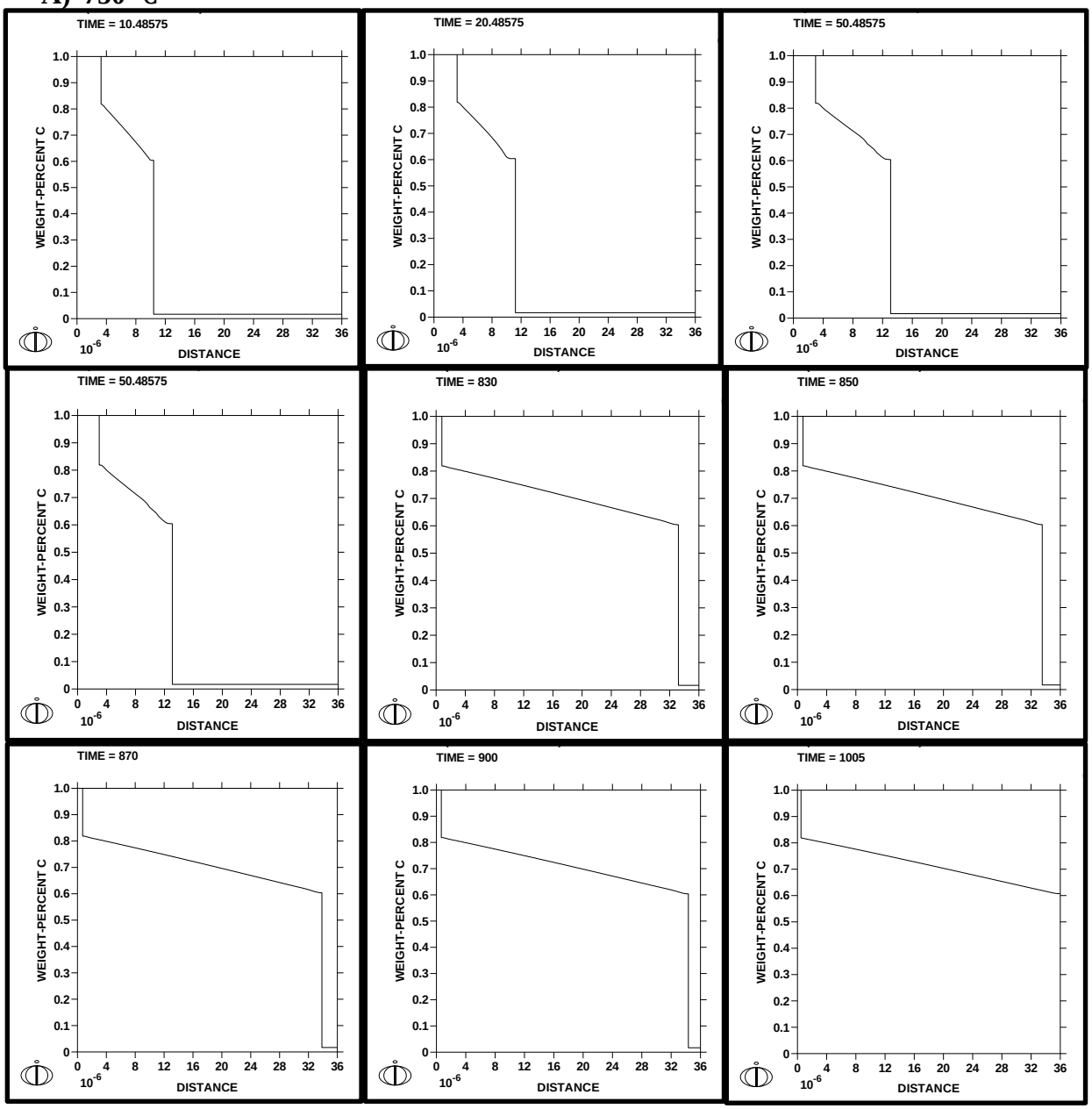

**B) 800** ℃

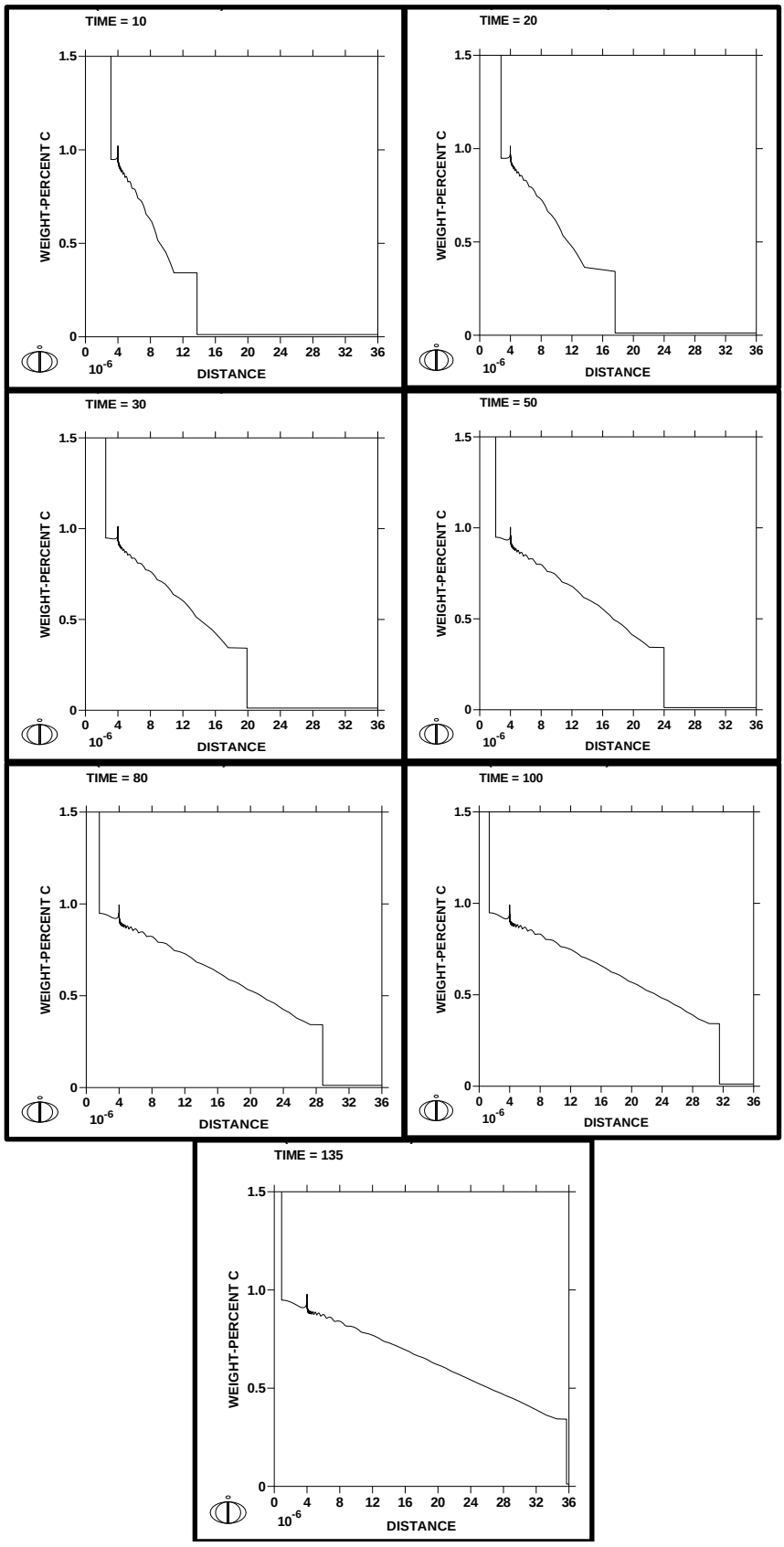
TIME = 10
TIME = 20
TIME = 30
TIME = 50
TIME = 80
TIME = 100
TIME = 135
WEIGHT-PERCENT C
1.5
1.0
0.5
0
0 4 8 12 16 20 24 28 32 36
10-6
DISTANCE

**C) 825 ℃**

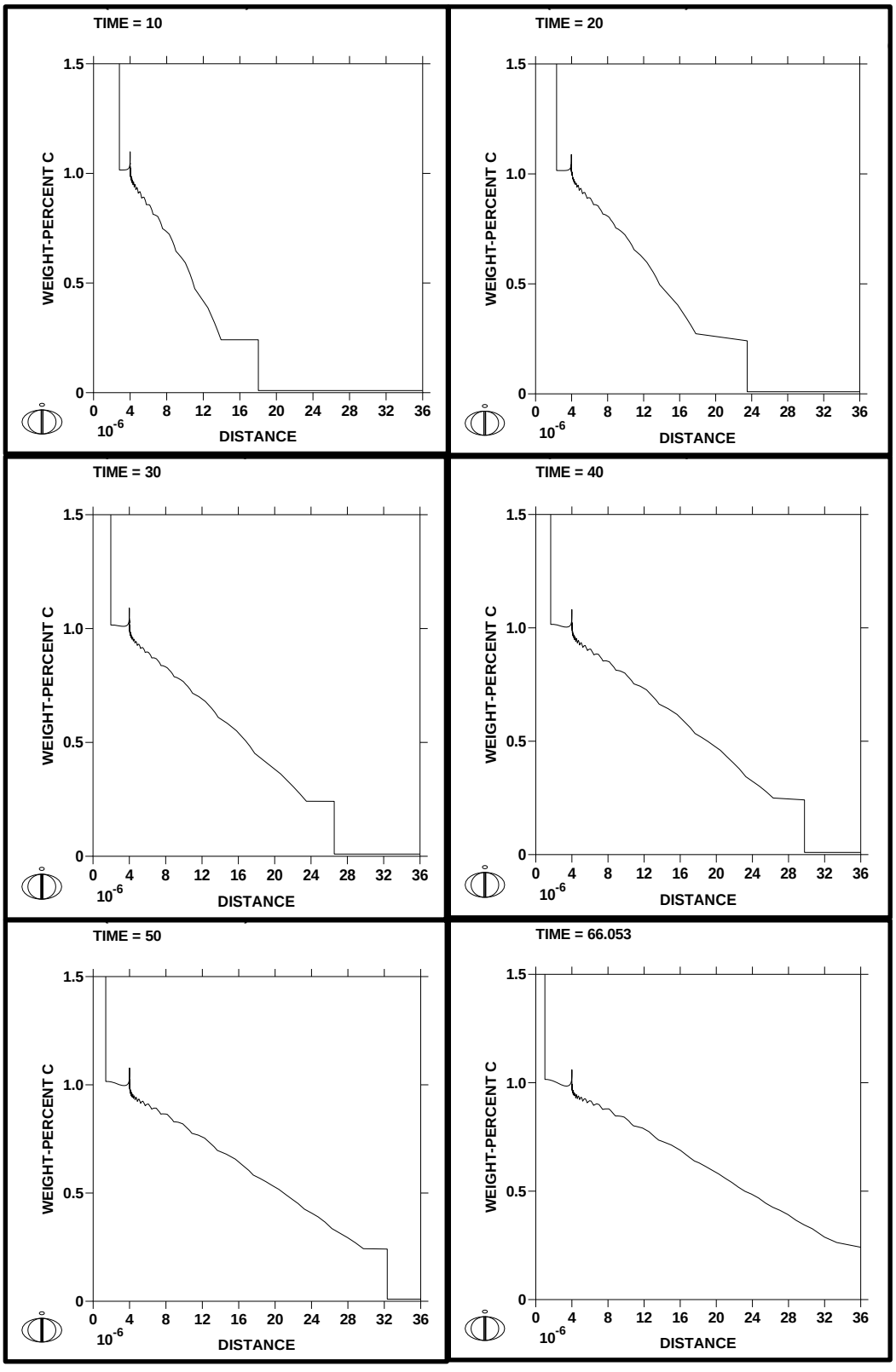
TIME = 10
TIME = 20
TIME = 30
TIME = 40
TIME = 50
TIME = 66.053
WEIGHT-PERCENT C
1.5
1.0
0.5
0
0 4 8 12 16 20 24 28 32 36
10-6
DISTANCE

**D) 850 ℃**

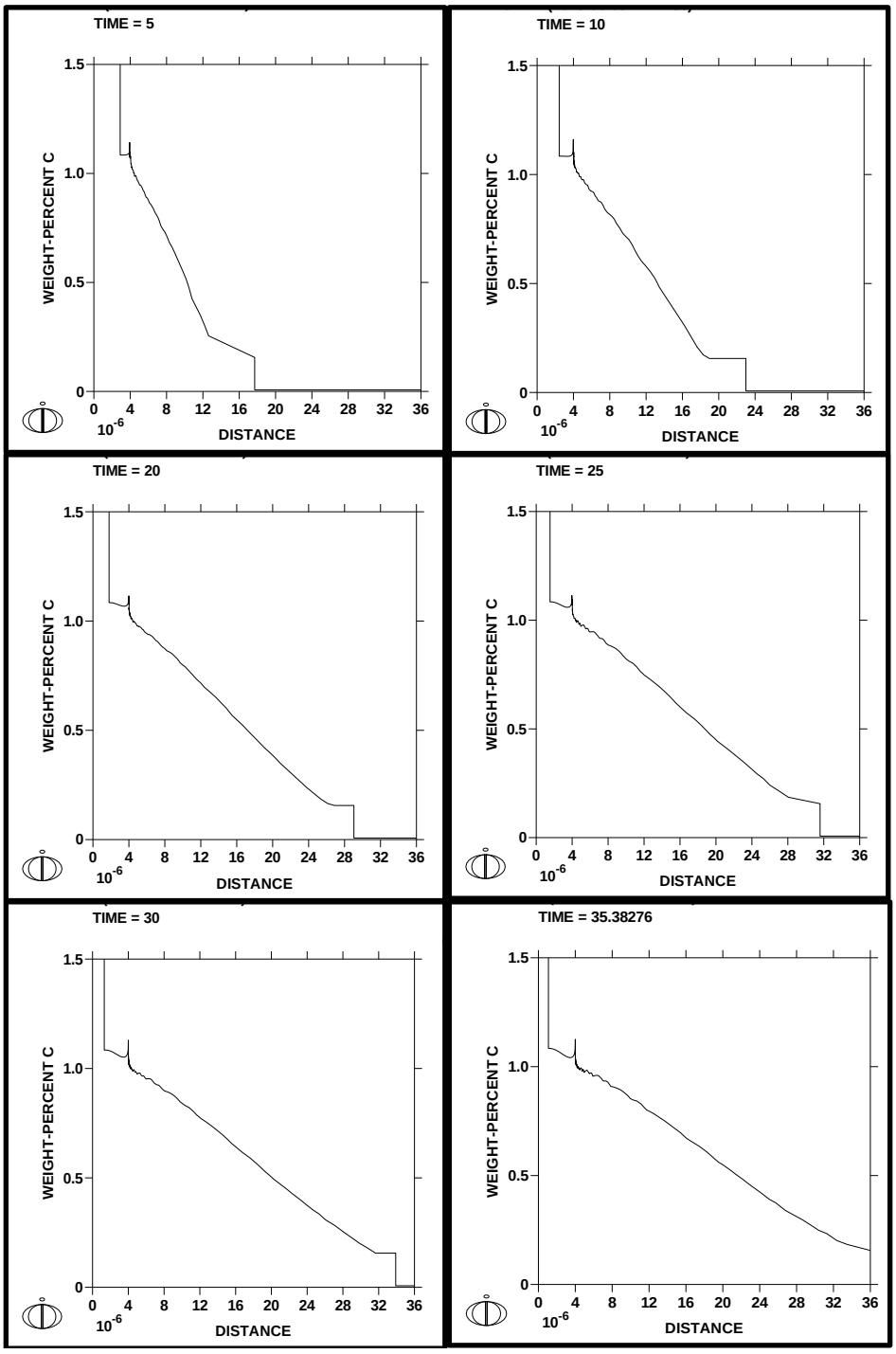
TIME = 5
TIME = 10
TIME = 20
TIME = 25
TIME = 30
TIME = 35.38276
WEIGHT-PERCENT C
1.5
1.0
0.5
0
0 4 8 12 16 20 24 28 32 36
10-6
DISTANCE

# APPENDIX-II

Result window of DICTRA simulations showing (step 1) weight percent carbon as a function of distance, at different heating rates (viz. 10, 20, 50, 100, 200, 300, 400, 500 ℃/$s$) at a constant temperature for different intercritical annealing temperatures viz. 750, 800, 85, 850 ℃. DISTANCE = distance from original cementite lamella of pearlite mixture in microns.

**A) 750** ℃

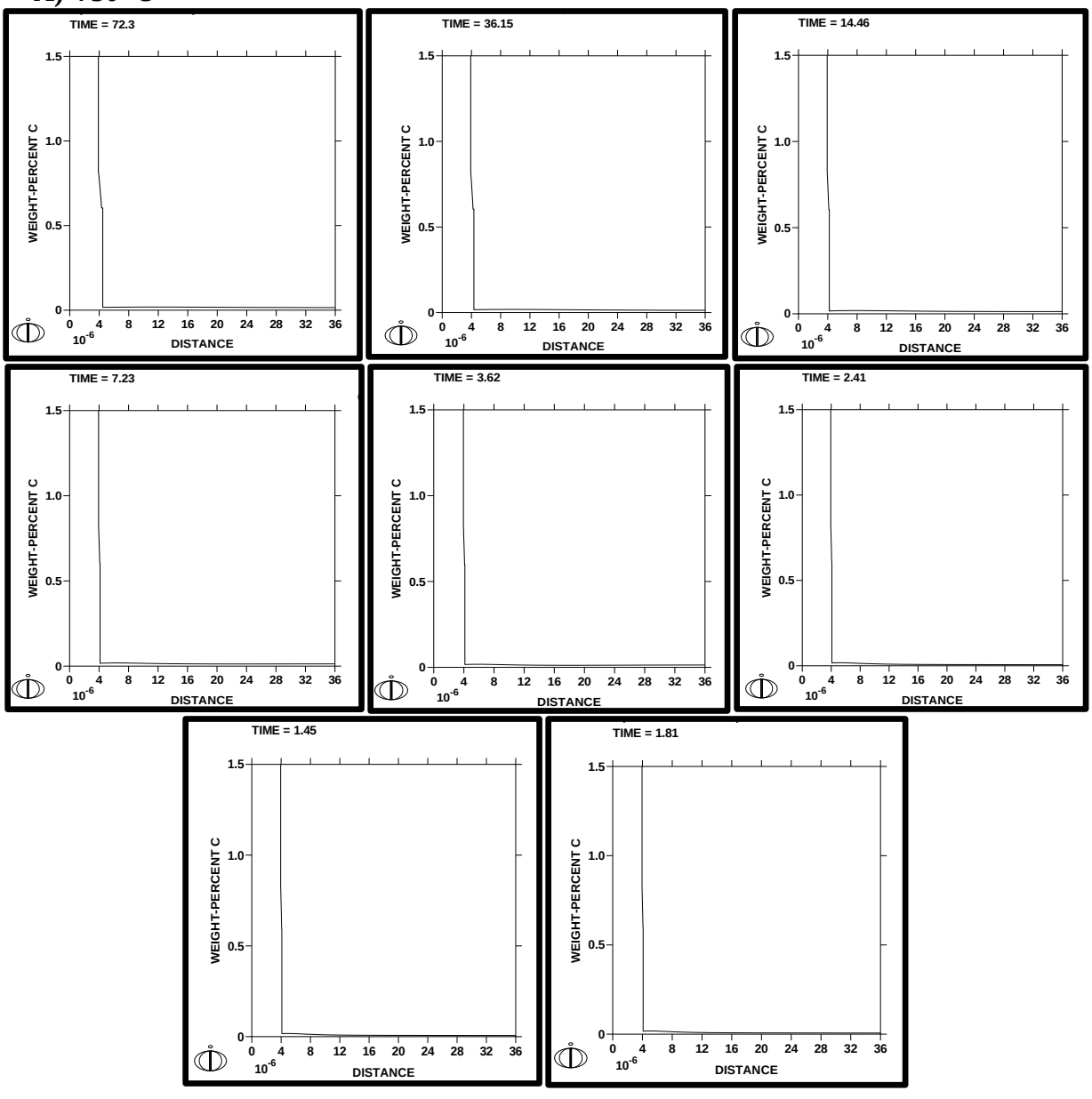

**B) 775 ℃**

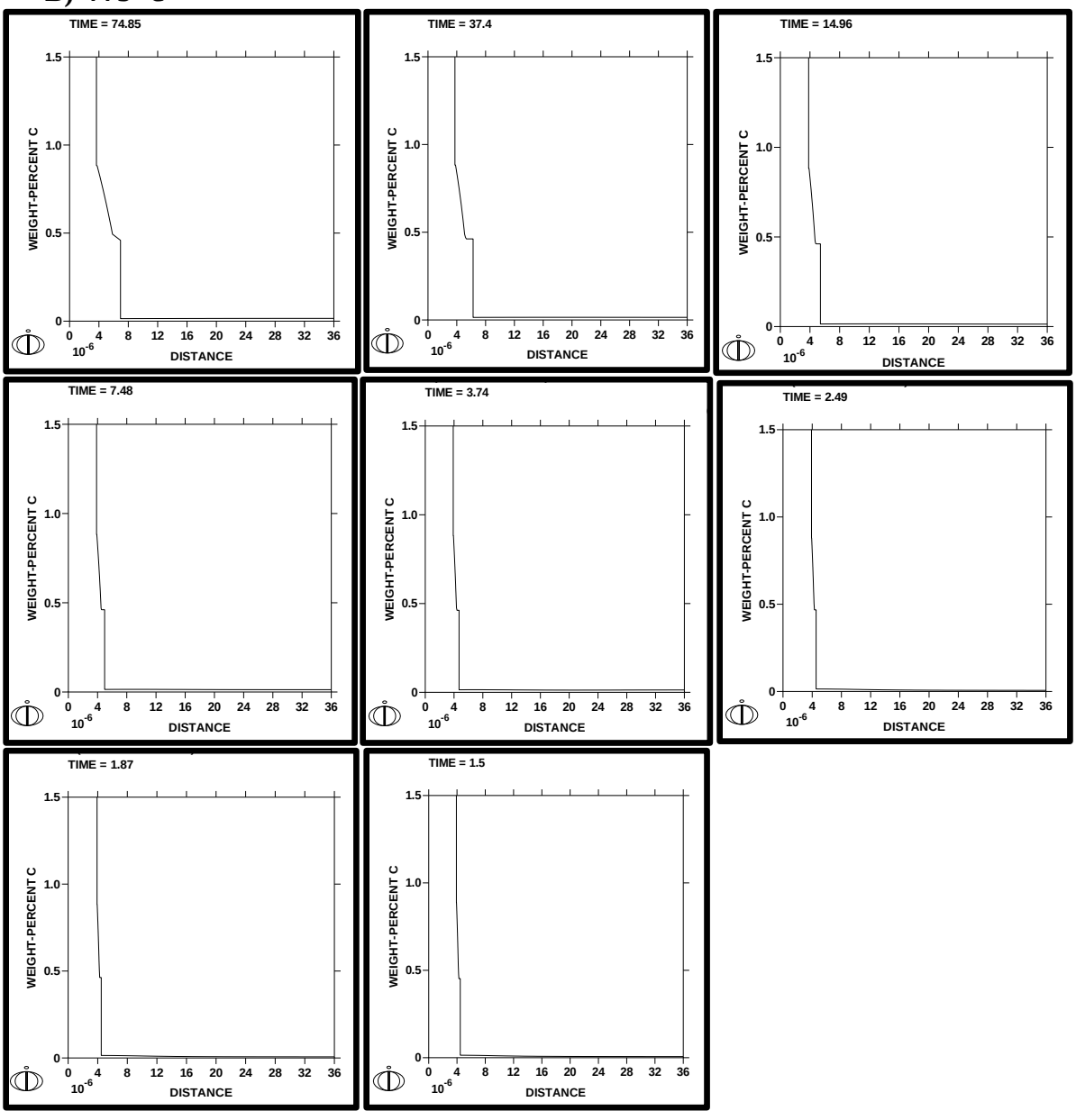
TIME = 74.85
TIME = 37.4
TIME = 14.96
TIME = 7.48
TIME = 3.74
TIME = 2.49
TIME = 1.87
TIME = 1.5
WEIGHT-PERCENT C
DISTANCE
10-6
0 4 8 12 16 20 24 28 32 36
0 0.5 1.0 1.5

**C) 825 ℃**

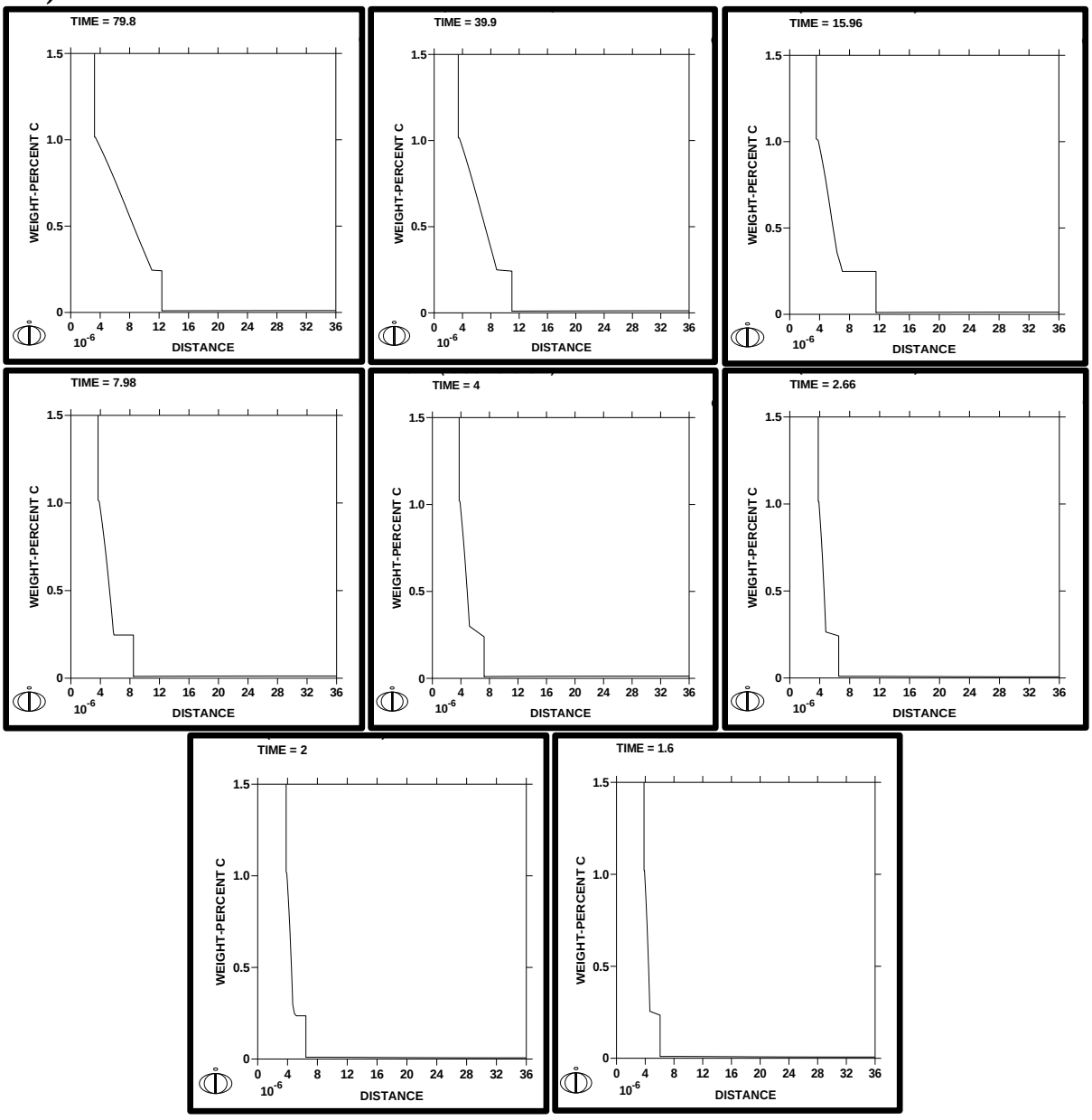
TIME = 79.8
TIME = 39.9
TIME = 15.96
TIME = 7.98
TIME = 4
TIME = 2.66
TIME = 2
TIME = 1.6
WEIGHT-PERCENT C
DISTANCE
10-6
0
0.5
1.0
1.5
0 4 8 12 16 20 24 28 32 36

**D) 850℃**

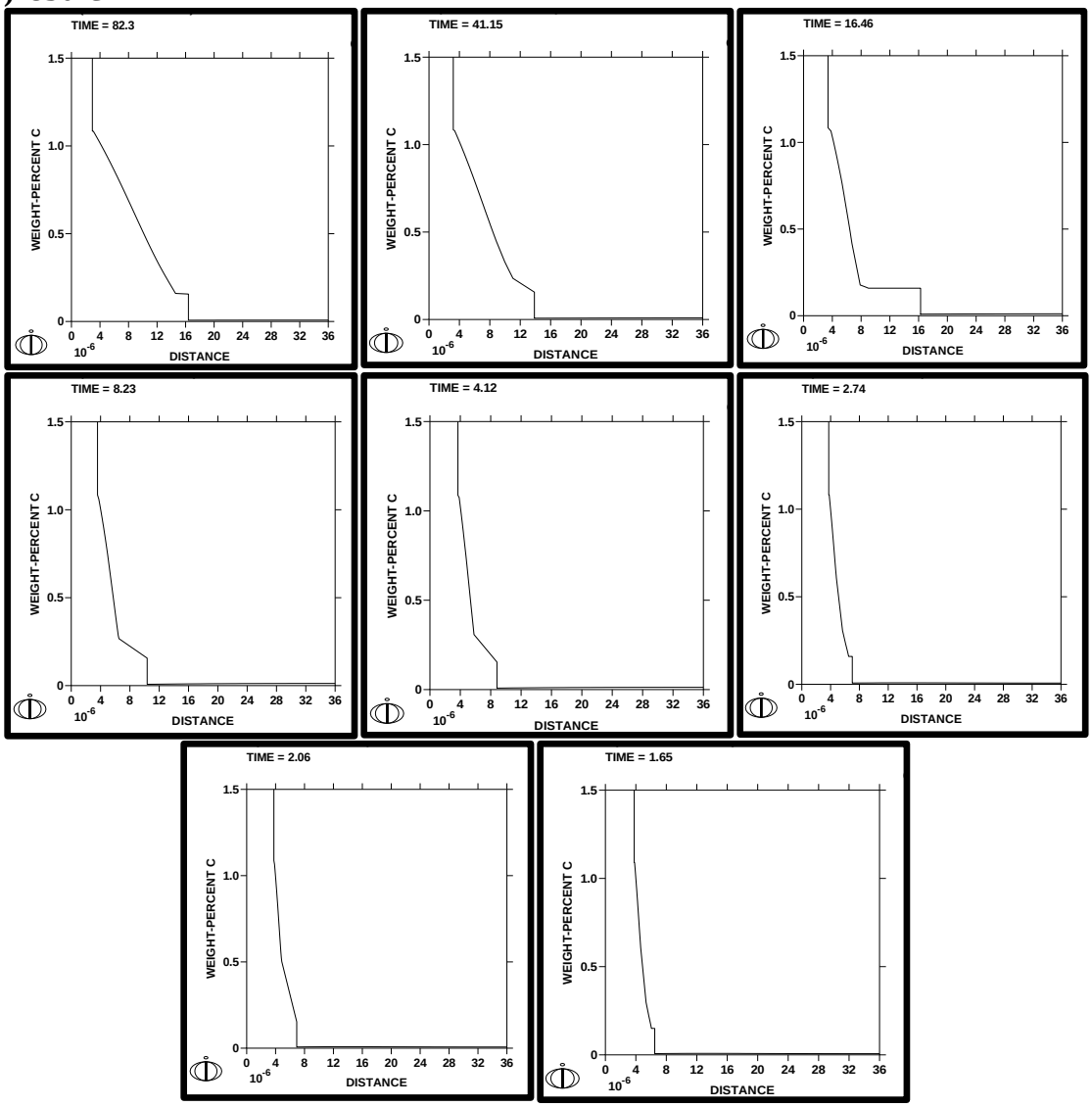
TIME = 82.3
TIME = 41.15
TIME = 16.46
TIME = 8.23
TIME = 4.12
TIME = 2.74
TIME = 2.06
TIME = 1.65
WEIGHT-PERCENT C
DISTANCE
10-6
0
0.5
1.0
1.5
0 4 8 12 16 20 24 28 32 36

# APPENDIX-III

Result window of DICTRA simulations showing stage 2 austenite volume faction as a function of time and weight percent carbon as a function of distance, at different heating rates viz. heating rates viz. 10, 20, 50, 100, 200, 300, 400, 500 ℃/s at a constant temperature of 750, 775, 800, 825, and 850 ℃.

**A) 750**℃

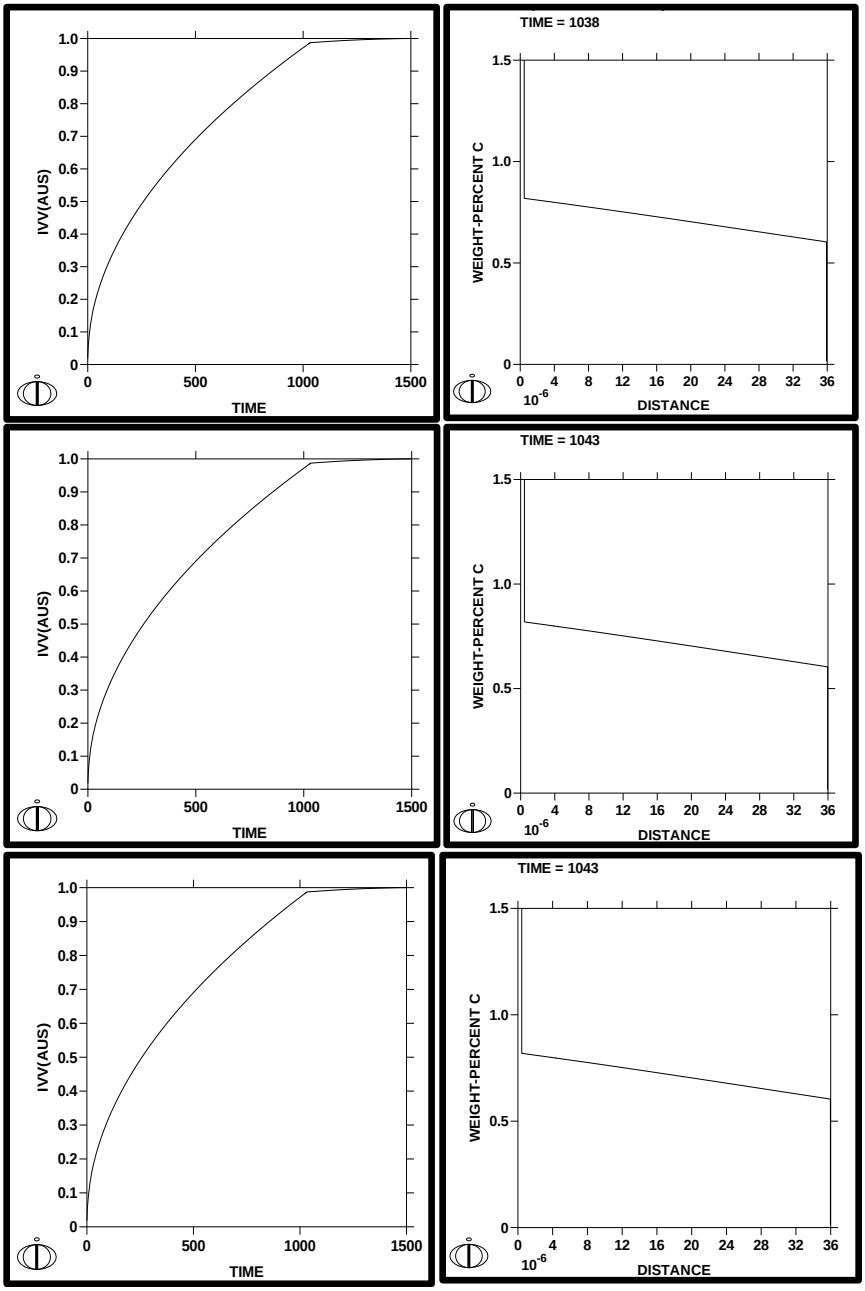

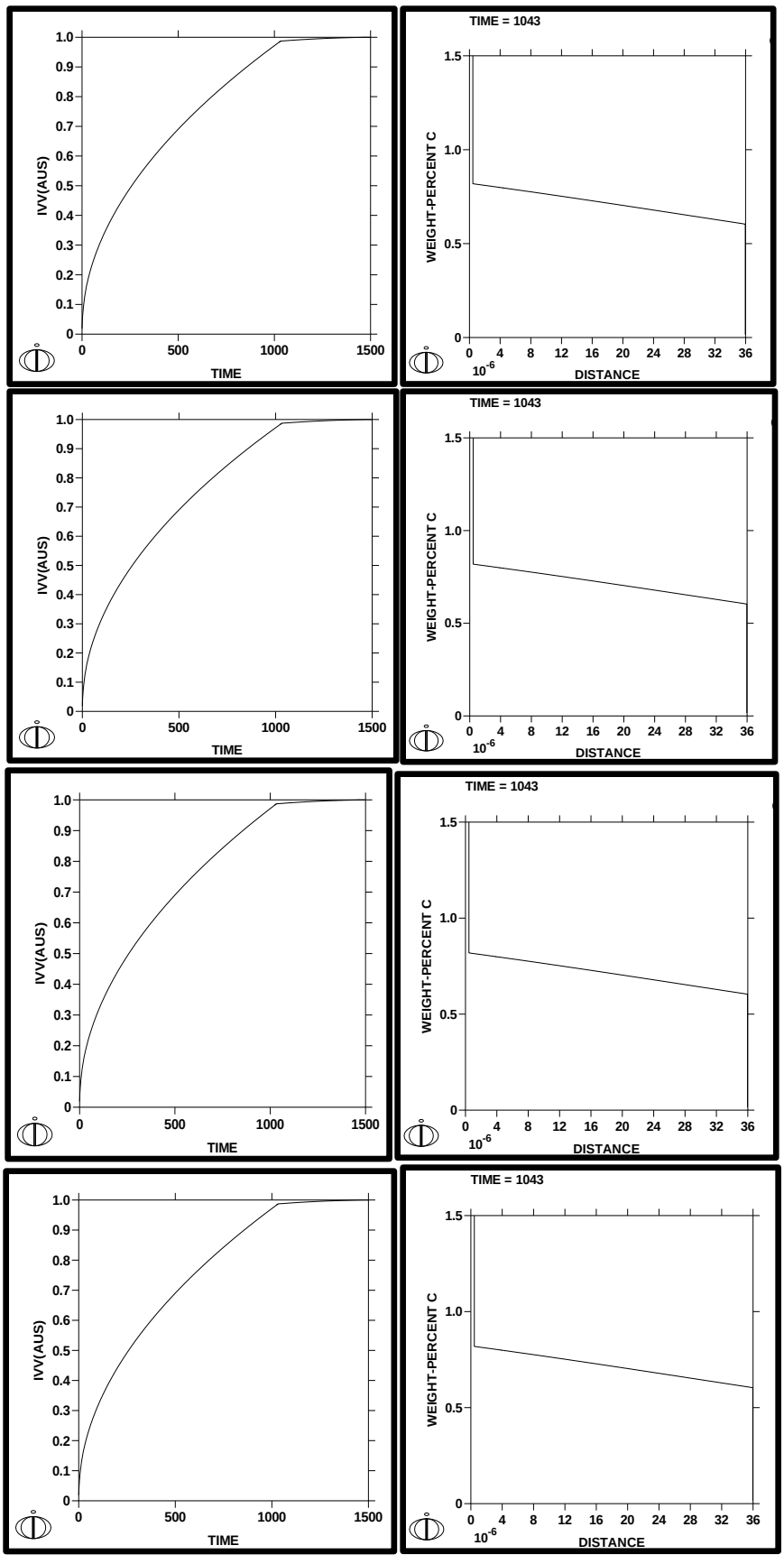
IVV(AUS)
TIME
0
0.1
0.2
0.3
0.4
0.5
0.6
0.7
0.8
0.9
1.0
0
500
1000
1500
TIME = 1043
WEIGHT-PERCENT C
DISTANCE
10-6
0.5
1.0
1.5
4
8
12
16
20
24
28
32
36

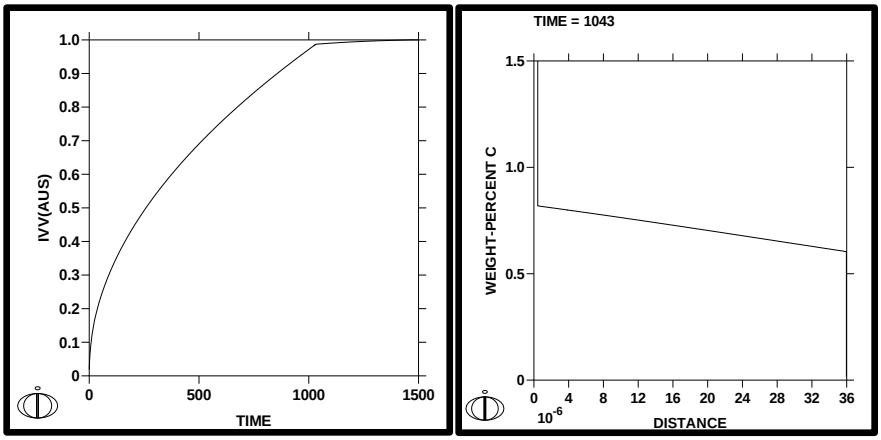
IVV(AUS)
TIME
TIME = 1043
WEIGHT-PERCENT C
DISTANCE
10-6

**B) 775 ℃**

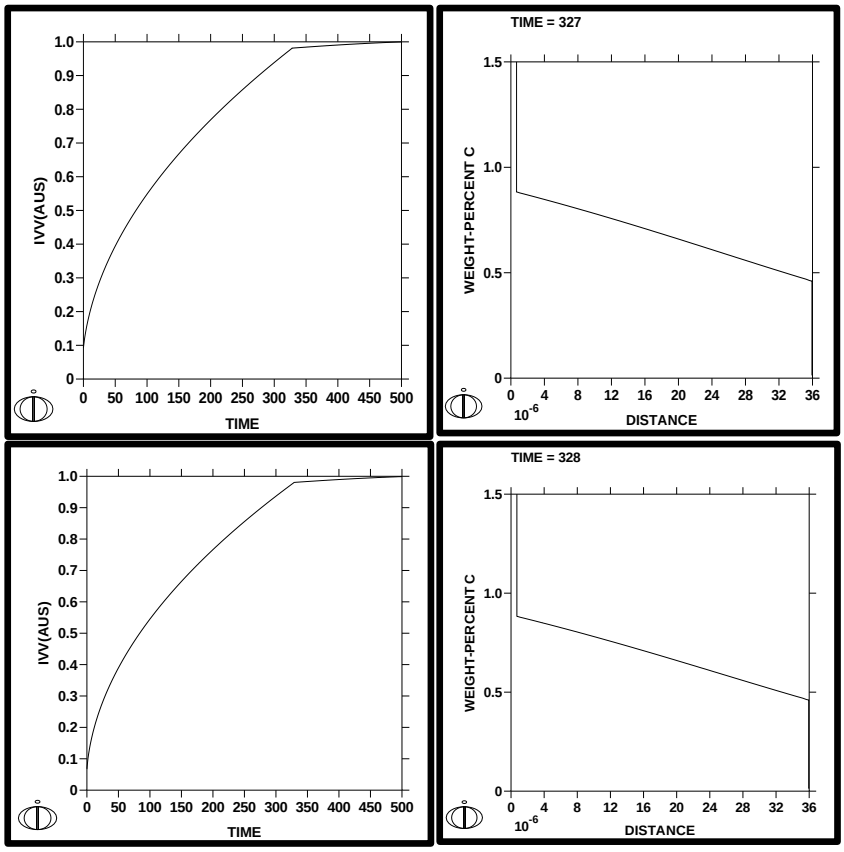
IVV(AUS)
TIME
TIME = 327
WEIGHT-PERCENT C
DISTANCE
10-6
IVV(AUS)
TIME
TIME = 328
WEIGHT-PERCENT C
DISTANCE
10-6

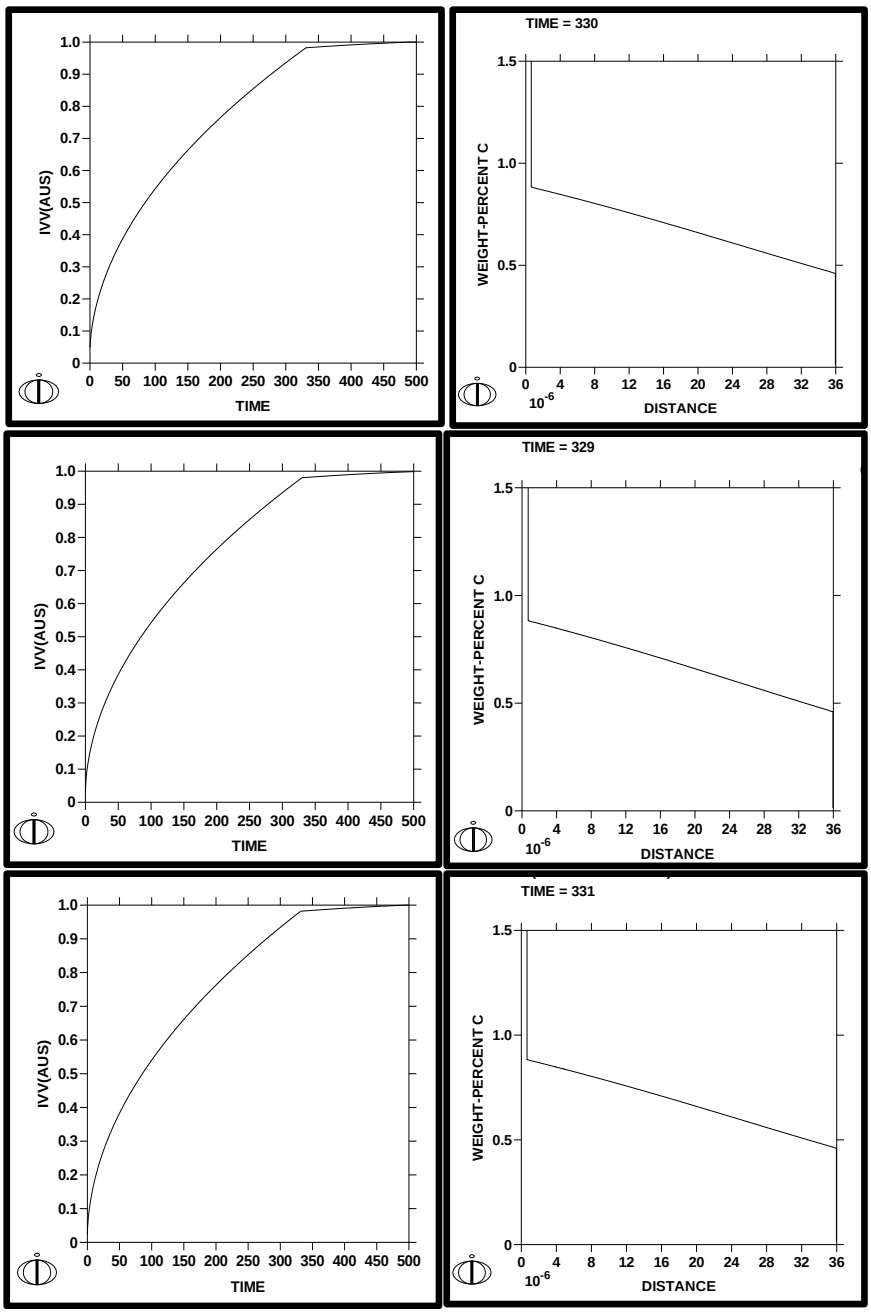
IVV(AUS)
TIME
TIME = 330
WEIGHT-PERCENT C
DISTANCE
10-6
TIME = 329
TIME = 331

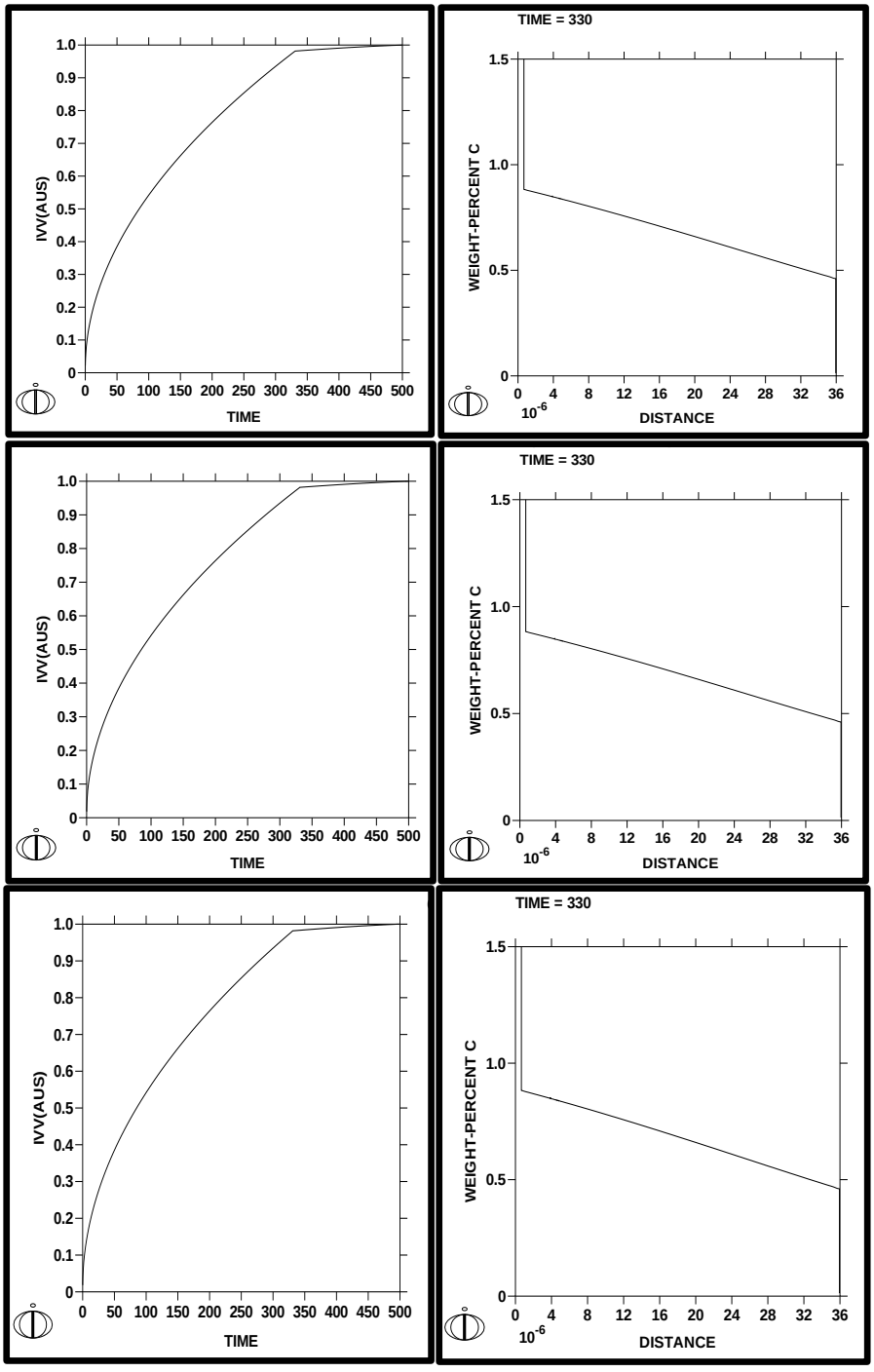
IVV(AUS)
TIME
TIME = 330
WEIGHT-PERCENT C
DISTANCE
10-6

**C) 800 ℃**

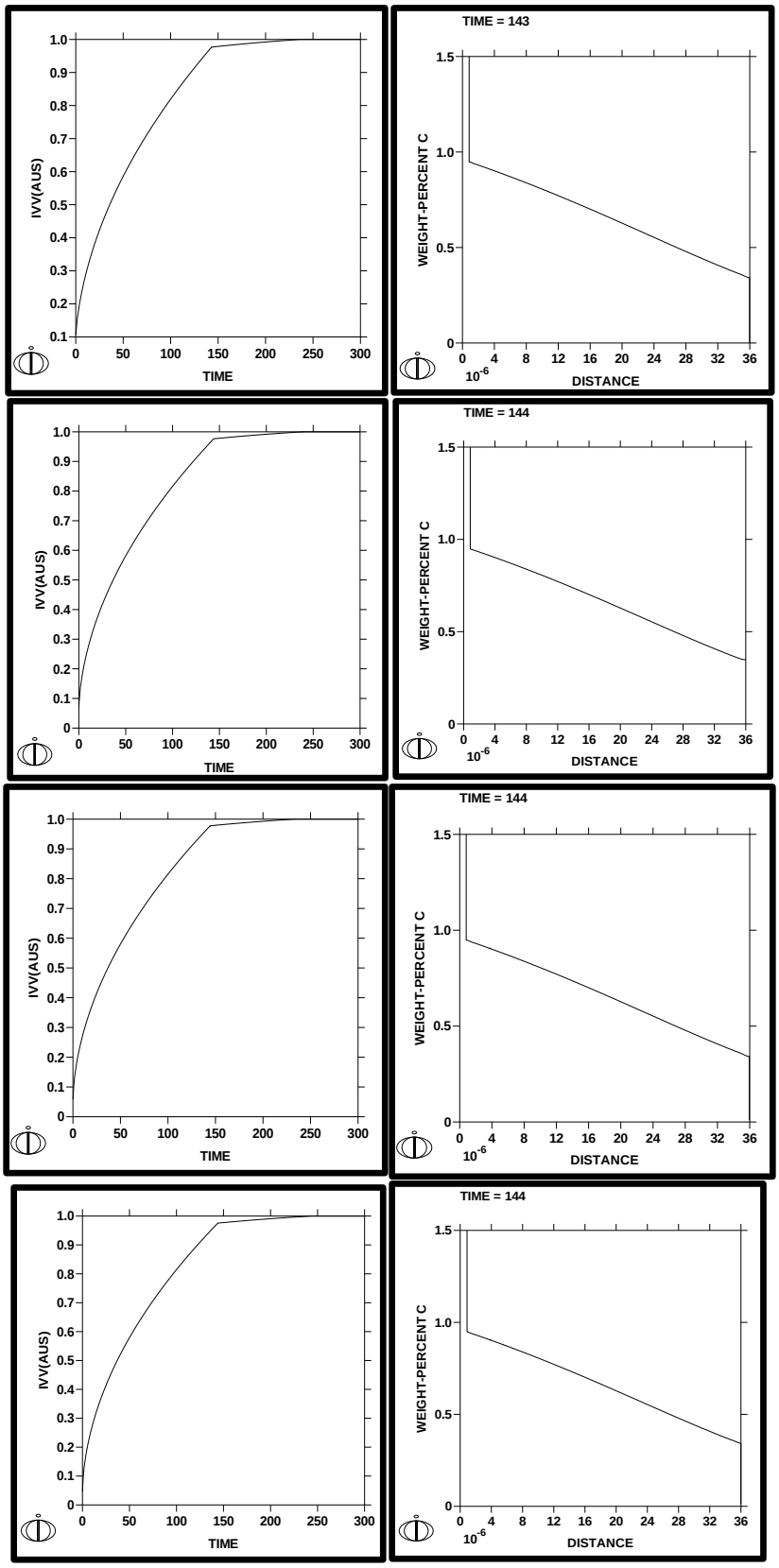
IVV(AUS)
TIME
TIME = 143
WEIGHT-PERCENT C
DISTANCE
10-6
IVV(AUS)
TIME
TIME = 144
WEIGHT-PERCENT C
DISTANCE
10-6
IVV(AUS)
TIME
TIME = 144
WEIGHT-PERCENT C
DISTANCE
10-6
IVV(AUS)
TIME
TIME = 144
WEIGHT-PERCENT C
DISTANCE
10-6

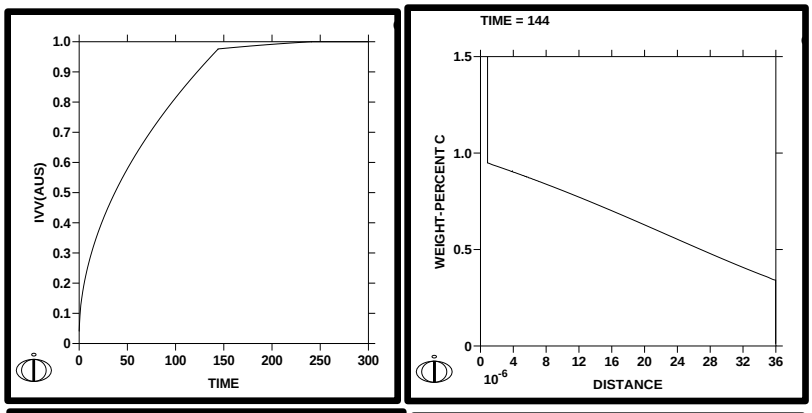
IVV(AUS)
TIME
TIME = 144
WEIGHT-PERCENT C
DISTANCE
10-6

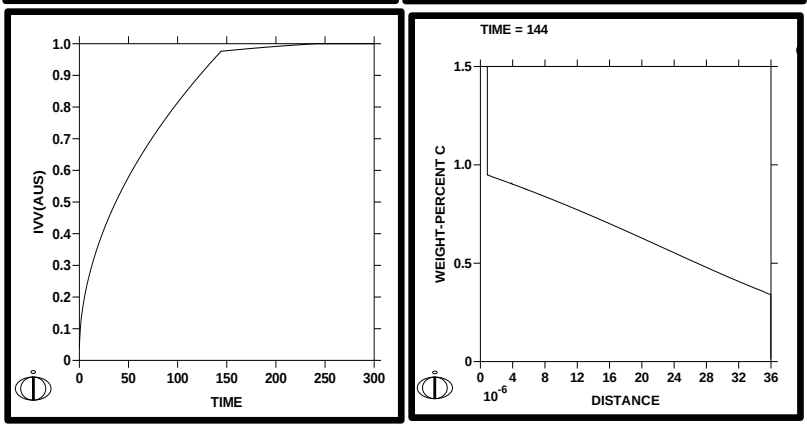
IVV(AUS)
TIME
TIME = 144
WEIGHT-PERCENT C
DISTANCE
10-6

**A) 825 ℃**

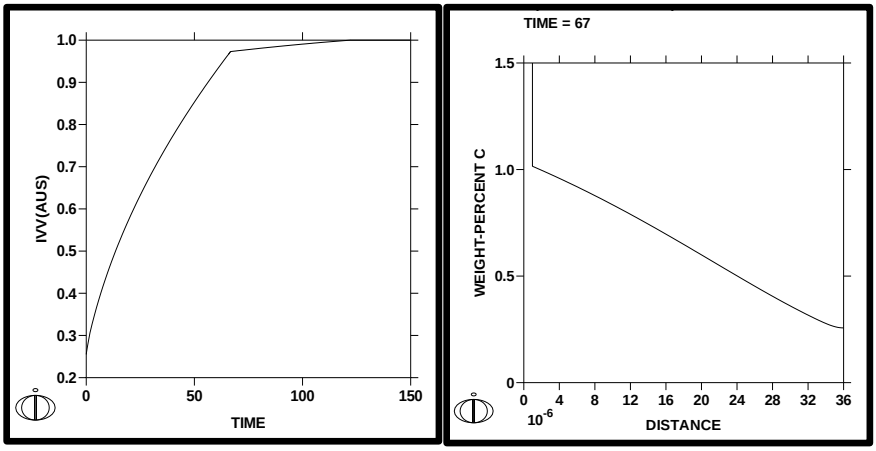
IVV(AUS)
TIME
TIME = 67
WEIGHT-PERCENT C
DISTANCE
10-6

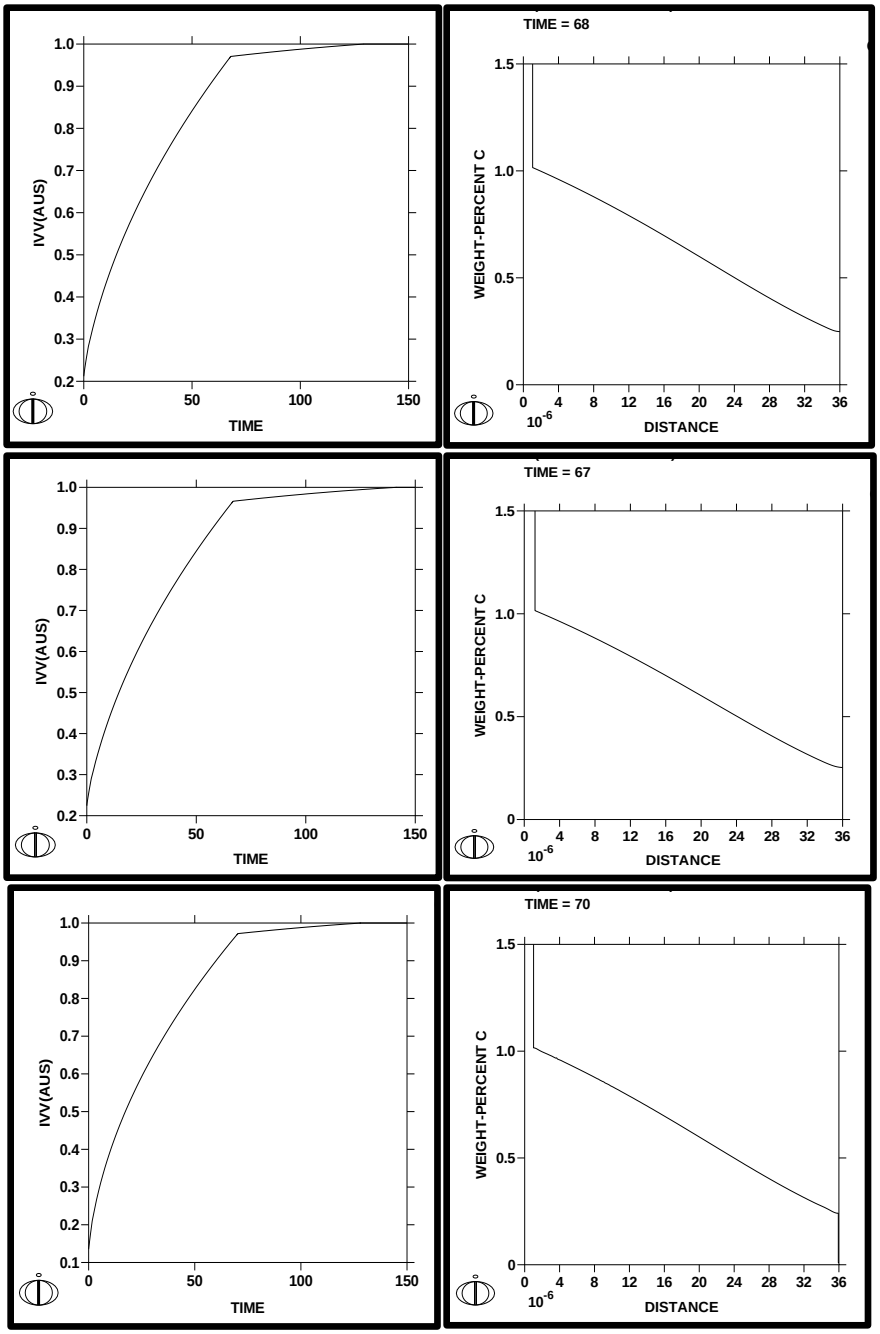
IVV(AUS)
TIME
WEIGHT-PERCENT C
DISTANCE
TIME = 68
TIME = 67
TIME = 70

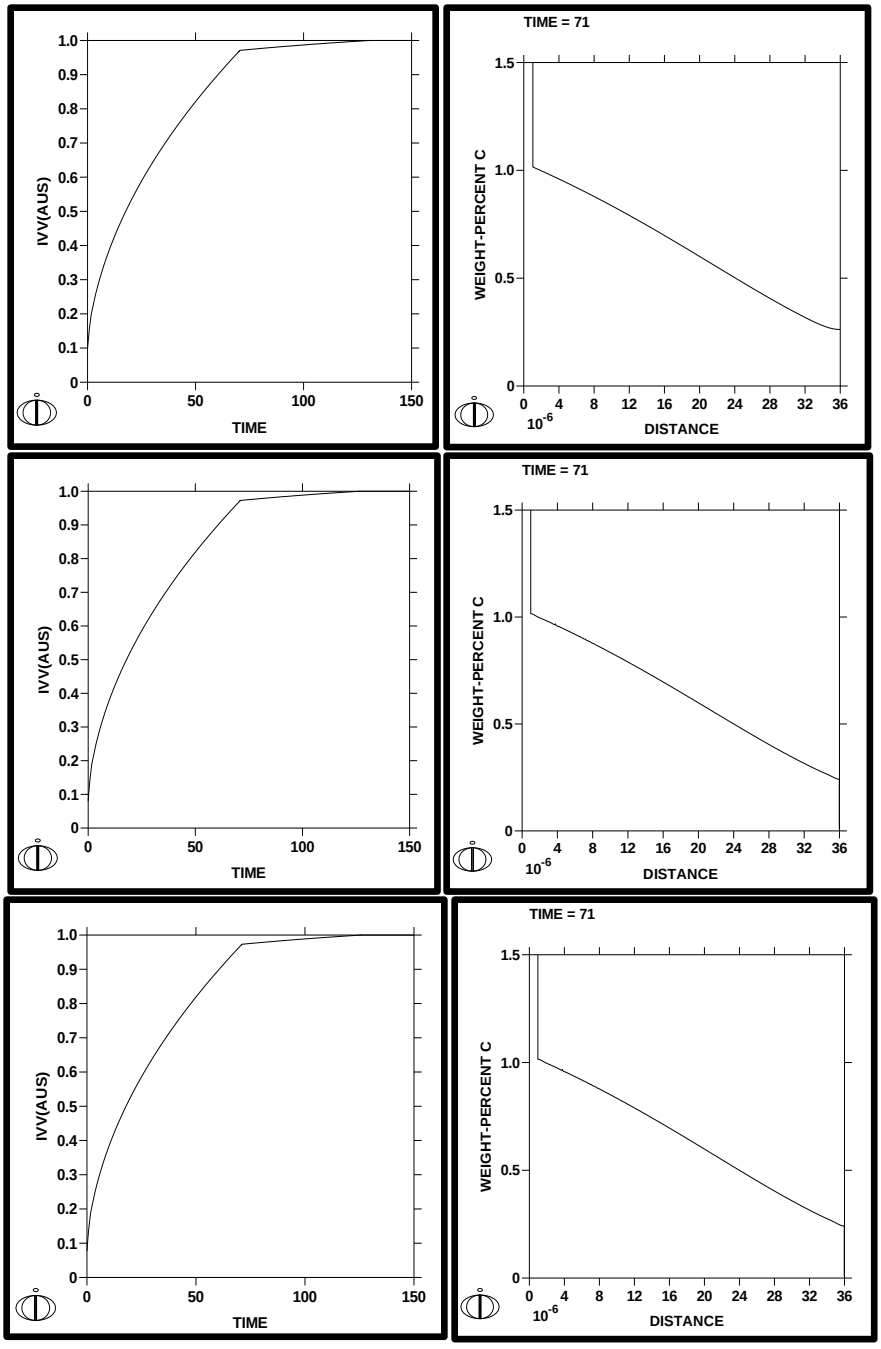
IVV(AUS)
TIME
TIME = 71
WEIGHT-PERCENT C
DISTANCE
10-6

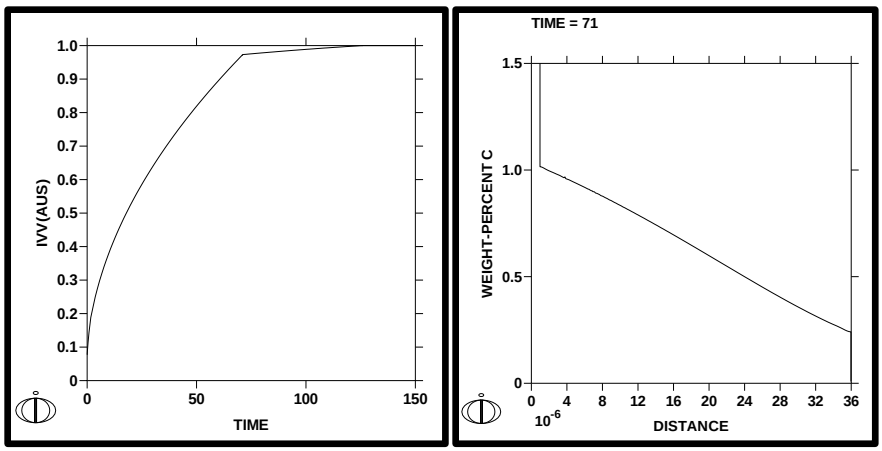
IVV(AUS)
1.0
0.9
0.8
0.7
0.6
0.5
0.4
0.3
0.2
0.1
0
0
50
100
150
TIME
TIME = 71
WEIGHT-PERCENT C
1.5
1.0
0.5
0
0
4
8
12
16
20
24
28
32
36
10-6
DISTANCE

**B) 850 ℃**

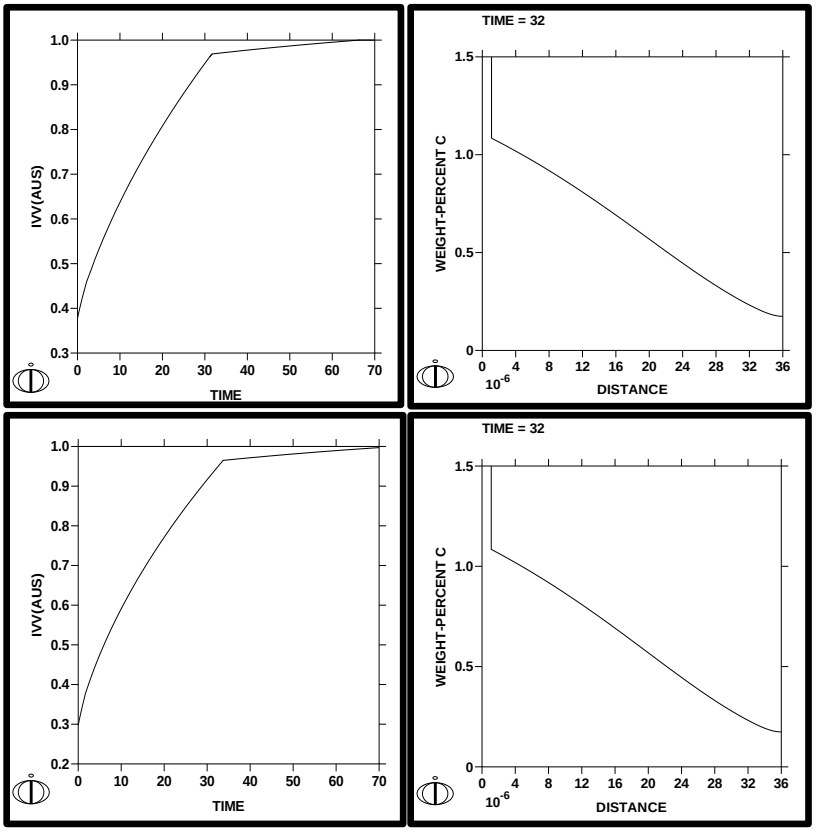
IVV(AUS)
1.0
0.9
0.8
0.7
0.6
0.5
0.4
0.3
0
10
20
30
40
50
60
70
TIME
TIME = 32
WEIGHT-PERCENT C
1.5
1.0
0.5
0
0
4
8
12
16
20
24
28
32
36
10-6
DISTANCE
IVV(AUS)
1.0
0.9
0.8
0.7
0.6
0.5
0.4
0.3
0.2
0
10
20
30
40
50
60
70
TIME
TIME = 32
WEIGHT-PERCENT C
1.5
1.0
0.5
0
0
4
8
12
16
20
24
28
32
36
10-6
DISTANCE

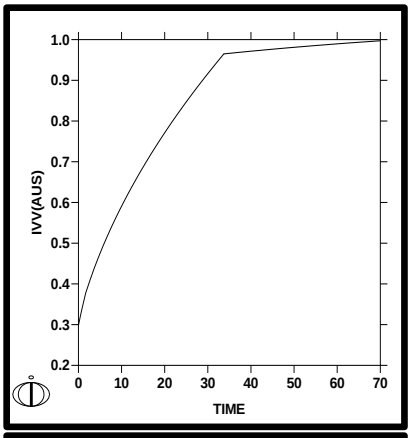
IVV(AUS)
1.0
0.9
0.8
0.7
0.6
0.5
0.4
0.3
0.2
0 10 20 30 40 50 60 70
TIME

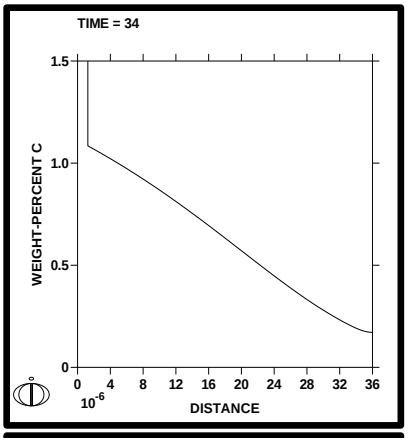
TIME = 34
WEIGHT-PERCENT C
1.5
1.0
0.5
0
0 4 8 12 16 20 24 28 32 36
10-6
DISTANCE

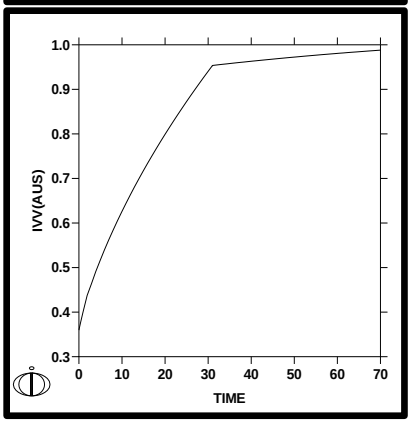
IVV(AUS)
1.0
0.9
0.8
0.7
0.6
0.5
0.4
0.3
0 10 20 30 40 50 60 70
TIME

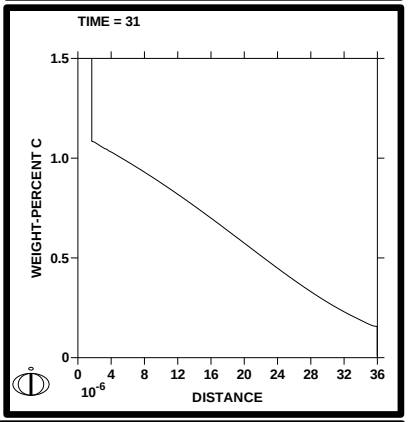
TIME = 31
WEIGHT-PERCENT C
1.5
1.0
0.5
0
0 4 8 12 16 20 24 28 32 36
10-6
DISTANCE

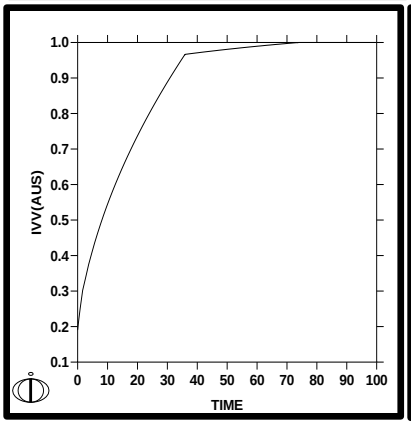
IVV(AUS)
1.0
0.9
0.8
0.7
0.6
0.5
0.4
0.3
0.2
0.1
0 10 20 30 40 50 60 70 80 90 100
TIME

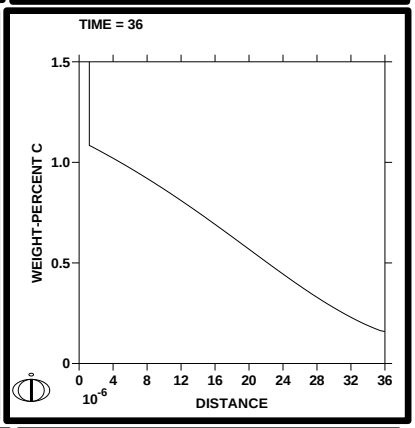
TIME = 36
WEIGHT-PERCENT C
1.5
1.0
0.5
0
0 4 8 12 16 20 24 28 32 36
10-6
DISTANCE

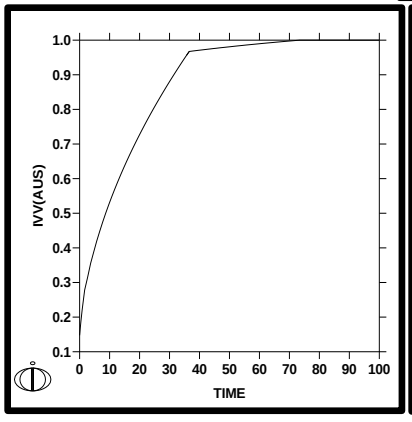
IVV(AUS)
1.0
0.9
0.8
0.7
0.6
0.5
0.4
0.3
0.2
0.1
0 10 20 30 40 50 60 70 80 90 100
TIME

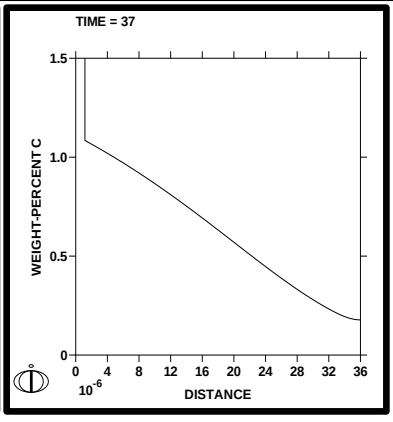
TIME = 37
WEIGHT-PERCENT C
1.5
1.0
0.5
0
0 4 8 12 16 20 24 28 32 36
10-6
DISTANCE

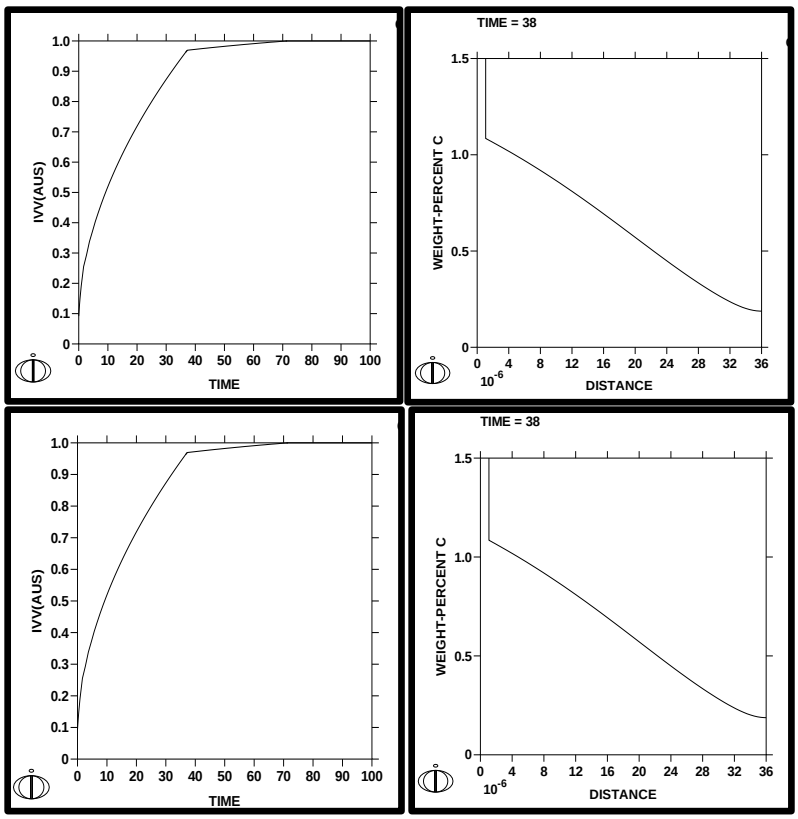
IVV(AUS)
TIME
TIME = 38
WEIGHT-PERCENT C
DISTANCE
$10^{-6}$
IVV(AUS)
TIME
TIME = 38
WEIGHT-PERCENT C
DISTANCE
$10^{-6}$

# APPENDIX-IV

Result window of DICTRA simulations showing weight percent carbon as a function of distance, at different annealing temperatures viz. 750, 775, 800, 825, 850 ℃ at a constant heating rates of 10, 20, 50, and 100 ℃/$s$. DISTANCE = distance from original cementite lamella of pearlite mixture in microns.

A) 775℃

i) 10 ℃/$s$

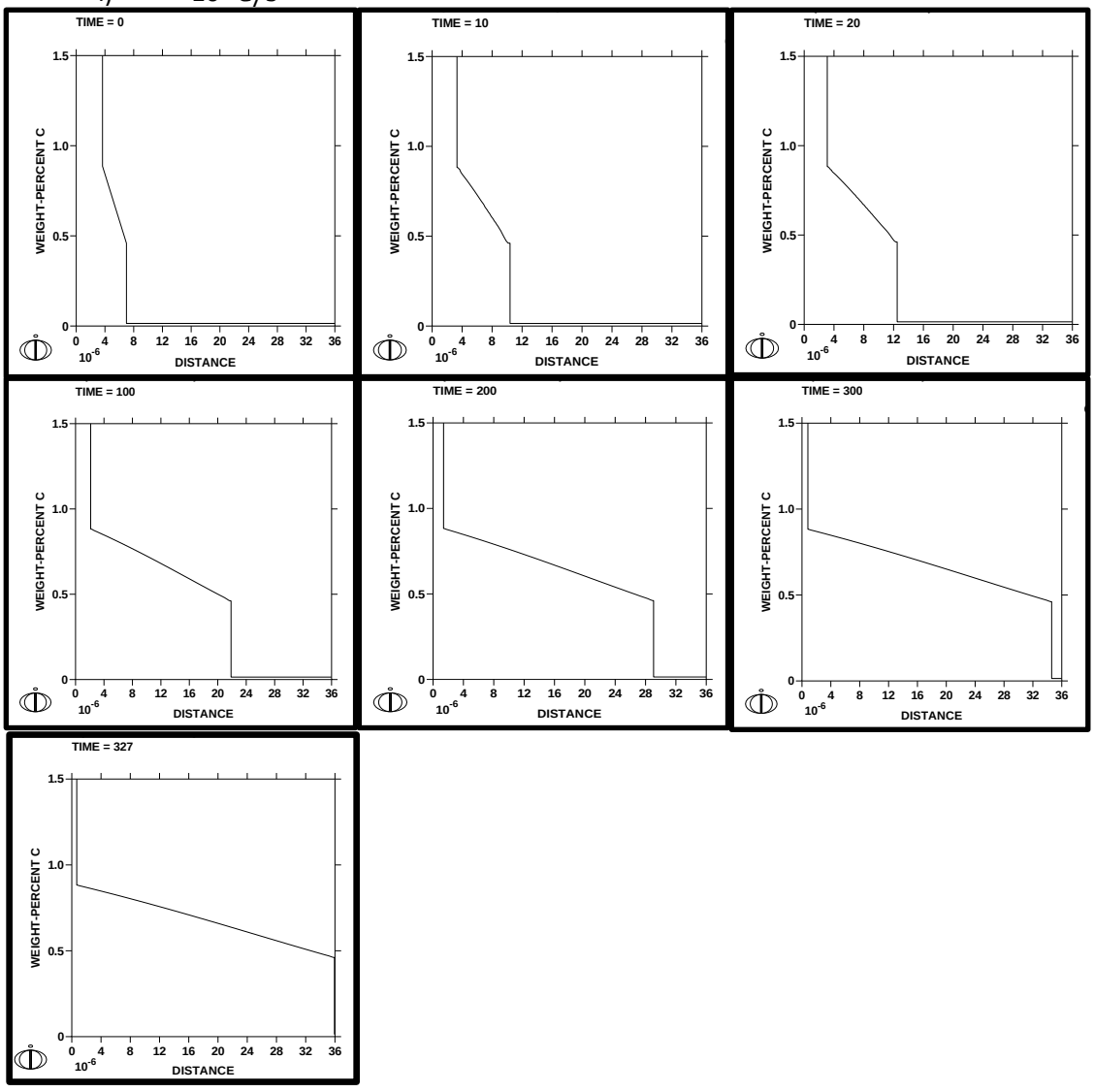

ii) 20 ℃/$s$

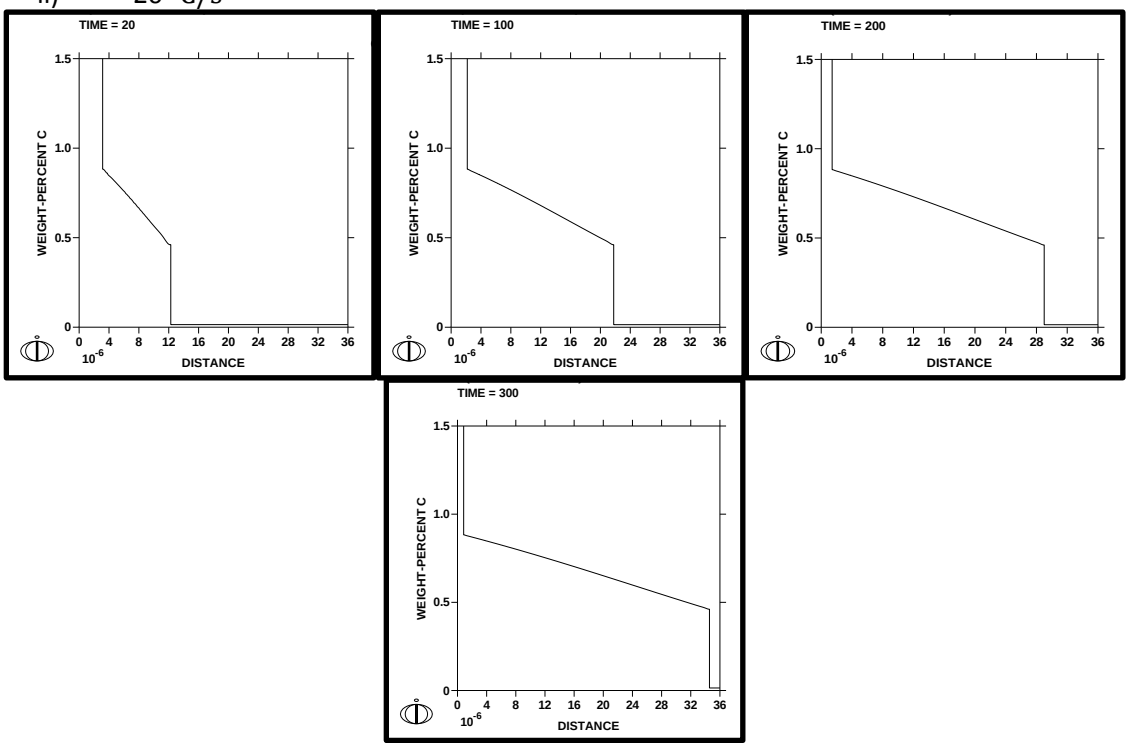


iii) 50 ℃/$s$

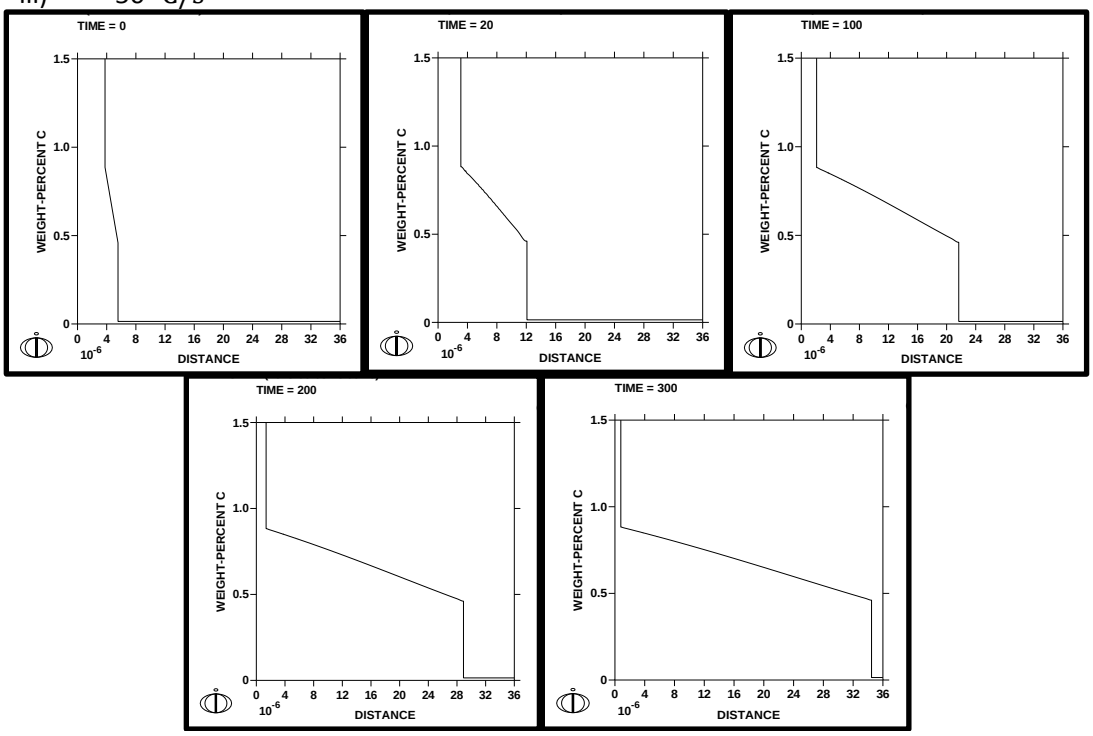

**B) 775** ℃

**i) 10** ℃/$s$

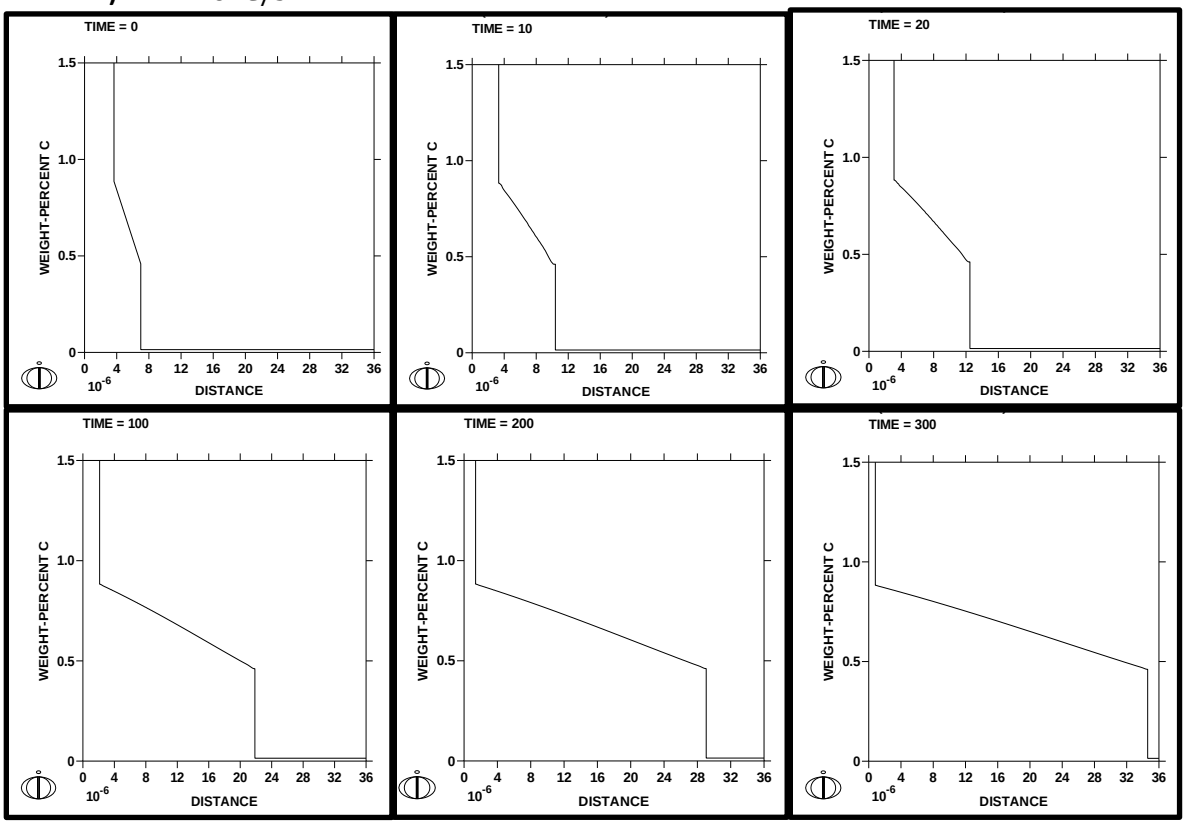


**ii) 20** ℃/$s$

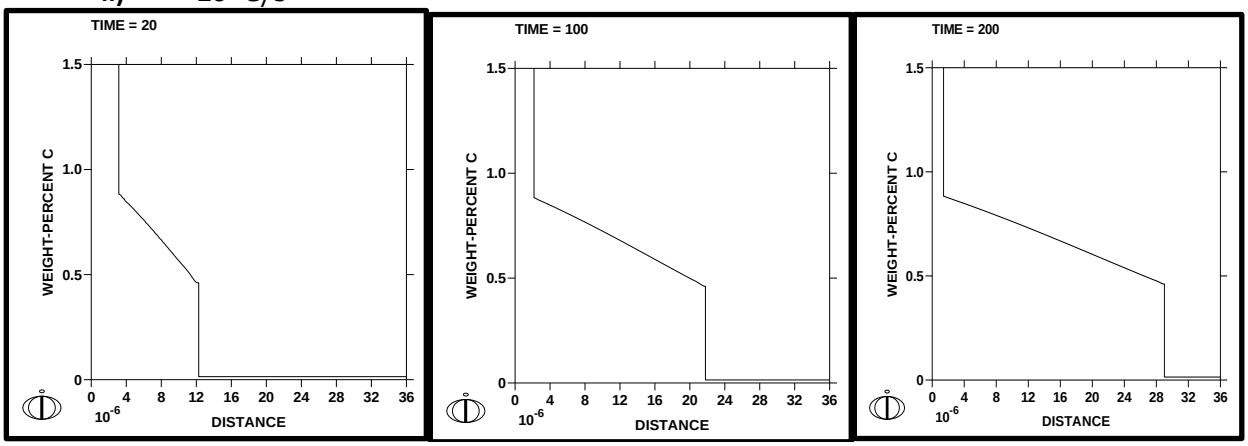

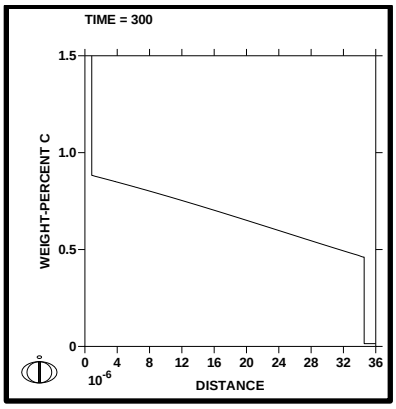


**iii)** **50** $℃/s$

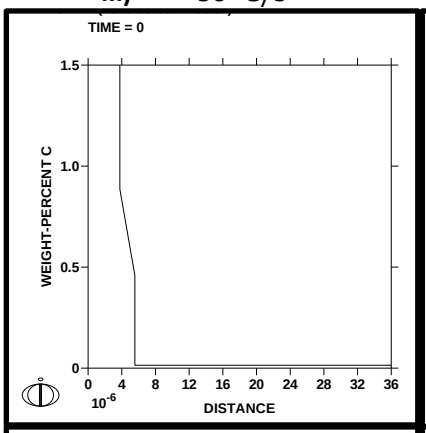


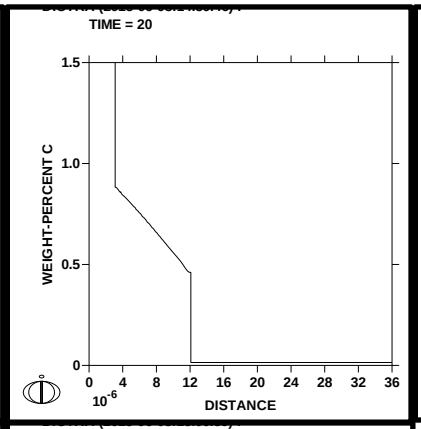


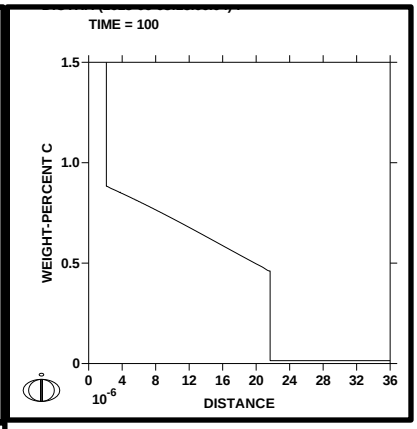


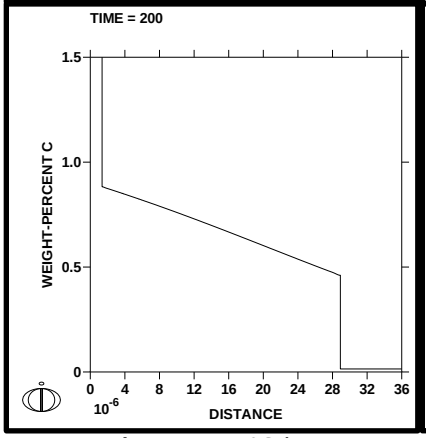


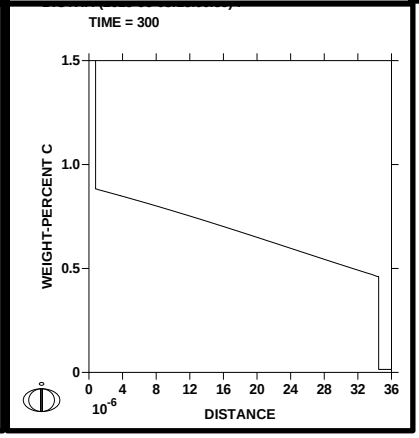


**iv)** **100** $℃/s$

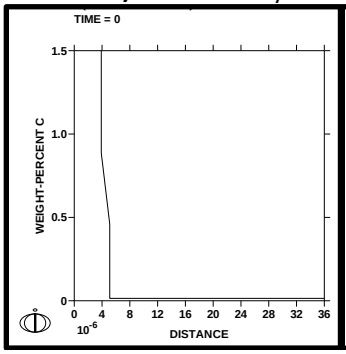


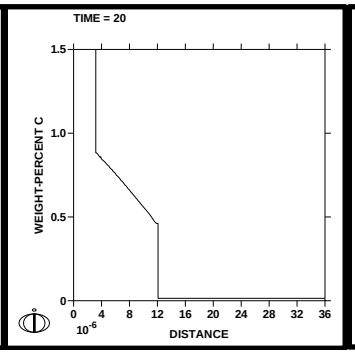


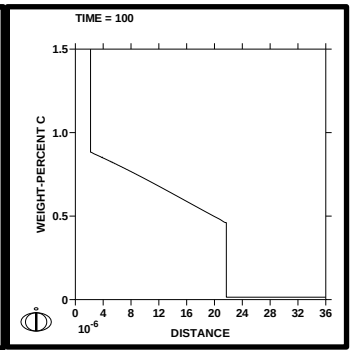

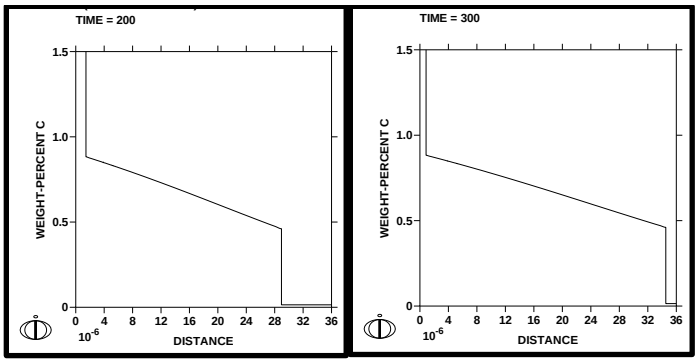


**C) 800** ℃

**10** ℃/$s$

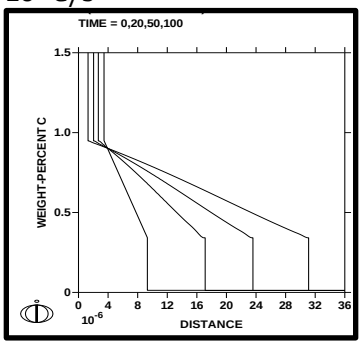


**20** ℃/$s$

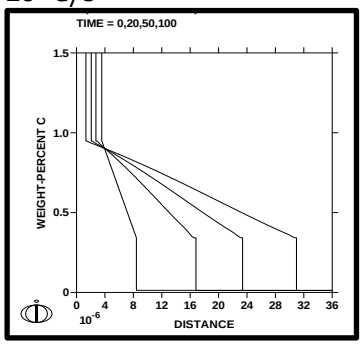


**50** ℃/$s$

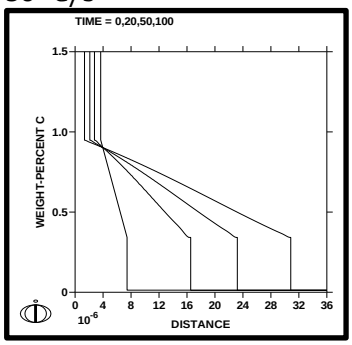


**100** ℃/$s$

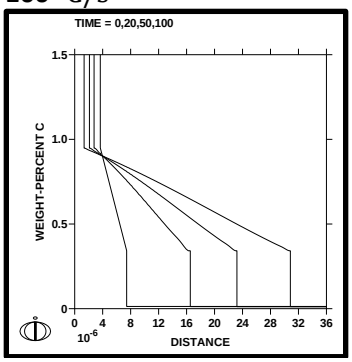


**D) 825** ℃

**10** ℃/$s$

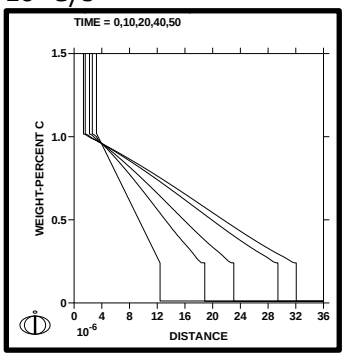


**20** ℃/$s$

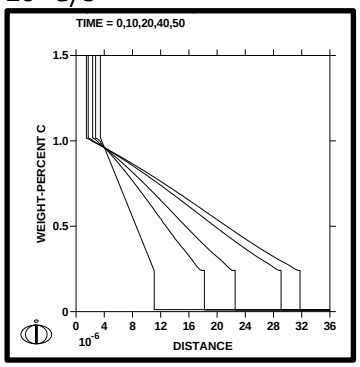


**50** ℃/$s$

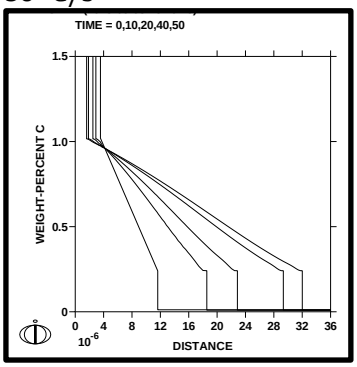

**100** ℃/$s$

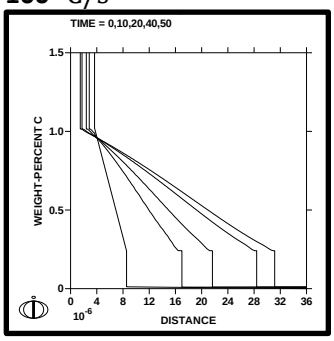


**E) 850** ℃

**10** ℃/$s$

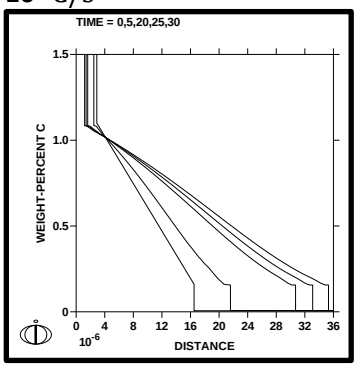


**20** ℃/$s$

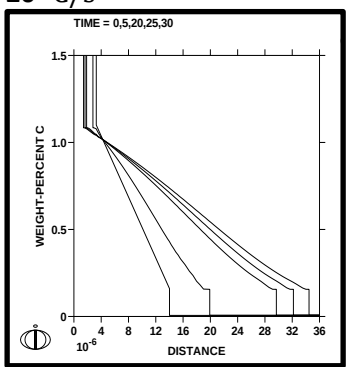


**50** ℃/$s$

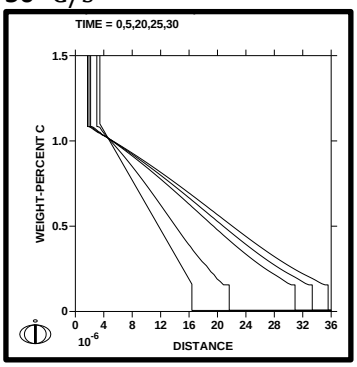


**100** ℃/$s$

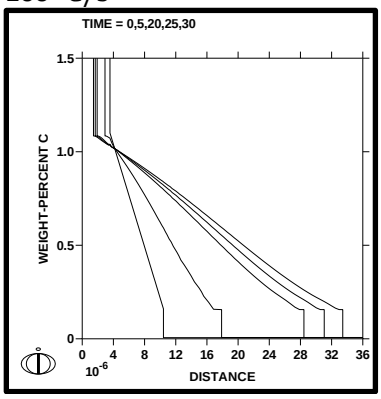

# APPENDIX-V

Table: Represents austenite formation at varying heating rates at different annealing temperatures (actual distance of austenite formed by DICTRA simulations).

| Heating rate | Austenite formed at 750 ℃ (μm) | Austenite formed at 775 ℃ (μm) | Austenite formed at 800 ℃ (μm) | Austenite formed at 825 ℃ (μm) | Austenite formed at 850 ℃ (μm) |
|---|---|---|---|---|---|
| 10 $℃/s$ | 0.66 | 3.33 | 5.86 | 9.18 | 13.61 |
| 20 $℃/s$ | 0.44 | 2.43 | 4.88 | 7.64 | 10.732 |
| 50 $℃/s$ | 0.44 | 1.78 | 3.77 | 6.696 | 9.072 |
| 100 $℃/s$ | 0.33 | 1.22 | 2.54 | 4.88 | 6.86 |
| 200 $℃/s$ | 0.32 | 0.88 | 2.1 | 3.54 | 5.31 |
| 300 $℃/s$ | 0.34 | 0.77 | 1.66 | 2.88 | 3.32 |
| 400 $℃/s$ | 0.34 | 0.66 | 1.44 | 2.77 | 3.22 |
| 500 $℃/s$ | 0.33 | 0.66 | 1.44 | 2.43 | 2.77 |

# APPENDIX-VI

Size distribution of phases for different annealing temperature of 775, 800, and 825 ℃ in hot rolled and cold rolled.

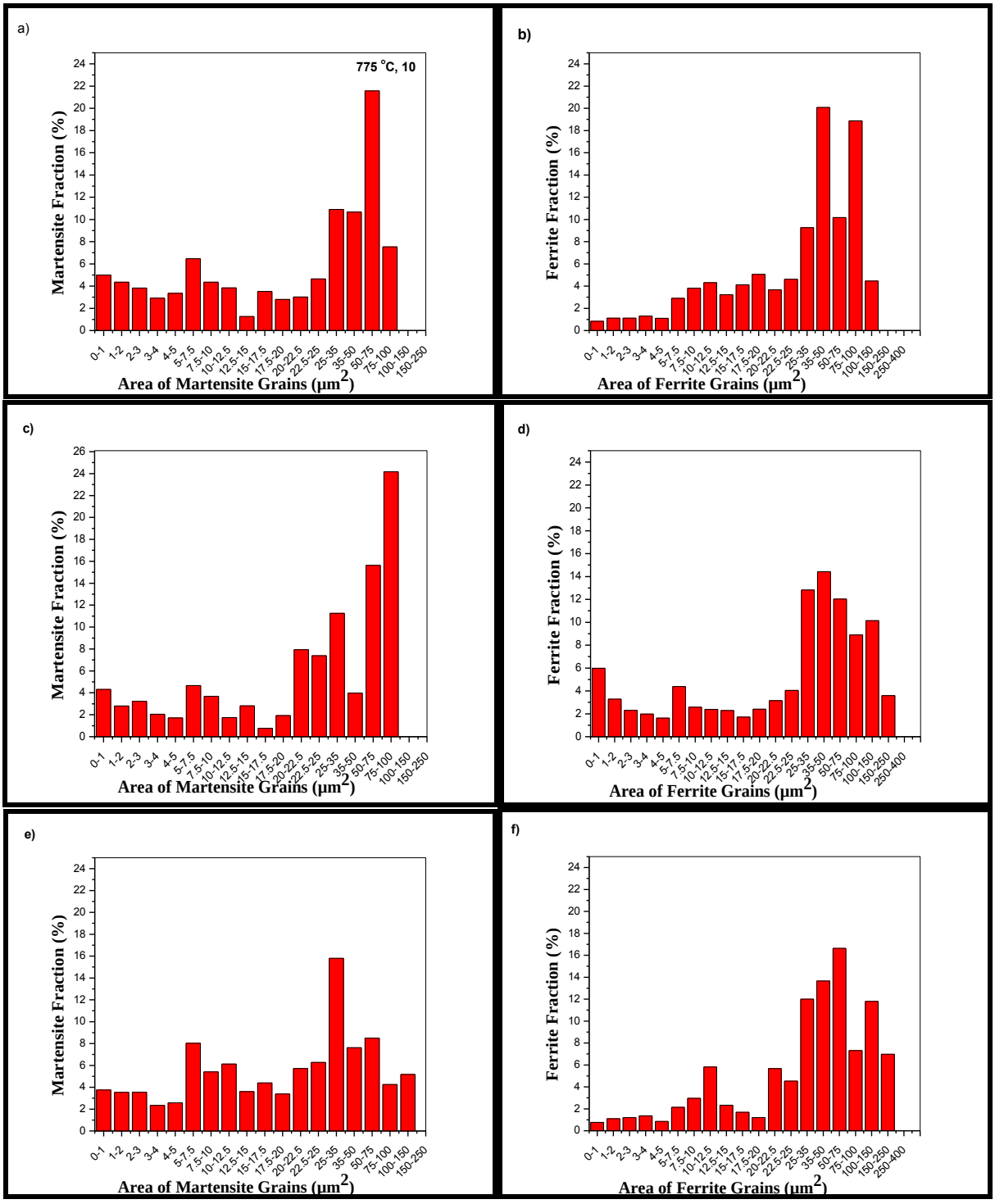


**Figure: Size distribution of phases in hot rolled specimens for different temperatures for (a, c, e) martensite (b, d, f) ferrite**

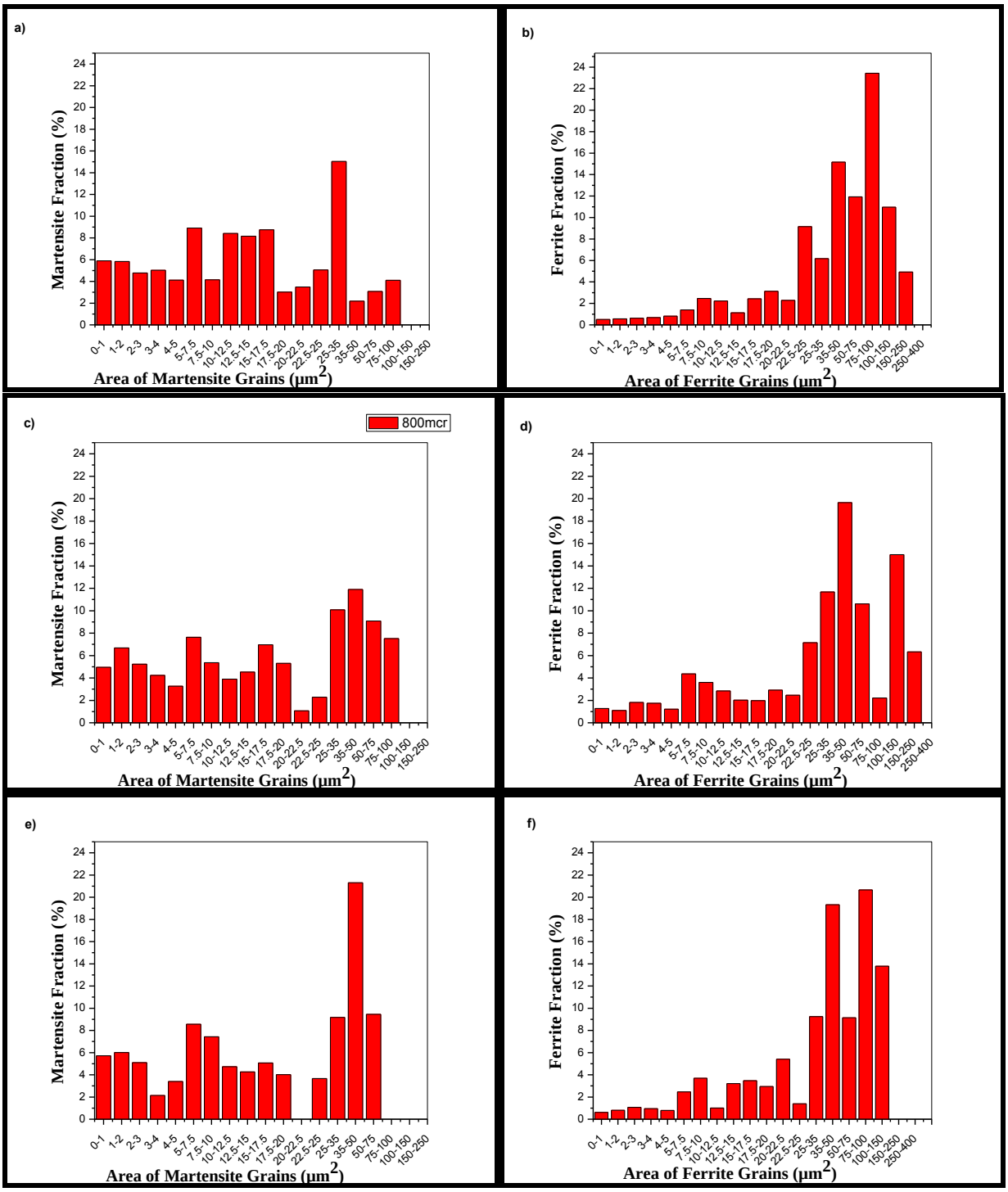


**Figure: Size distribution of phases in cold rolled specimens for different temperatures for (a, c, e) martensite (b, d, f) ferrite.**